The Effect of Energy Input on Flotation Kinetics

By

Mehdi Safari

B.Sc. and M.Sc. in Mining/Chemical Engineering and Mineral Processing

A thesis submitted to the University of Cape Town in fulfilment of the requirements for the degree of Doctor of Philosophy

Centre for Minerals Research
Department of Chemical Engineering
University of Cape Town
August 2017

ACKNOWLEDGEMENTS

This is not a very easy part for me because I believe that everybody that I have met up to this point has contributed in their own way to me being at this point in my life and hence achieving the things I have so far.

I would like to express my sincere thanks to my supervisor, Professor David Deglon, and co-supervisor, Martin Harris, for their assistance/guidance and enthusiasm, constant support and patience in this study. They allowed me the freedom to accomplish my studies as I wished. Thank you for the invaluable insights and input, and keeping the project interesting.

I would also like thank and acknowledge the following:

To Joachim Macke, Bill Randall, Izak van der Westhuizen and Granville de la Cruz for assisting with the construction of the pilot oscillating grid cell used in this study.

Heather Sundstrom for her assistance with my numerous administrative and purchasing issues.

Shireen Govender, thank you for all of your assistance during my project in the CMR laboratory.

Kenneth Maseko for his assistance during my time in the CMR laboratory.

The staff and students of the Centre for Minerals Research for their valuable assistance, comments, constructive advice and providing a stimulating environment for learning and growing.

My parents and sisters, for their continuous encouragement and moral support throughout the years. Without your love and support from the other side of the world I would not have made it this far.

Thank you to the University of Cape Town and the AMIRA P9P project for funding this research and the continued interest in the project.

DECLARATION

I know the meaning of plagiarism and declare that all the work in the document, save for that which is properly acknowledged, is my own. No portion of the work referred to in this thesis has been submitted in support of an application for another degree or qualification of this or any other university or other institute of learning.

Mehdi Safari
August 2017

CERTIFICATION BY SUPERVISOR

In terms of paragraph GP 8 of the rules for the degree of PhD I certify that I approve of the incorporation in this thesis of material that has been published.

Professor David Deglon (Supervisor)
Department of Chemical Engineering
University of Cape Town
Private Bag
Rondebosch, 7700

LIST OF PUBLICATIONS

Journal Publications

Safari, M., Deglon, D.A., An Attachment-Detachment Kinetic Model for the Effect of Energy Input on Flotation, Minerals Engineering Volume 117, 2018, pp. 8-13.

Safari, M., Harris, M., Deglon, D.A., The effect of energy input on the flotation of a platinum ore in a pilot-scale oscillating grid flotation cell, Minerals Engineering 110, 2017, pp. 69-74.

F., Testa, Safari, M.C., Deglon, D.A., Filho, L.L., 2017. Influence of agitation intensity on flotation rate of apatite particles. REM: R. Esc. Minas, Ouro Preto, 70(4), 2017, pp. 491-495.

Safari, M., Harris, M.C., Deglon, D.A., Filho, L.L., Testa, F., 2016. The effect of energy input on flotation kinetics. International Journal of Mineral Processing 156C, 2016, pp. 108-115.

Peer-Reviewed Conference Proceedings

Safari, M., Harris, M.C., Deglon, D.A., 2016. The effect of energy input on the flotation of a platinum ore in a pilot-scale oscillating grid flotation cell. In Proceedings of XXVIII International Mineral Processing Congress, Canada, Quebec, 11-15 September. ISBN: 978-1-926872-29-2.

Safari, M., Harris, M.C., Deglon, D.A., 2014. The effect of energy input on the flotation kinetics of galena in an oscillating grid flotation cell. In Proceedings of XXVII International Mineral Processing Congress, Santiago, 20-24 October. ISBN 978-956-9393-15-0.

Conference Papers

Safari, M., Harris, M.C., Deglon, D.A., 2015. The effect of energy input on the flotation kinetics. Flotation'15, Cape Town, South Africa, 1-9.

Safari, M., Harris, M.C., Deglon, D.A., 2015. A preliminary phenomenological model for determining the effect of energy input on the flotation rate. MinProc 2015, Cape Town, South Africa.

Safari, M., Harris, M.C., Deglon, D.A., 2013. The effect of energy input on the flotation kinetics of galena in an oscillating grid flotation cell. Flotation'13, Cape Town, South Africa, 1-10.

SYNOPSIS

Energy/power input in a flotation cell is an important parameter which, if optimised, can increase the flotation rate. The optimum energy/power input within a flotation cell is still a matter of conjecture and there is a need for a better understanding of the effect of energy input on flotation kinetics. This study investigates the effect of energy/power input on flotation kinetics in an oscillating grid flotation cell (OGC). The OGC decouples the processes of solid suspension and bubble generation as well as producing relatively isotropic and homogeneous turbulence with zero mean flow. Due to this, oscillating grids provide a potentially ideal environment for investigating the effects of energy input on flotation kinetics, which cannot be achieved in a mechanical flotation cell. The first objective of this thesis was to determine the effect of energy/power input on the flotation kinetics of sulphide minerals (galena, pyrite & pentlandite) and oxide minerals (apatite & hematite) in a laboratory scale oscillating grid flotation cell. The second objective was to compare the results from the laboratory OGC to comparative studies in the flotation literature and to fundamental models for particle-bubble contacting. The third objective was to determine whether the experimental results from the laboratory OGC are consistent with those from a pilot-scale OGC operating on a platinum ore.

Galena, pyrite, pentlandite (-150 μm), apatite (-650 μm) and hematite (-75 μm) were floated in the laboratory OGC at energy inputs from 0.1 to 5.0 W/kg, using 0.13, 0.24, 0.58 and 0.82 mm bubble sizes (d_{10}), and at three collector dosages. Platinum ore (-75 μm) was floated in the pilot-scale OGC at energy inputs from 0 to 2.5 W/kg, using 0.71 and 1.47 mm bubble sizes (d_{10}). The effect of energy input on flotation kinetics was interpreted through trends in experimental flotation rate constants, simulated flotation rate constants and attachment-detachment flotation rate constants. Here, simulated flotation rate constants were calculated using a literature fundamental model for flotation in turbulent systems. This model is based on suitable expressions for the collision frequency, collision efficiency, attachment efficiency and stability efficiency, Attachment-detachment flotation rate constants were calculated using a kinetic model which allows for the two separate processes of bubble-particle collision/attachment and detachment. This model is based on kinetic expressions using empirical correlations for the attachment and detachment rate constants.

Experimental flotation results show that the effect of energy input on the flotation rate is strongly dependent on the particle size and particle density and less dependent on bubble size and contact angle. Flotation rates generally increase with increasing particle size, decreasing bubble size and increasing contact angle, as is commonly found in the literature. Increasing energy input generally leads to an increase in the flotation rate for fine particles, an optimum flotation rate for intermediate particles and a decrease in the flotation rate for coarse particles. The optimum in the flotation rate for minerals with higher density is at a lower energy input than that for lower density minerals. The changes (increases/decreases) in the flotation rate with increasing energy input are very large for most of the conditions, indicating that this is an important parameter in flotation. Pilot scale results generally support the trends observed in the laboratory OGC. These findings are attributed to the effect of energy/power input on bubble-particle collection which is a balance between two competing effects, those of bubble-particle collision/attachment and those of bubble-particle detachment. Increasing energy input generally leads to significant increases in the flotation rate of fine particles, due to increased bubble-particle collision/attachment. Increasing energy input generally leads to an optimum flotation rate for intermediate particles, due to a combination of increased bubble-particle collision/attachment and detachment. For coarse particles, increasing energy input leads to significant increases in bubble-particle detachment. The relationship between the flotation rate and energy input is often described as $k \propto \varepsilon^N$, in the absence of significant bubble-particle detachment. The typical values of N are in the range of 0.44-0.75 for theoretical studies and 0.7-1 for experimental studies. The values of N found in the current study are in the range of 0.7-1, which suggests that bubble-particle collision/attachment has a stronger dependence on energy input than theory suggests.

Simulated flotation results for fine particles compare well to the experimental data in terms of both trends and magnitude. This suggest that the turbulent collision model used is appropriate for fine particles. For intermediate particles there are differences between the simulated flotation rate constants and the experimental data, primarily in terms of trends. For coarse particles there are very large differences between simulated flotation rate constants and the experimental data. This is attributed to under prediction of the collision frequency/efficiency and incorrect prediction of the stability efficiency. Here, the stability efficiency is considered to be under predicted at low energy inputs and over predicted at high energy inputs. This suggests that the stability efficiency has a much stronger dependence on energy input than theory suggests. Attachment-detachment results show that the attachment rate constant has a stronger dependence on energy input than theory suggest, supporting finding from the experimental results and simulated results for coarser particles. In addition, the detachment rate constant has a much stronger dependence on energy input than theory suggests, supporting findings from both the experimental and simulated results.

Based on the objectives of this study and literature reviewed, the following hypotheses were made at the outset 1) Increasing energy/power input will increase the rate of flotation of fine particles but will result in an optimum for intermediate and coarse particles. The position of this optimum will depend

on the particle density, bubble size and contact angle. 2) Fundamental models based on the RMS turbulent velocity will be appropriate for describing flotation kinetics as turbulence in the oscillating grid cell is relatively homogeneous and isotropic and 3) Trends in flotation results for a laboratory and pilot-scale oscillating grid flotation cell will be comparable as the distribution of turbulence in OGCs at equivalent specific power inputs is scale independent. Hypothesis 1 was found to be valid for both fine and intermediate particles, but for coarse particles increasing energy input resulted in sharp decreases in the flotation rate. In addition, the increase in the flotation rate with increasing energy input was found to be more dependent on the particle size and particle density than the bubble size and contact angle. Hypothesis 2 was found to be valid for fine particles but not for intermediate or coarse particles. Here, it was found that the processes of bubble-particle collision/attachment and detachment have a stronger dependence on energy input than theory suggests. Hypothesis 3 was supported by general trends in results for the laboratory and pilot-scale oscillating grid flotation cells, but was not convincingly demonstrated.

TABLE OF CONTENTS **Page**

ACKNOWLEDGMENTS II
DECLARATION III
CERTIFICATION BY SUPERVISOR IV
LIST OF PUBLICATIONS V
SYNOPSIS VI
TABLE OF CONTENTS IX
LIST OF FIGURES XII
LIST OF TABLES XV
NOMENCLATURE XVI

CHAPTER 1: INTRODUCTION 1
1.1. BACKGROUND 1
1.2. RESEARCH OBJECTIVES 2
1.3. HYPOTHESES 3
1.4. RESEARCH SCOPE AND LIMITATIONS 3
1.5. THESIS OUTLINE 4

CHAPTER 2: LITERATURE REVIEW 5
2.1. FLOTATION CELLS 5
2.1.1. Mechanical Flotation Cells 6
2.1.2. Column Flotation Cells 7
2.1.3. Novel Flotation Cells 8
2.1.3.1. Reactor/Separator Cells 8
2.1.3.2. Agitated Columns 9
2.1.3.3. Other Novel Cells 10
2.2. OSCILLATING GRIDS 12
2.2.1. Background 13
2.2.2. Turbulence Fundamentals 13
2.2.2.1. Turbulent Flow 13
2.2.2.2. The Turbulent Energy Spectrum 14
2.2.2.3. Macro and Micro Scales of Turbulence 15
2.2.3. Oscillating Grid Turbulence 15
2.2.3.1. Single/Double Grids 16
2.2.3.2. Multiple Grids 18
2.2.3.3. Deviations from Ideal Hydrodynamic Behavior 19
2.2.4. Mean Energy Input in Oscillating Grid Agitation 19
2.3. EFFECT OF ENERGY INPUT ON FLOTATION KINETICS 21
2.3.1. Theoretical Findings 21
2.3.1.1. Particle - Bubble Collision Mechanism 22
2.3.1.2. Particle - Bubble Collision Frequency 23
2.3.1.3. Particle - Bubble Collection Efficiency 25
2.3.1.3.1. Particle - Bubble Collision Efficiency 25
2.3.1.3.2. Particle - Bubble Attachment Efficiency 28

2.3.1.3.3. Particle - Bubble Stability Efficiency 29
2.3.1.4. Summary of Theoretical Findings 32
2.3.1.4.1. Effect of Particle Size 32
2.3.1.4.2. Effect of Bubble Size 32
2.3.1.4.3. Effect of Contact Angle 33
2.3.1.4.4. Effect of Energy Input 34
2.3.2. Experimental Findings 34
2.3.2.1. Effect of Particle Size 34
2.3.2.2. Effect of Bubble Size 35
2.3.2.3. Effect of Contact Angle 36
2.3.2.4. Effect of Energy Input 37
2.3.2.4.1. Stirred Cells 37
2.3.2.4.2. Oscillatory Baffled Column 41
2.3.2.4.3. Oscillating Grid Cell 42
2.3.2.5. Summary of Experimental Findings 44
2.4. FLOTATION MODELLING 45
2.4.1. Fundamental Models 45
2.4.2. Kinetic Models 47
2.4.3. Phenomenological Models 48
2.4.4. Empirical Models 50
2.5. SUMMARY OF LITERATURE REVIEW 51

CHAPTER 3: MATERIALS AND METHODS 52

3.1. LABORATORY OGC 52
3.1.1. Aeration System 53
3.1.2. Recycle System 54
3.1.3. Froth Removal System 54
3.1.4. Energy Input Measurements 54
3.1.5. Bubble Size Measurements 56
3.1.6. Contact Angle Measurements 56
3.1.7. Materials and Reagents 59
3.1.8. Experimental Conditions and Procedures 62
3.1.9. Experimental Program 63
3.2. PILOT SCALE OGC 64
3.2.1. Aeration System 65
3.2.2. Recycle System 65
3.2.3. Froth Removal System 66
3.2.4. Energy Input Measurements 66
3.2.5. Bubble Size Measurement 66
3.2.6. Materials and Reagents 68
3.2.7. Experimental Conditions and Procedures 68
3.2.8. Experimental Program 69
3.3. ERROR ANALYSIS 70

CHAPTER 4: RESULTS AND DISCUSSION 72

4.1. LABORATORY OSCILLATING GRID CELL 72
4.1.1. The Effect of Principal Parameters on Flotation Kinetics 73

4.1.1.1. Effect of Particle Size 73
4.1.1.2. Effect of Bubble Size 74
4.1.1.3. Effect of Contact Angle 76
4.1.2. The Effect of Energy Input on Flotation Kinetics 78
4.1.2.1. Sulphide Minerals 78
4.1.2.1.1. Fine Particles 78
4.1.2.1.2. Intermediate Particles 80
4.1.2.1.3. Coarse Particles 81
4.1.2.2. Oxide Minerals 83
4.1.2.2.1. Apatite 83
4.1.2.2.2. Hematite 84
4.1.3. Relative Effect of Energy Input on Flotation Kinetics 84
4.1.4. Simulated Effect of Energy Input on Flotation Kinetics 86
4.1.4.1. Flotation Rate Constant Calculations 87
4.1.4.2. The Simulated Effect of Principal Parameters on Flotation Kinetics 87
4.1.4.2.1. Effect of Particle Size 87
4.1.4.2.2. Effect of Bubble Size 89
4.1.4.3. The Simulated Effect of Energy Input on Flotation Kinetics 91
4.1.4.3.1. Fine Particles 91
4.1.4.3.2. Intermediate Particles 92
4.1.4.3.3. Coarse Particles 94
4.2. Pilot Scale Oscillating Grid Cell 96
4.2.1. The Effect of Energy Input on Flotation Kinetics 96
4.3. Flotation Modelling 98
4.3.1. The Attachment-Detachment Kinetic Model 98
4.3.1.1. Model Development 98
4.3.1.2. Model Testing 100
4.3.2. Empirical Correlations for the Rate Constants 102
4.3.2.1. Attachment Rate Constant 103
4.3.2.2. Detachment Rate Constant 103
4.3.3. The Flotation Rate Constant 104
4.4. Summary of the Effect of Energy Input on Flotation Kinetics 106

CHAPTER 5: CONCLUSIONS AND RECOMMENDATIONS 108

5.1. The Effect of Principal Parameters on Flotation Kinetics 109
5.2. The Effect of Energy Input on Flotation Kinetics 109
5.3. Recommendations for Future Work 111

REFERENCES 113

APPENDICES 126

A.1: Galena Flotation Data 126
A.2: Pyrite Flotation Data 127
A.3: Pentlandite Flotation Data 129
A.4: Apatite Flotation Data 131
A.5: Hematite Flotation Data 131

LIST OF FIGURES Page

Figure 2.1: Schematic of a modern mechanical flotation cell (TankCell®, Outotec, 2016) 6

Figure 2.2: Schematic of a modern column flotation cell (Metso, 2015) 7

Figure 2.3: Schematic of a Jameson flotation cell (Xtrata Jameson Cell) 9

Figure 2.4: Schematic of a fluidised bed flotation cell (Eriez HydroFloat Separator, 2014) 11

Figure 2.5: Staged Flotation Reactor (Courtesy Woodgrove Technologies Inc., 2015) 12

Figure 2.6: Schematic representation of a turbulent energy spectrum (Deglon, 1998) 14

Figure 2.7: Typical diagram of oscillating grid set-ups and oscillating grid turbulence (adapted) 16

Figure 2.8: Diagram of single and double oscillating grids (adapted from Villermaux et al., 1995) 17

Figure 2.9: (a) Distribution of TKE generated by a single oscillating grid (5 Hz and 30 mm) (Orlins and Gulliver, 2003), (b) Determination of turbulence in a two grid system (Janzen, 2006) 17

Figure 2.10 a,b: RMS turbulent velocity in OGC and fluid velocity in stirred cell (adapted from Bache & Rasool 2001) 18

Figure 2.11: Graph showing u'2 variation with tank height, at 2 Hz and 18 mm amplitude (Bache and Rasool, 2001) 19

Figure 2.12: Particle colliding with a bubble at its equator 26

Figure 2.13: Flotation rate constant versus particle size for the flotation of quartz (2.5 ppm CTAB) in a stirred cell, at three agitation rates and bubble sizes (adapted from Ahmed and Jameson, 1985) 39

Figure 2.14: Flotation rate constant versus energy input for the flotation of quartz -100 µm in a stirred cell, for 0.13 mm and 0.82 mm bubbles (adapted from Deglon, 1998) 40

Figure 2.15: (a) Effect of density on flotation rate constant (• quartz : 2.65 g/cm3, □ chalcopyrite :4.1 g/cm3, ... 40

Figure 2.16: Flotation rate constant versus energy input for the flotation of moderately hydrophobic quartz in an oscillatory baffled column, for four particle size classes (adapted from Anderson, 2008) 42

Figure 2.17: Flotation rate constant versus energy input for the flotation of -48 +26 µm quartz in an oscillating grid cell, for three bubble sizes (adapted from Changunda et al., 2008) 43

Figure 2.18: Flotation rate constant versus energy input for the flotation of quartz in an oscillating grid cell, for 0.24 mm bubbles and three particle size classes (adapted from Changunda et al) 43

Figure 2.19: Flotation rate constant versus power intensity for all bubble and particle sizes (Massey et al., 2012) 44

Figure 3.1: The laboratory oscillating grid flotation cell 52

Figure 3.2: Flow diagram of OGC aeration system..... 53

Figure 3.3: Schematic of sintered glass discs placement with detail of rotation..... 54

Figure 3.4: OGC froth removal system (galena concentrates)..... 54

Figure 3.5: Energy input measurement and calibration testing with galena sample 55

Figure 3.6: Schematic of Washburn technique, as described by Washburn 1921..... 57

Figure 3.7: Capillary penetration method for galena contact angle measurement using KRUSS Force Tensiometer 57

Figure 3.8: Surface tension measurements using KRUSS Force Tensiometer (K12 and K100) 58

Figure 3.9: Wetting kinetics for galena powder in water (red line) and hexane (blue line) (53˚)..... 58

Figure 3.10: Pentlandite sample preparation 59

Figure 3.11: Rotary dividers used to randomly split mineral particles 59

Figure 3.12: Malvern Mastersizer™..... 60

Figure 3.13: Particle size distribution (PSD) of sulphide and oxide minerals..... 61

Figure 3.14: Vertical sections of sulphide minerals for mineralogical study using QEMSCAN 61

Figure 3.15: QEMSCAN results for galena and pyrite feed samples 62

Figure 3.16: Pilot scale oscillating grid flotation cell..... 64

Figure 3.17: CPT porous metal and CPT cavitation tube..... 65

Figure 3.18: Pilot-scale oscillating grid flotation cell during operation at the Baobab Concentrator .. 66

Figure 3.19: Anglo Platinum Bubble Sizer used for pilot scale OGC..... 67

Figure 3.20: Bubble size distribution in pilot scale OGC using Anglo Platinum Bubble Sizer..... 67

Figure 3.21: PGM samples preparation..... 68

Figure 4.1: Flotation rate constant (min-1) versus particle size (µm) for three bubble sizes and high collector dosage at low energy input (0.5 W/kg), A: Galena, B: Pyrite, C: Pentlandite 73

Figure 4.2: Flotation rate constant (min-1) versus bubble size (mm) for the flotation of all particle sizes and all collector dosages at low energy input (0.5 W/kg), A: Galena, B: Pyrite, C: Pentlandite .. 75

Figure 4.3: Flotation rate constant (min-1) versus contact angle for the flotation of all particle sizes and all bubble sizes at low energy input (0.5 W/kg), A: Galena, B: Pyrite, C: Pentlandite..... 77

Figure 4.4: Flotation rate constant (min-1) versus energy input (W/kg) for the flotation of fine particles (-19 µm), all bubble sizes and collector dosages, A: Galena, B: Pyrite, C: Pentlandite 79

Figure 4.5: Flotation rate constant (min-1) versus energy input (W/kg) input for the flotation of intermediate particles (+19-38 µm), all bubble sizes and collector dosages, A: Galena, B: Pyrite, ... 80

Figure 4.6: Flotation rate constant (min-1) versus energy input (W/kg) for the flotation of coarse particles (+38-150 µm), all bubble sizes and collector dosages, A: Galena, B: Pyrite, C: Pentlandite .. 82

Figure 4.7: Flotation rate constant (min-1) versus energy input (W/kg) for three particle sizes and two collector dosages..... 83

Figure 4.8: Flotation rate constant (min-1) versus energy input (W/kg) for two particle sizes and three bubble sizes 84

Figure 4.9: Percentage change in the flotation rate constants, relative to the rate at low energy input (0.5 W/kg), versus energy input for all particle sizes, bubble sizes and moderate collector dosage, sorted for all minerals based on their density, A: Ga, B: He, C: Py, D: Pen, E: Ap 86

Figure 4.10: Flotation rate constant (min-1) (k), collision efficiency (Ec), attachment efficiency (Ea), stability efficiency (Es) versus particle size (µm) for three bubble sizes and high collector dosage (θ=90) at low energy input (0.5 W/kg), A: Galena, B: Pyrite, C: Pentlandite..... 88

Figure 4.11: Flotation rate constant (min-1) (k), collision efficiency (Ec), attachment efficiency (Ea), stability efficiency (Es) versus bubble size (mm) for three particle size fractions (µm) and high collector dosage (θ=90) at low energy input (0.5 W/kg), A: Galena, B: Pyrite, C: Pentlandite..... 90

Figure 4.12: Flotation rate constant (min-1) (k), collision efficiency (Ec), attachment efficiency (Ea), stability efficiency (Es) versus energy input (W/kg) for the flotation of fine particles (-19 µm), all bubble sizes and high collector dosage (θ=90), A: Galena, B: Pyrite, C: Pentlandite..... 92

Figure 4.13: Flotation rate constant (min-1) (k), collision efficiency (Ec), attachment efficiency (Ea), stability efficiency (Es) versus energy input (W/kg) for the flotation of intermediate particles (+19 -38 µm), all bubble sizes and high collector dosage (θ=90), A: Galena, B: Pyrite, C: Pen..... 93

Figure 4.14: Flotation rate constant (min-1) (k), collision efficiency (Ec), attachment efficiency (Ea), stability efficiency (Es) versus energy input (W/kg) for the flotation of coarse particles (+38-150 µm), all bubble sizes and high collector dosage (θ=90), A: Galena, B: Pyrite, C: Pentlandite..... 95

Figure 4.15: Normalized flotation rate constant versus energy input for the flotation of PGM minerals with three particle size fractions, two bubble sizes and plant collector dosage, A: Primary cleaner tail, B: Secondary rougher feed 97

Figure 4.16: Model predicted versus experimental flotation rate constant (-ln(k)) for full experimental data set 100

Figure 4.17: Experimental (symbols) and predicted (dash lines) flotation rate constant (min-1) versus energy input (W/kg) for all the pyrite experimental data 101

Figure 4.18: Model predicted versus experimental flotation rate constant (min-1)..... 102

Figure 4.19: Variation of predicted flotation rate constants (min-1) versus particle size (µm) and energy input (W/kg) for the pyrite sample with high collector dosage (Contact angle = 90°) and 0.1 mm bubble size 105

Figure 4.20: Variation of predicted flotation rate constants (min-1) versus particle size (µm) and energy input (W/kg) for the pyrite sample with high collector dosage (90°) , 0.9 mm bubble size .. 106

LIST OF TABLES Page

Table 2.1: Scales of microturbulence relevant to flotation (Massey, 2011) 15
Table 2.2: Estimation of energy input in oscillating grid cells (summary of main equations) 20
Table 2.3: Collision mechanism in turbulence (Anderson, 2008)..... 22
Table 2.4: Values of the parameters B and n of Equation (2.31) (Yoon and Luttrell, 1989) 27
Table 2.5: Experimental studies on the effect of energy input on flotation kinetics..... 37
Table 2.6: Values for the constant N in the relationship k $\propto$ εN 51

Table 3.1: Physical specifications for the laboratory scale oscillating grid flotation cell 53
Table 3.2: Sintered glass frit pore sizes and corresponding mean bubbles sizes produced (laboratory scale OGC) 56
Table 3.3: Specific gravity, specific surface area and bulk elemental composition of mineral samples..... 60
Table 3.4: Particle size analysis of galena feed sample, as given by the Malvern Mastersizer 60
Table 3.5: Experimental conditions..... 63
Table 3.6: Summary of flotation tests..... 64
Table 3.7: Physical specifications for the pilot scale oscillating grid flotation cell..... 65
Table 3.8: Mean bubbles sizes produced by CPT Porous Metal and Cavitation Tube spargers (pilot scale OGC)..... 68
Table 3.9: Experimental conditions..... 69
Table 3.10: Table of summarized experiments conducted in the pilot scale oscillating grid cell..... 69
Table 3.11: Experimental programme for the pilot scale oscillating grid cell..... 70

Table 4.1: Empirical exponents for all experimental data 99
Table 4.2: Comparison of empirical exponents to the flotation literature..... 103

Table A.1: Flotation rates for Galena particles floated with 0.13 mm bubbles..... 126
Table A.2: Flotation rates for Galena particles floated with 0.58 mm bubbles..... 126
Table A.3: Flotation rates for Galena particles floated with 0.82 mm bubbles..... 127
Table A.4: Flotation rates for Pyrite particles floated with 0.13 mm bubbles..... 127
Table A.5: Flotation rates for Pyrite particles floated with 0.58 mm bubbles..... 128
Table A.6: Flotation rates for Pyrite particles floated with 0.82 mm bubbles..... 128
Table A.7: Flotation rates for Pentlandite particles floated with 0.13 mm bubbles..... 129
Table A.8: Flotation rates for Pentlandite particles floated with 0.58 mm bubbles..... 129
Table A.9: Flotation rates for Pentlandite particles floated with 0.82 mm bubbles..... 130
Table A.10: Flotation rates for Apatite particles floated with 0.58 mm bubbles..... 131
Table A.11: Flotation rates for Hematite particles floated at moderate collector dosage..... 131

NOMENCLATURE

A	Tank cross sectional area (m^2)
Bo	Bond number (Dimensionless)
Bo_m	Modified Bond number (Dimensionless)
C	Concentration of particles in the pulp - volumetric concentration (kgm^{-3})
C_o	Initial concentration of particles in the pulp (kgm^{-3})
C_d	Drag coefficient (Dimensionless)
C_s	Concentration of particles on bubble surfaces (kgm^{-2})
d_{10}	Arithmetic mean diameter (m)
d_{32}	Sauter mean diameter (d_s) (m)
d_{80}	80 Percentile particle size (m)
d_b	Mean bubble size (m)
d_c	Critical diameter (m)
d_p	Mean particle size (m)
E_a	Efficiency of attachment (Fractional)
E_c	Efficiency of collision (Fractional)
E_{coll}	Efficiency of collection (Fractional)
E_d	Efficiency of detachment (Fractional)
$E_{k\text{-}A}$	Kinetic energy of attachment (J)
$E_{k\text{-}D}$	Kinetic energy of detachment (J)
E_1	Surface energy barrier (J)
E_S	Efficiency of stability (Fractional)
F	Force (N)
F_{det}	Force of detachment (N)
f	Oscillating frequency (s^{-1})
g	Gravitational acceleration (m^2s^{-2})
G	Shear rate of a fluid (s^{-1})
G_{fr}	Volumetric flowrate (m^3s^{-1})
H	Tank height (m)
J_g	Superficial gas velocity (ms^{-1})
k	Flotation rate constant (s^{-1})

k_c	Flotation rate constant in the collection zone (s^{-1})
k_a	Attachment rate constant (s^{-1})
k_d	Detachment rate constant (s^{-1})
L	Macro length scale (m)
M	Grid mesh space (m)
m_b	Mass of bubble (kg)
m_L	Mass of the fluid being agitated (kg)
m_p	Mass of particle (kg)
n	Number of grids
N_b	Number of bubbles per unit volume (m^{-3})
N_p	Number of particles per unit volume (m^{-3})
P	Power input (W)
Q	Gas flowrate (m^3s^{-1})
r	Eddies radii (m)
R	Recovery (fractional)
Re	Reynolds number (Dimensionless)
S	Stroke length (m)
S	Specific bubble surface area (m^2m^{-3})
S_A	Solids area of the grid (%)
S_b	Bubble surface area flux (s^{-1})
St	Stokes number (Dimensionless)
TKE	Turbulent kinetic energy of turbulence (Jkg^{-1}) or (m^2s^{-2})
t	Time (s)
t_{ind}	Induction time (s)
u	Mean velocity (ms^{-1})
u_b	Bubble rise velocity (ms^{-1})
u'	Fluctuating velocity (ms^{-1})
u'_{eff}	Effective root mean square (RMS) turbulent velocity (ms^{-1})
V	Tank volume (m^3)
V_o	Initial tank volume (m^3)
w	Wave number (m^{-1})
W_A	Work of adhesion (J)

x_e	Entrainment fraction (Fractional)
x_g	Gas flow fraction (Fractional)
Y	Displacement in oscillating system (m)
$\dot{Y}$	Velocity in oscillating system (ms^{-1})
$\ddot{Y}$	Acceleration in oscillating system (m^3s^{-2})
Z_{pb}	Number of particle-bubble collisions per unit volume-time ($m^{-3}s^{-1}$)

Greek Letters

γ	Interfacial tension (Nm^{-1})
ε	Specific energy input/turbulent energy dissipation rate (Wkg^{-1} / kWm^{-3})
$\bar{\varepsilon}$	Average energy input in bulk tank (Wkg^{-1})
η	Kolmogorov microscale length (m)
ω	Kolmogorov microscale velocity ($rad.s^{-1}$)
θ	Static contact angle (°)
θ_a	Adhesion angle (°)
θ_t	Tangency angle (°)
λ	Eulerian micro length scale or turbulent eddy scale (m)
Λ	Eulerian macro length scale or macro scale of turbulence (m)
«	Viscosity (Pa)
ν	Kinematic viscosity (m^2s^{-1})
ρ_f	Fluid density (kgm^{-3})
ρ_l	Liquid density (kgm^{-3})
ρ_s	Solid/particle density (kgm^{-3})
σ	Surface tension (Nm^{-1})
τ	Lag time (s)
τ_g	Gas residence time (s)
τ_{gs}	Gas residence time based on surface area (s)
τ_p	Pulp residence time (s)

Subscripts

a	Attachment
b	Bubble
c	Collision
d	Detachment
f	Fluid
i	Size fraction/size class
l	Liquid
p	Particles
s	Stability

Abbreviations

AMIRA	Australian Mining Industry Research Association
CMR	Centre for Mineral Research
OK	Outokumpu® (flotation cell manufacturer)
P9	Project 9 - Different Modules (AMIRA project numbering system)
PGM	Platinum Group Metals
PSD	Particle Size Distribution
RPM	Revolutions per Minute
RTD	Residence Time Distribution
SD	Standard Deviation
UCT	University of Cape Town

Parameters

c, n, m	Empirical exponents and constants

#All the units specified in the nomenclature are applicable in this thesis unless otherwise indicated in the text, tables or figures.

Chapter 1: Introduction

Flotation is a separation method used for the beneficiation of a considerable portion of the world's mineral ores. It is responsible for the beneficiation of in excess of two billion tons of over one hundred different mineral species annually (Nguyen and Schulze, 2004). The process of flotation selectively separates minerals by exploiting differences in the physical and chemical properties of the various species. The addition of flotation reagents selectively renders the surfaces of mineral particles either hydrophobic or hydrophilic. The hydrophobic particles become attached to gas bubbles and are carried upwards through the slurry to a froth layer that forms at the top of the flotation cell. Due to the extensive use industrially, any inefficiencies in flotation translate into an enormous loss of revenue and an unnecessary waste of these reserves. These losses are expected to compound in the coming decades as, due to the preferential processing of high quality ores, mining companies are forced to treat more and more complex and finely disseminated ore bodies. As lower grade, finely disseminated ore bodies are mined flotation faces rising challenges. There is therefore an increased need to understand flotation in order to increase the efficiency of this process. Global resource companies are currently operating under very challenging economic and regulatory conditions. Many mineral producers also face pressure to reduce their energy consumption for both economic and environmental reasons. These pressures may become key drivers of technological change in and of themselves. These factors represent significant challenges to the industry and create a climate supportive of technological innovation.

1.1. Background

Energy/power input in a flotation cell is an important parameter which, if optimised, can increase the flotation rate. The optimum energy input within a flotation cell is still a matter of conjecture and there is a need to better understand the effect of energy/power input on flotation kinetics and the sub-processes of flotation. For successful flotation to occur, three processes must take place i.e. solids suspension, gas dispersion and particle-bubble contacting. Energy/power input is known to play an important role in each process but in a mechanical flotation cell, energy input has an effect on all of these processes simultaneously. This makes it extremely difficult to investigate and optimise energy input for each of these sub-processes individually.

There is a considerable body of experimental and theoretical evidence to suggest that energy input plays an important role in flotation kinetics (improving particle-bubble contacting), particularly in the finer particle size where flotation efficiency is poor (Deglon, 2005). A number of excellent studies into the effect of energy on flotation kinetics have been carried out in impeller stirred cells (Ahmed and Jameson, 1985; Deglon, 2002; Pyke et al., 2003; Sherrell, 2004; Newell and Grano, 2006). These cells have a number of limitations, such as the influence of the impeller on particle suspension and bubble break-up (Grau and Heiskanen, 2005). In addition, turbulence is highly inhomogeneous, being orders of magnitude higher near the impeller than elsewhere in the cell (Deglon, 1998; Koh and Schwarz, 2003; Schubert, 1999, 2008). This complicates the investigation of the effect of energy input on flotation kinetics as particle-bubble contacting is considered to be driven by turbulence, with many flotation theories/models based on the assumption of homogeneous, isotropic turbulence.

Anderson developed a novel oscillating baffled cell (OBC) (Anderson et al., 2009). The OBC decoupled the processes of solid suspension, bubble generation and energy input. Anderson investigated the effects of energy input on the flotation kinetics of -100 µm quartz particles. This study was limited to very low energy inputs of up to 1 W/kg. Results showed that the unique bulk oscillatory motion of the fluid in the cell had a strong effect on flotation kinetics at very low energy inputs. However as a research tool it is not ideal due to the complex oscillatory nature of the flow. A novel oscillating grid cell was developed by Changunda 2009 and Massey 2011. The OGC decoupled the processes of solid suspension and bubble generation as well as producing relatively isotropic and homogeneous turbulence with zero mean flow. Due to this, oscillating grids provide a potentially ideal environment for investigating the effects of energy input on flotation kinetics, which cannot be achieved in mechanical flotation cell. Results showed that the effect of energy input on flotation kinetics is strongly dependent on both particle and bubble size. These studies were limited to the flotation of quartz.

This study investigates the effect of energy/power input on the flotation kinetics of sulphide minerals (galena, pyrite & pentlandite) and oxide minerals (apatite & hematite) in a laboratory scale OGC and the flotation of a platinum ore in a pilot-scale OGC.

1.2. Research objectives

The objective of this study was to investigate the effect of energy/power input on flotation kinetics in an oscillating grid cell. The study was composed of three parts which were carried out to achieve the following objectives:

1. To determine the effect of energy/power input on the flotation kinetics of sulphide minerals (galena, pyrite & pentlandite) and oxide minerals (apatite & hematite) in a laboratory scale oscillating grid flotation cell.

2. To compare the results from the laboratory OGC to comparative studies in the flotation literature and to fundamental models for particle-bubble contacting.

3. To determine whether the experimental results from the laboratory OGC are consistent with those from a pilot scale OGC operating on a real platinum ore.

1.3. Hypotheses

Based on the objectives of this study and literature reviewed, the following hypotheses are made:

1. Increasing energy/power input will increase the rate of flotation of fine particles but will result in an optimum for intermediate and coarse particles. The position of this optimum will depend on the particle density, bubble size and contact angle.

2. Fundamental models based on the RMS turbulent velocity will be appropriate for describing flotation kinetics as turbulence in the oscillating grid cell is relatively homogeneous and isotropic.

3. Trends in flotation results for a laboratory and pilot-scale oscillating grid flotation cell will be comparable as the distribution of turbulence in OGCs at equivalent specific power inputs is scale independent.

These hypotheses are based primarily on the trends observed in flotation data from both experimental and theoretical studies for impeller stirred cells. However, as indicated previously, the impeller influences processes such as bubble break-up and turbulence in these cells is highly inhomogeneous, being orders of magnitude higher near the impeller than elsewhere in the cell. This has led to some contention in the flotation literature. For example, some authors argue that the process of particle-bubble collision/attachment is dominated by turbulence in the impeller zone whereas others argue that detachment dominates in this region. This study presents a comprehensive set of flotation results, from a cell with relatively homogeneous turbulence, and should clarify whether the hypotheses derived from the flotation literature are consistent.

1.4. Research scope and limitations

The scope of the research is limited to the effects of energy/power input, particle size, bubble size, particle hydrophobicity and mineral type (galena, pyrite, pentlandite, apatite and hematite) on the flotation rate constant. Flotation experiments are limited to the pulp phase. This study excludes the effect of other factors such as pulp chemistry and froth effects on the flotation rate.

1.5. Thesis Outline

Chapter 2 presents a review of the flotation literature relevant to this study. Firstly, the current ranges of flotation cell technologies in industry and novel flotation cells are highlighted in this chapter. Secondly, the characteristics of oscillating grid turbulence and turbulence fundamentals are reviewed with specific emphasis on the hydrodynamic and energy/power characteristics of the cell. Thirdly, the existing body of knowledge on the effect of energy input on flotation kinetics is reviewed from both a theoretical and experimental point of view. Chapter 2 ends by reviewing flotation models. Chapter 3 describes the experimental apparatus, materials and methods used in this study in both the laboratory and pilot scale OGC. Chapter 4 presents and discusses the results obtained from the flotation experiments performed in the laboratory and pilot scale OGC. The focus of this chapter is to present and discuss the effect of energy input on flotation kinetics. Furthermore, a kinetic model for determining the effect of energy input on the flotation rate constant is presented. Finally Chapter 5 presents conclusions and recommendations for future work.

Chapter 2: Literature Review

In the past two decades a considerable amount of research has been undertaken in flotation, especially in the three major areas of flotation reagent, flotation cell and flotation fundamentals research. Research into flotation reagents has focused on the development of new reagents and an understanding of the role of these reagents in the subprocesses of flotation. Research into flotation cells has focused on the development of new flotation cell technologies from a better understanding of the impact of cell hydrodynamics on the subprocesses of flotation. Research into flotation fundamentals impacts on both the aforementioned areas of research and has focused on improving flotation efficiency through an understanding of the fundamental mechanisms of the subprocesses of flotation. The research presented in this thesis aims to gain a greater understanding of the influence of energy/power input on flotation kinetics, though fundamental mechanisms are explored where appropriate. In addition, the effects of physical factors (particle size, bubble size and particle density) and chemical factors (collector dosage - contact angle) which have a significant influence on flotation kinetics are investigated in this study.

The following chapter reviews the literature relevant to flotation subprocesses, oscillating grids and modelling, for both theoretical and experimental studies. In order to set the scene for this study the various types of flotation cells used in industrial applications and novel flotation cells, are reviewed in Section 2.1. The characteristics of oscillating grid turbulence and turbulence fundamentals are reviewed in Section 2.2. Section 2.3 provides a review of the theoretical and experimental findings of the effect of energy input on flotation kinetics. The fundamental theories of flotation are reviewed in Section 2.3.1, along with models which describe them. There have been numerous experimental studies on flotation kinetics, which are reviewed in Section 2.3.2 with a focus on the effects of particle size, bubble size, contact angle and energy input on flotation kinetics. This chapter ends of by reviewing flotation models such as fundamental, kinetics, integrated (fundamental-kinetics) and empirical models (Section 2.4) and reviewing the purpose of this research (Section 2.5).

2.1. Flotation Cells

Since the inception of froth flotation in 1905, numerous flotation machine designs have been proposed, particularly in the last 50 years. Traditionally, flotation has been performed in mechanically

agitated tanks and the minerals processing industry has been particularly slow in its uptake of new cell technologies. The primary reason for this is that the development and testing of new flotation cell designs is costly and inherently risky to any mining company. Plant trials of large prototype cells are often costly, both in installation costs and in the potentially large losses of valuable mineral during testing. Despite this, many new flotation technologies have found increasing application in industry. The most common types of flotation cells used in industry are mechanical cells and, to a lesser extent, column cells. In addition to these cells there are numerous novel cells which have been developed. This section will outline some of the different cells used, and briefly discuss the benefits and limitations of each.

2.1.1. Mechanical Flotation Cells

Mechanical or conventional flotation cells are the most commonly used cells in industry, and are considered the industry standard. They utilise an impeller, consiting of a rotor and stator, for the functions of particle suspension, bubble break-up and particle-bubble contacting. Many different cell designs have been used over the years but the most notable trend in design has been in the cell size. Conventional cell size has increased exponentially, particularly since the advent of rounded tank cells in the late 1980's. The volume of such cells may vary from 1 L for laboratory use, to up to 600 m^3 in industry. Recent developments in mechanical cell design have typically centred on the use of larger cells, a trend which is driven by the economic benefits of using larger equipment. The metallurgical effects of using large cells are not fully understood, however there is evidence to suggest that cell size may be increased without loss of metallurgical performance (Yianatos et al., 2008). The typical energy input used in industrial mechanical cells ranges from 0.6-3 kW/m^3 (Deglon et al., 2000; Lelinski et al., 2011), although energy levels of up to 12 kW/m^3 have been used in some fine particle applications. A schematic of a modern mechanical flotation cell is depicted in Figure 2.1.

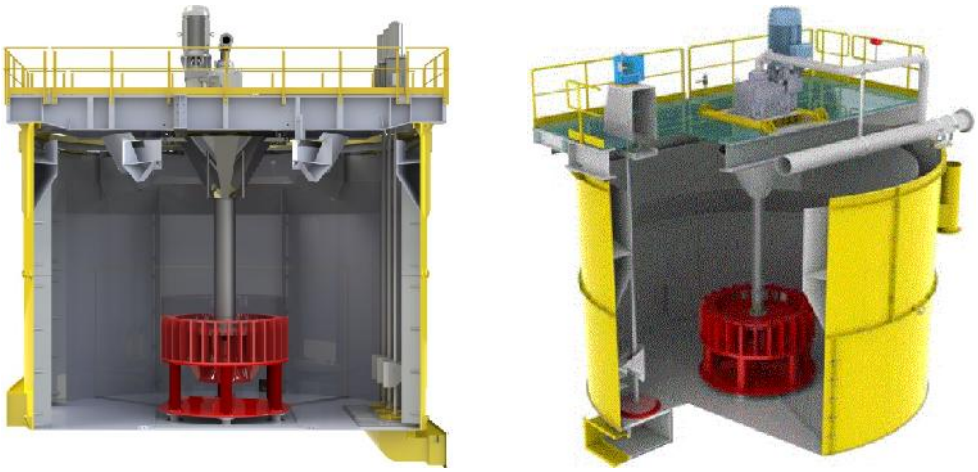

Figure 2.1: Schematic of a modern mechanical flotation cell (TankCell®, Outotec, 2016)

Mechanical cells have an inherently inhomogeneous distribution of energy input through the cell, with high energy input found near the impeller and much lower levels in the bulk of the cell (Deglon, 1998;

Koh and Schwarz, 2003; Newell and Grano, 2007; Schubert, 2008). The fact that the processes of particle suspension, bubble break-up and energy generation are all interdependent makes it difficult or impossible to optimise the conditions for flotation (Schubert, 1999; 2008). Despite these weaknesses, the robustness of the design has meant that mechanical cells overwhelmingly dominate in industrial applications, despite competition from several other cell technologies. Numerous studies have however shown that these cells may have considerable weaknesses in the flotation of fine particles since the flotation rate decreases significantly with decreasing particle size (Ahmed and Jameson, 1985; Deglon, 1998; Feng and Aldrich, 1999; Pyke, 2004). It is speculated that these problems are likely to become more acute in future, with mining companies seeking to recover ever finer and more complex ore types, thus providing greater scope for the application of novel cell technologies.

2.1.2. Column Flotation Cells

Column flotation cells are used industrially, though to a lesser extent than mechanical cells. One of the first alternative cell designs to be developed was the column flotation cell which was first successfully trialled in the late 1960's (Wheeler, 1988). This design was based on the chemical engineering concept of a counter-current mass transfer system and was the first attempt to decouple the subprocesses of solid suspension, gas dispersion and particle-bubble contacting. Column cells operate by introducing ore near the top of the column and sparging air from the bottom. This produces a counter-current flow in the collection zone, which promotes particle-bubble contacting. Industrially these cells are operated with deep froths of approximately 1 m, which have wash water added, aiding in the removal of entrained fine particles (Bergh and Yianatos, 2003). A schematic of a modern column flotation cell is shown in Figure 2.2.

Figure 2.2: Schematic of a modern column flotation cell (Metso, 2015)

The advantages of these devices include low installation and operating costs as well as the ability to operate at high froth depths, thus allowing significantly higher grade concentrates to be produced compared to a conventional cell. The technology was slow to gain favour industrially and it was not

until 1981 that the first commercial flotation column was installed at Les Mines Gaspe (Quebec, Canada) for Molybdenum cleaning. It was found that one stage of column flotation was able to replace seven stages of conventional cell cleaning (Finch and Dobby, 1990). Since then, the technology has gained popularity, particularly in base metal and coal applications. Although column cells have achieved many successes industrially, they still suffer from two inherent flaws. Firstly, coarse particles have large settling velocities and therefore tend to have a shorter residence time in the cell, making them more difficult to recover. Secondly, fine particles generally lack the inertia to overcome the streamlines around bubbles and are therefore less likely to collide with approaching bubbles.

2.1.3. Novel Flotation Cells

Numerous novel flotation cells have been developed in an attempt to exploit or improve the various subprocesses of flotation since the inception of the flotation process. These improvements have largely been instigated by a better understanding of flotation fundamentals which has led to an appreciation of the micro-environment necessary for optimising flotation performance. This has been complemented by a better understanding of flotation cell hydrodynamics which has led to an improved understanding of the effects of energy input on the micro-environment in the flotation cell. Despite these improvements, however, the influence of energy input on hydrodynamics, particle-bubble contacting, attachment and detachment in flotation cells still remains poorly understood. It is the problems with both fine and coarse particle recovery that have been the focus of many subsequent novel cell developments. Most of these systems attempt to improve the fine and coarse particle recovery by increasing the shear rate in the contacting zone, or by further decoupling the collection and cleaning functions of the cell. Much of the development of new flotation technologies has centred on the generation of small bubbles and the development of reactor/separator type cells. Fine bubble generation has been developed through methods such as improved sparger design, dissolved air flotation and electro flotation. Reviews on these subjects can be found in Finch 1995, Rodrigues and Rubio 2007 and Miettinen et al. 2010. This section will review some of the major types of novel cells which provide alternative turbulent environments for flotation which have found particular industrial success.

2.1.3.1. Reactor/Separator Cells

One of the major developments in flotation cell design was the development of “reactor separator” type cells. These cells work by separating the contacting and separation functions of the cell, thus allowing independent optimisation of each function. The literature is filled with many examples of such designs such as the Flotaire Cell (Gruber and Kelahan, 1988), the Pneumatic Cell (Changgen and Bahr, 1992), the Contact cell (Amelunxen, 1993) and the LM flotation cell (Xinghau, 1998), but perhaps the best known and most successful design is the Jameson cell. The concept of the reactor/separator type cell is to separate the processes of particle bubble contacting and the removal of the particle-bubble aggregates from the pulp. This is generally achieved by mixing the bubbles and

slurry in a vertical downcomer which supplies the turbulence for contacting. The downcomer then discharges into a quiescent zone where the aggregates are allowed to rise to the surface. This separation of the contacting and separation allows for each to be independently optimised. A schematic of a Jameson cell is shown in Figure 2.3.

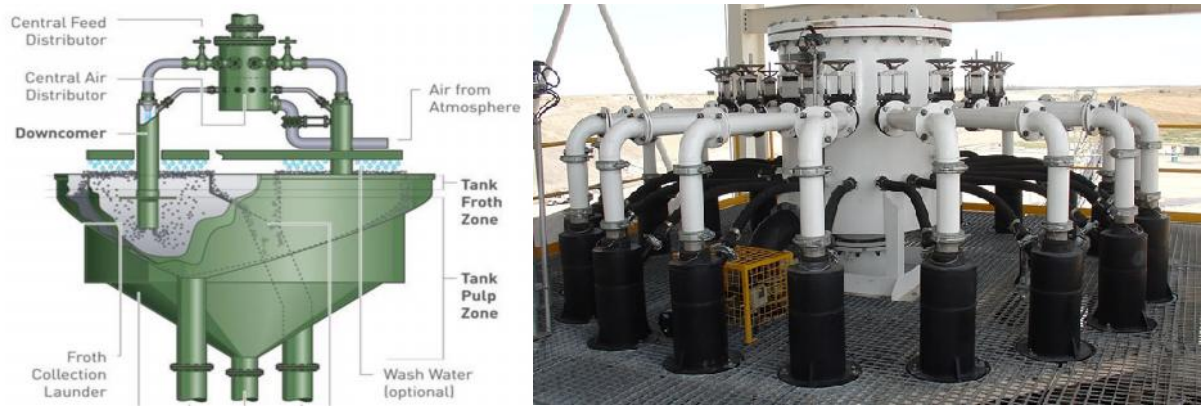

Figure 2.3: Schematic of a Jameson flotation cell (Xtrata Jameson Cell)

Since the first installation at Mount Isa Mines in 1986, the Jameson cell has achieved many successes and there are currently more than 341 installations worldwide (Glencore Technology, 2015). The design has also been extensively developed since its first introduction and modern Jameson cells consist of up to 20 parallel downcomers incorporating sophisticated slurry injection systems which maximise air entrainment (Jameson, 2007). Jameson cells have been shown to be particularly effective in fine coal flotation, and are able to produce high throughputs when compared with MicroCell^{TM} and Packed Column technologies (Mohanty and Honaker, 1999). Their weakness lies in the short contacting time of the slurry in the downcomer, which is usually of the order of 10 seconds. This means that weakly hydrophobic particles only have a limited opportunity to successfully contact bubbles and be recovered. The cell design is therefore thought to be best suited to the flotation of highly hydrophobic material such as coal and chalcopyrite. In addition the cells require a highly stable feed rate and good control systems to prevent fluctuations in performance. This weakness has however been somewhat mitigated in recent designs by incorporating a slurry recycle to stabilise the feed rate.

2.1.3.2. Agitated Columns

One of the first attempts to improve fine and coarse particle recovery in column flotation was the introduction of agitated flotation columns. The first examples of this column was the HydroChem column (Schneider and Van Weert, 1988), which consisted of a standard flotation column fitted with a series of alternating impellers and spinning discs down its length. The configuration was designed to create a tanks-in-series type mixing profile down the column length. This column achieved some success but failed to improve coarse particle recovery due to the high detachment rates associated with spinning discs. Later, Harris et al. 1992 tested a hybrid flotation cell, which consisted of a Leeds batch cell design combined with a 2 inch column section fitted to the top of the cell. This design was found

to significantly improve coarse particle recovery relative to a standard column cell and was able to produce a much higher grade than a batch flotation cell. This work was then extended by Breytenbach 1995, who developed an agitated column by added four impellers down the length of a flotation column. It was found that quartz flotation rates could be increased substantially over a standard column cell, and that fine particle (-40 µm) recoveries were superior to those in a standard batch cell and a Jameson cell. Ityokumbul et al. 2000 tested the same design on the flotation of pyrite with a particle size of 62% passing 25 µm. It was found that the recovery of pyrite increased with increasing energy input, however above 0.3 kW/m^3 the grade decreased sharply. The oscillatory baffled column is a design which produces turbulence in a column through a unique oscillatory flow (Anderson, 2008). Experiments floating -100 µm quartz found that the flotation rates could be greatly increased with low energy inputs of up to 0.05 kW/m^3. An attribute of the oscillatory flow was that the flotation rate could be increased 1.4 to 1.6 fold over a conventional column, regardless of the fluid viscosity. It was therefore speculated that this device shows potential for the flotation of viscous, non-Newtonian slurries. This cell is discussed in more detail in Section 2.3.2.3.2.

Despite this evidence of significant improvements in flotation rate, agitated columns have yet to be tested industrially. Some exceptions were the earlier column designs such as the WEMCO/Leeds cell (Degner and Sabey, 1988) and the OK cell (Ulan et al., 1991) of the late 1980's and early 1990's which incorporated agitation into their designs. These cells were applied in limited instances but were distinctly different in their design compared with the aforementioned agitated columns, in that the impeller was located at the base of the column as in a conventional cell. The role of the impeller was more for promoting better gas dispersion and solid suspension than for optimising particle-bubble contacting. For this reason the cells only achieved limited success and were eventually replaced by conventional cell technologies. Given the significant improvements in fine particle recovery achievable using agitated columns, it is believed that a distinct opportunity still exists for the application of this technology to industrial slurries. It is speculated that such a column, combined with a modern micro-bubble generation apparatus may be able to achieve good fine particle performance by optimising the energy input independently of gas dispersion effects.

2.1.3.3. Other Novel Cells

Many other novel flotation devices have been suggested over the years, mostly in the waste water treatment and paper deinking industries where flotation is used for the removal of waste products. Comprehensive reviews of such technology are given in Finch and Hardie 1999 and Rubio et al. 2002. Notable examples include the cells such as the Centrifloat® and the Air-Sparged Hydrocyclone (Ye et al., 1988), which make use of the shear rate under a centrifugal flow field to induce greater particle bubble contacting. Other novel techniques include electro flotation and dissolved air flotation for the generation of microbubbles, and even cavitation air flotation which attempts to seed bubbles directly onto particle surfaces.

Jameson proposed two new flotation devices in 2010. The first is the Concorde cell, which operates by forcing pressurised, aerated slurry through a choke into an open cell, creating a supersonic shockwave. This shockwave is reported to produce very high energy inputs (100 kW/m^3). Experimental results in fine PGM flotation have indicated that the cell produces substantially increased flotation rates over conventional cells. The second device proposed by Jameson is the fluidised bed flotation cell, which is focused on coarse particle flotation. The fluidised bed concept aims at producing high levels of contacting at low energy inputs, so as to minimise the detachment of coarse particles. This is achieved by having a high concentration of solids in the cell and pumping aerated slurry upwards through the cell. The air then has to force its way through the particles, creating the environment for contacting. Experiments have shown improved flotation of coarse galena (850µm) using such a device.

HydroFloat was developed by Eriez recently and operates much like a traditional hindered-bed separator or teeter bed (Figure 2.4). The fluidization (teeter) water is supplied through a network of pipes that extend across the bottom of the entire cross-sectional area of the separation chamber. The teeter bed is continuously aerated by injecting compressed air and a small amount of frothing agent into the fluidization water. The bubbles attach to the hydrophobic particles, reducing their density till they rise through the teeter bed and are floated off. The use of the dense-phase, fluidized bed eliminates axial mixing, increases coarse particle residence time, and increases the flotation rate by promoting bubbleparticle interactions. As a result, the rate of recovery is high for both coarse liberated and semi-liberated particles. Hydrophilic particles that do not attach to the air bubbles continue to move down through the teeter bed and eventually settle into the dewatering cone. These particles are discharged as a high solids stream (e.g., 75% solids) through a control valve at the bottom of the separator. The valve is actuated in response to a signal provided by a pressure transducer mounted to the side of the separation chamber. This configuration allows a constant effective density to be maintained within the teeter bed.

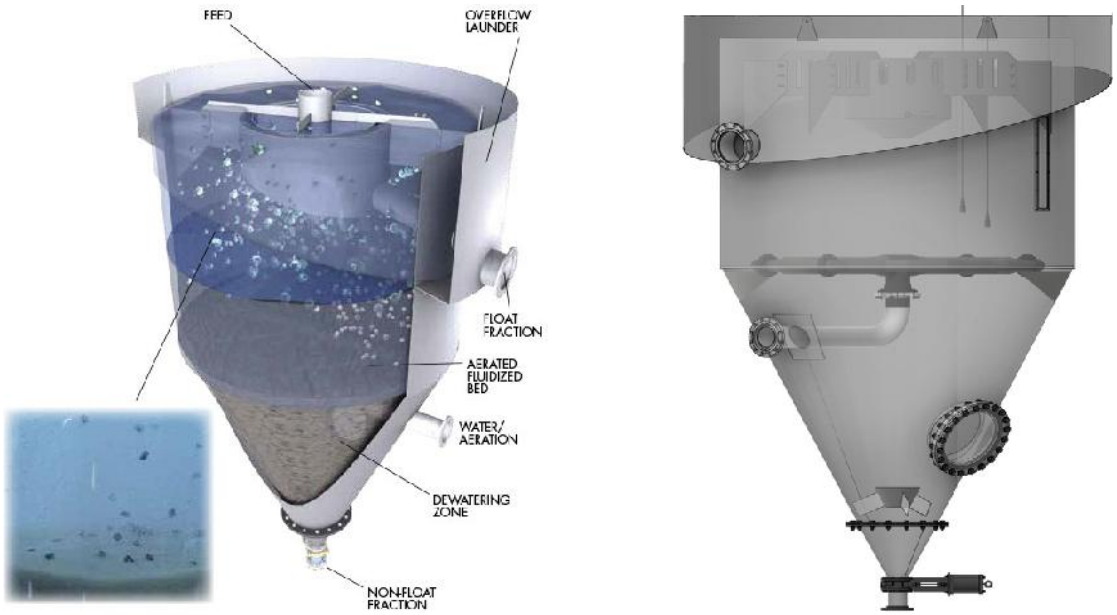

Figure 2.4: Schematic of a fluidised bed flotation cell (Eriez HydroFloat Separator, 2014)

The Staged Flotation Reactor (SFR) (Figure 2.5) is a recent development in the minerals industry. By sequencing the three processes-particle collection, bubble/slurry disengagement, and froth recovery-and assigning each to a purpose-built chamber, the SFR aims to optimize each of the three processes independently. The SFR incorporates an agitator in the first (collection) chamber designed to provide high energy input and induce multiple particle passes through the high shear impeller zone, hence giving high collection efficiency. Slurry flows by gravity through the reactor stages, that is, there is no need to apply agitation to suspend solids, only for particle collection. As such, impeller speed can be adjusted online in correlation with desired recovery without sanding. The second tank is designed to deaerate the slurry (bubble disengagement) and rapidly recover froth to the launder without dropback. The froth recovery unit is tailored for use of wash water and for high solids flux. Efficient particle collection and high froth recovery translate into fewer, smaller cells, resulting in a smaller footprint and building height, with lower power consumption, and the potential for good selectivity in both roughing and cleaning applications.

Figure 2.5: Staged Flotation Reactor (Courtesy Woodgrove Technologies Inc., 2015)

2.2. Oscillating Grids

Oscillating grids originated from the classical experimental studies on ‘grid turbulence’, in which regions of near homogeneous, isotropic turbulence were obtained by passing fluid through a stationary grid (Mohamed and LaRue, 1990) or dropping a grid through a stationary fluid (Dickey and Mellor, 1980). However, due to the rapid decay of turbulence downstream from the grid, these configurations proved impractical for many experimental studies (Srdic et al., 1996). As a consequence, oscillating grid systems were developed, whereby a grid was continually moved back and forth through the fluid, resulting in a more practical ‘static turbulent region’ for conducting experiments. Numerous studies on oscillating grids have shown that regions of near homogeneous, isotropic turbulence can be attained in vessels using this form of agitation. The background, turbulence of oscillating grids and determination of mean energy input in oscillating grids agitation were described in Sections 2.2.1 to 2.2.3.

2.2.1. Background

Oscillating grids produce turbulence which, at a distance away from the grid, is considered to be near homogeneous and isotropic. In addition they have zero mean-flow and the energy input can be easily varied. These properties make oscillating grids useful tools for investigating areas which operate in turbulent regimes. Due to the near ideal nature of the turbulence generated, oscillating grids have been used in many areas of research including turbulent characteristics behind grid (Taylor, 1935; Baines and Peterson, 1951; Comte and Corrsin, 1966; Dickey and Mellor, 1980), various stroke and frequency oscillating grids in ambient fluids (Kostazos et al., 1994), sediment suspension (Rouse, 1939; Brunk et al., 1996; Medina et al., 2001), particle turbulence interaction (Ettema et al. 1984; Nielson, 1993; Lyn, 1995), mixing processes in a stratified fluid and entrainment (Rouse, 1955; Thompson and Turner, 1975; Hopfinger and Toly 1976), turbulence and the gas transfer processes (Brumley and Jirka, 1987; Jirka, 1991; Herlina and Jirka, 2008), combustion (De Silva and Fernando, 1994), resuspension (Orlins and Gulliver, 2003), sedimentation (Huppert et al., 1995), mixing across density layers (McDougall, 1979), coagulation (Shy et al., 1996; Brunk et al., 1998), two grids turbulence (Shy et al., 1997; Ott and Mann, 2000; Janzen, 2003), precipitation (Mokgethi, 2010) and flotation (Changunda et al., 2008; Massey et al., 2012).

2.2.2. Turbulence Fundamentals

Flotation is directly influenced by the turbulent environment in which it occurs. It is therefore important to understand turbulence in order to appreciate how it may affect the process of flotation. Turbulence in itself is a complex topic and only a brief overview is given here. This section is derived from the review in Nguyen and Schulze 2004.

2.2.2.1. Turbulent Flow

The instantaneous fluid velocity at a point in a turbulent environment is composed of two parts. These are the mean velocity of the bulk fluid flowing in the system at that point, and a fluctuating component known as the instantaneous fluctuating velocity (u'). This fluctuating velocity is the action of turbulent eddies in the system, and it is this velocity which is thought to be of importance in flotation. The root mean squared (RMS) fluctuating velocity can be defined as $u' = \sqrt{u^2}$ in each direction. If the velocity is denoted u, v and w in the x, y and z direction respectively, then the total kinetic energy (TKE) can be described as:

$$TKE = \frac{1}{2}(u'^2 + v'^2 + w'^2) \tag{2.1}$$

If the turbulence is assumed to be isotropic, then the RMS turbulent velocities are equal in all directions. Therefore u'=v'=w' and Equation 2.1 becomes:

$$TKE = \frac{3}{2}u'^2 \qquad \text{(Isotropic turbulence)} \tag{2.2}$$

This assumption of isotropy is made for most collision models for flotation; however it is not strictly true in most flotation devices. The rate of turbulent energy input (ε) can be defined as:

$$£ = A\frac{TKE^{3/2}}{L} \tag{2.3}$$

where A= 0.85 (Wu and Patterson, 1989), L is the macro length scale, which is typically half the height of the turbine blades (Jenne and Reuss, 1999). In flotation literature and practice the average energy input ($\bar{£}$) is commonly used, which can be determined from the power input into the system (P) and the mass of the fluid being agitated (m_L).

$$\bar{£} = \frac{\bar{P}}{m_L} \tag{2.4}$$

This assumes that the energy input is homogeneous in the cell which is generally not the case; however it serves as measure of the overall energy input in a flotation cell.

2.2.2.2. The Turbulent Energy Spectrum

The eddies in a turbulent system are described as a spectrum of different sizes (λ) through which the energy cascades. The total kinetic energy as described in Section 2.2.2.1 is due to the action of all the eddies in the spectrum. Energy is continuously transferred, through turbulent shear stress, from large eddies to successively smaller eddies until the smallest possible eddies are reached, which then dissipate the energy as heat. A schematic of the turbulent energy spectrum is shown in Figure 2.6.

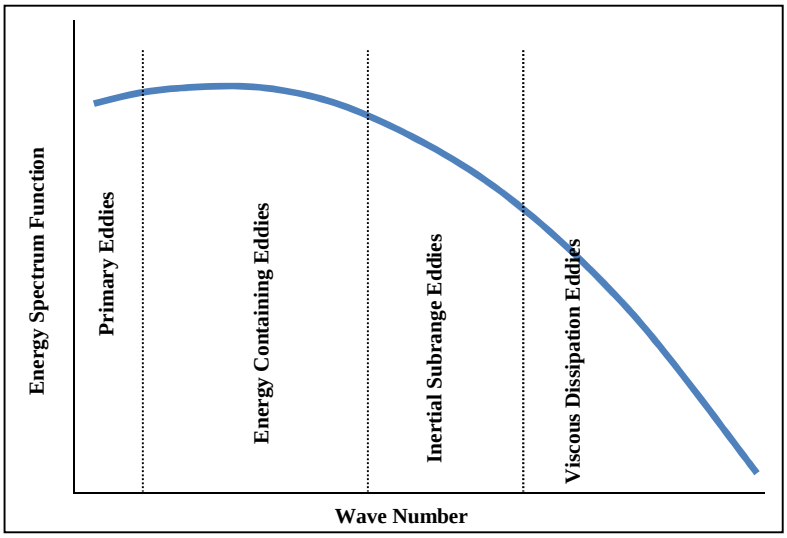

Figure 2.6: Schematic representation of a turbulent energy spectrum (Deglon, 1998)

Energy is initially input into a system through some external means (for example an impeller or an oscillating grid) to form primary eddies. The energy is transferred to smaller eddies which contain the majority of the energy in the system and are known as the energy containing eddies. As the eddy size decreases the number of eddies increases, but the total energy contained in that eddy size decreases. Eddies smaller than the energy containing eddies are known as the inertial subrange eddies, as inertial forces are dominant in them. The smallest eddies in the spectrum dissipate the energy as heat through molecular friction and are known as the dissipative eddies.

2.2.2.3. Macro and Micro Scales of Turbulence

The eddies in the turbulent energy spectrum have defined scales which can be quantified. The large scale primary and energy containing eddies are thought to have a size (Λ) which is in the order of magnitude of the turbulence generating device (for example the impeller), and are known as the macroscale of turbulence. Smaller scale eddies in the inertial and dissipative subranges are thought to be independent of the external means of energy input, and the turbulence is often referred to as microturbulence. In 1941 Kolmogorov proposed that these smallest eddies are dependent entirely on the energy input (ε) and the kinematic viscosity of the fluid (ν). The smallest possible eddies are known as the Kolmogorov microscale, and have a length (η) and velocity (ω) defined as:

$$\eta = \left(\frac{\nu^3}{\varepsilon}\right)^{0.25} \tag{2.5}$$

$$\omega = (\nu\varepsilon)^{0.25} \tag{2.6}$$

Microturbulence can be separated into the inertial and dissipative subranges. Eddies that have radii $r < (5 \text{ to } 10)\ \eta$ are considered to be in the dissipative subrange and are laminar. Eddies with radii $0.06\ \Lambda > r > (15 \text{ to } 20)\ \eta$ are considered to be in the inertial subrange and are turbulent within themselves. The scale of the largest laminar eddies and smallest turbulent eddies, at typical flotation energy inputs, are given in Table 2.1.

Table 2.1: Scales of microturbulence relevant to flotation (Massey, 2011)

Energy Input (kW/m^3)	Largest Laminar eddies (μm)	Smallest Turbulent eddies (μm)
1	160 – 320	470 – 630
3	120 – 240	360 – 480
5	105 – 210	310 – 420

From Table 2.1 it can be seen that, in a typical flotation environment, particles smaller than 100 μm would be contained within laminar eddies. However, bubbles would typically be approximately 1 mm in size, and would therefore be influenced mainly by the turbulent eddies in the inertial subrange.

2.2.3. Oscillating Grid Turbulence

Oscillating grid turbulence is generated by moving either a single grid or multiple grids at a stroke length (S) and frequency (f) in a fluid. The movement of the grid openings through the fluid generates jets and wakes which interact, and create turbulence (Yan et al., 2010). Typical oscillating grid set-ups (single grid and two grids) are illustrated in Figure 2.7. The turbulence in the system occurs in two distinct areas, namely the area swept by the grid known as the internal zone, and the area which is not swept by the grid known as the external zone. The turbulence generated by the grids is directional, the horizontal plane is taken to be the x and y directions whilst the vertical (direction of oscillation) is the z direction.

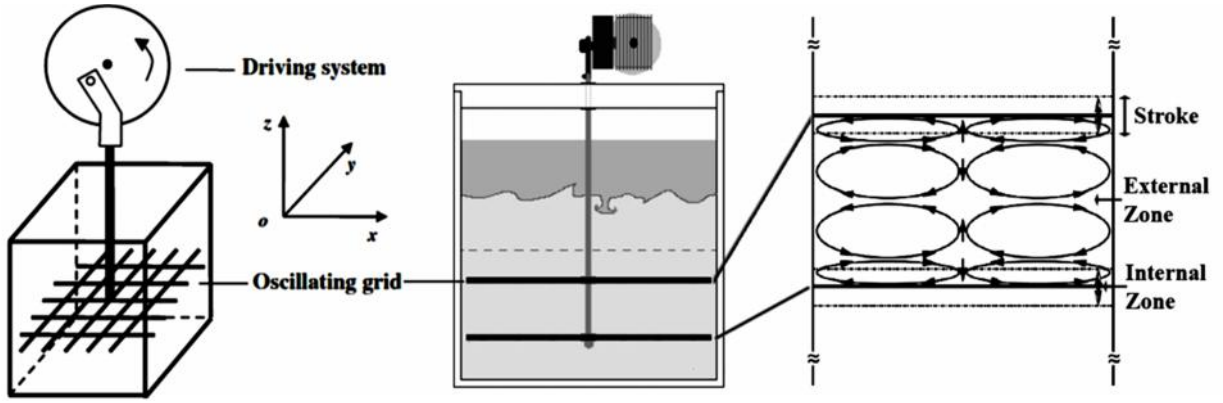

Figure 2.7: Typical diagram of oscillating grid set-ups and oscillating grid turbulence (adapted from Sanchez and Redond 1998, Yan et al. 2010, Blum et al. 2009)

2.2.3.1. Single/Double Grids

Typical oscillating grid set-ups are illustrated in Figure 2.8, which shows both a single and double grid set-up. The majority of studies into oscillating grid turbulence have been conducted using single oscillating grids (Hopfinger and Toly, 1976; McDougall, 1979; De-Silva and Fernando, 1994; Huppert et al., 1995; Liem et al., 1999; Orlins and Gulliver, 2003) and are reviewed briefly here. Hopfinger and Toly gave the following relationship (c.f. Table 2.2) describing the RMS fluid velocities in the external region generated by a single oscillating grid:

$$u' = v' = C_1 M^{0.5} S^{1.5} f Z^{-1} \quad \text{(Horizontal (x,y) plane)}$$
$$w' = C_2 M^{0.5} S^{1.5} f Z^{-1} \quad \text{(Vertical (z) plane)} \qquad (2.7)$$

where Z is the distance in the z axis away from the grid, M is the spacing of the mesh in the grid, and C_1 and C_2 are constants given as 0.25 and 0.27 respectively. The horizontal RMS velocities in the x and y directions (u′ and v′) are equal, although the vertical RMS velocity in the z direction is slightly larger. It is due to this, that this type of turbulence is considered to be nearly isotropic. Orlins and Gulliver 2003 confirmed the Hopfinger and Toly 1976 expressions by conducting tests using a two-component Laser Doppler Velocimeter (LDV) system. A LDV system uses a laser, beam splitter, fiber optic probe and a signal processor to measure the velocity field inside the tank. The measured TKE (turbulent kinetic energy) in a single oscillating grid is depicted in Figure 2.9a. It is illustrated that the turbulence is laterally homogeneous and decreases away from the grid. Turbulence in a two grid system is shown in Figure 2.9b (Janzen, 2006). Brunk et al. 1998 measured the turbulence parameters in the internal region in a single grid system. It was found that the TKE in the internal region did not vary greatly with distance from the centre of oscillation.

It is illustrated in Figure 2.9 that the turbulence is laterally homogeneous and decreases away from the grid, as indicated by Equations 2.7. The TKE is higher at the areas opposite the nodes of the grid; this is a characteristic of oscillating grids which is considered to be unavoidable. Shy et al. 1997 found that this difference between node and hole decreases as one measures further away from the grid. Equation 2.7 is only applicable for turbulence in the external region and does not describe the turbulence in the

internal region. Bache and Rasool 1996 studied the turbulence in the internal zone of a single grid system. It was found that the areas swept by the grid have significantly higher RMS velocities and energy input levels than in the remainder of the cell. Brunk et al. 1998 measured the turbulence parameters in the internal region in a single grid system. It was found that the TKE in the internal region did not vary greatly with distance from the centre of oscillation.

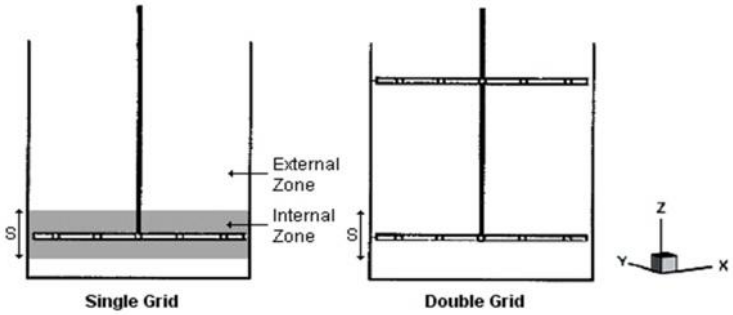

Figure 2.8: Diagram of single and double oscillating grids (adapted from Villermaux et al., 1995)

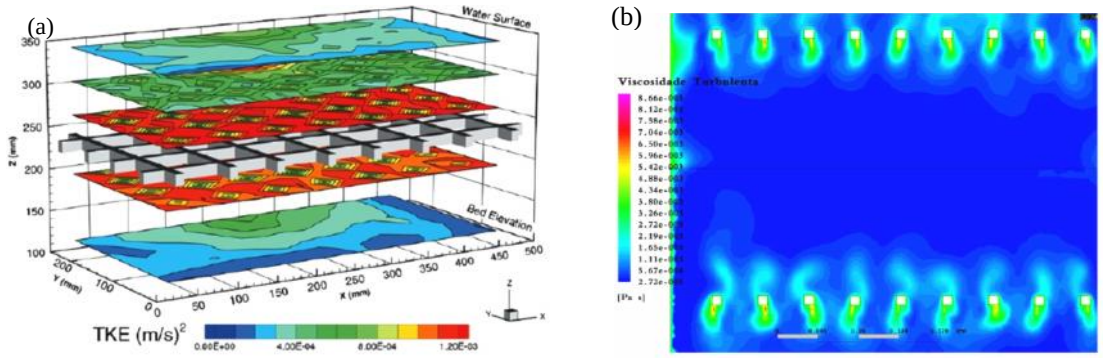

Figure 2.9: (a) Distribution of TKE generated by a single oscillating grid (5 Hz and 30 mm) (Orlins and Gulliver, 2003), (b) Determination of turbulence in a two grid system (Janzen, 2006)

However, the one-grid configuration produces a bias in the RMS velocity in the direction of oscillation. To compensate for the bias produced by the one-grid configuration, the two-grid configuration became a popular choice amongst authors such as Villermaux et al. 1995, Srdic et al. 1996, Shy et al. 1997, Eidelman et al. 2002, Janzen 2003 and 2006. The spatial decaying turbulence of both grids interacts to form a substantial nearly isotropic stationary region in between the grids which is often the domain of interest. Matsunga et al. 1999 obtained theoretical predictions of the TKE and energy input (ε), for oscillating grid turbulence using the k-ε turbulence model. Janzen et al. 2003 compared their findings to those of Matsunga et al. 1999 and obtained vertical profiles of the turbulent kinetic energy with the theoretical predictions of the k-ε turbulence model. They concluded that the profiles generated by the analytical solution agreed with those of the experimental turbulent kinetic energy data. However use of a k-ε model to describe turbulence created by oscillating grids is questionable. The turbulence created by oscillating grids has a zero mean shear, but this model is built in the framework of turbulence with a mean shear and the constants of the steady k-ε model were determined from experiments with mean shear flows.

2.2.3.2. Multiple Grids

It has been shown in Equation 2.7 and Figure 2.9a that the turbulence in a single oscillating grid system degrades with distance from the grid. In order to remedy this researchers have used two grids which generate a stationary zone of interest between them (Villermaux et al., 1995; Srdic et al., 1996; Shy et al., 1997). Villermaux et al. 1995 proposed that the RMS velocities are additive when considering multiple grids and the effective turbulent RMS velocity (u'_{eff}) can be given as:

$$u'_{eff} = 2^{\frac{1}{3}} u' \tag{2.8}$$

where u′ is the RMS velocity for one of the grids. This equation was experimentally validated by Shy et al. 1997, who also determined that the area between the grids was nearly isotropic and stationary. Bache and Rasool 2001 developed an oscillating multi-grid mixer capable of generating large regions of near homogenous isotropic turbulence through the vessel. Figure 2.10 shows the variation of the RMS turbulent velocity through the oscillating multi-grid mixer and fluid velocity in a stirred cell. The turbulence does vary throughout the oscillating multi-grid mixer but this is insignificant in comparison to the orders of magnitude variations found in stirred cells (Lee and Yianneskis, 1988; Schafer et al., 1997). In an oscillating multi-grid mixer, the coefficient of variation of the RMS turbulent velocity is around 14% (Figure 2.10 a), however in a stirred cell, variation of the fluid velocity near the impeller is more than 1000 % (Figure 2.10 b).

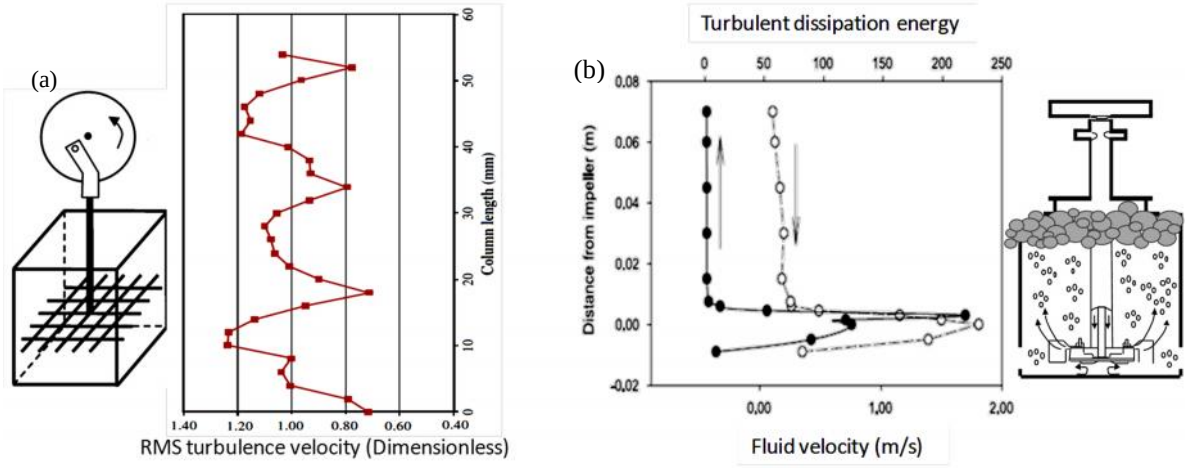

Figure 2.10 a,b: RMS turbulent velocity in OGC and fluid velocity in stirred cell (adapted from Bache & Rasool 2001)

Bache and Rasool investigated the turbulence in a multiple grid cell and they found that eddy motion was higher in the z direction. In the areas swept by the grid it was found that $w'^2 \approx 4u'^2$, and due to this an average intensity per direction (u'^2) was defined in order to account for this anisotropy in the system. The measured value of u'^2 for the length of the oscillating grid cell, from Bache and Rasool 2001, is shown in Figure 2.11.

$$u'^2 = \frac{1}{3}(2u'^2 + w'^2) \tag{2.9}$$

It can be seen in Figure 2.11 that u'^2 was relatively constant throughout the cell. Note that in Figure 2.11 the stroke length is equal to the spacing between the grids and therefore the entire length is swept

by the grids. It is assumed that for a multi-grid scenario, under these conditions, the turbulence can be considered relatively homogeneous and isotropic throughout the cell.

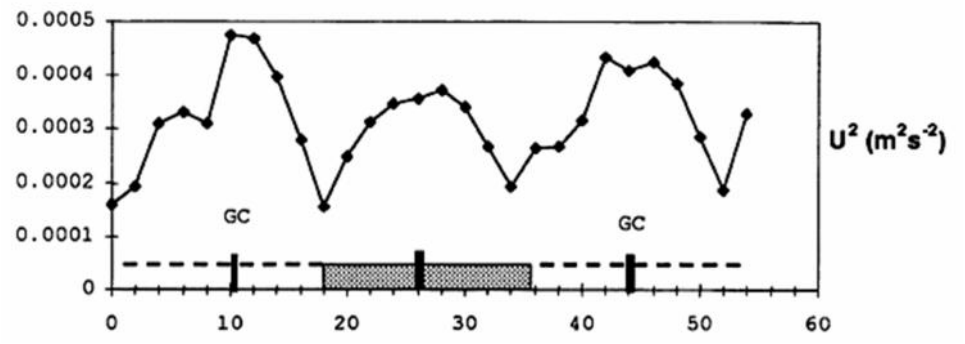

Figure 2.11: Graph showing u'^2 variation with tank height, at 2 Hz and 18 mm amplitude (Bache and Rasool, 2001)

2.2.3.3. Deviations from Ideal Hydrodynamic Behavior

There is evidence that, at high frequencies, oscillating grid turbulence deviates from being isotropic. It has been suggested by McDougall 1979 that 7 Hz should be the highest frequency used (known as the "off" frequency) since after this point u′, v′ and w′ no longer increase linearly with frequency, and therefore Equation 2.7 no longer holds. Shy et al. 1997 found that in the case of a double grid system this effect began at approximately 9 Hz. These observations are however made in the external region only and it is not known how higher frequencies may affect the internal region.

There have been reports of undesired circulatory flows in single grid cells (McDougall, 1979; McKenna and McGillis, 2004). It was found that these flows were dependent on initial starting conditions and McDougall noted that they began when seeding material was added. They concluded that circulatory flows are a feature of oscillating grid turbulence, but they are relatively benign if sufficiently spaced sampling points are used. These observations have only been made in single grid systems and it is not known if they may be a feature in multiple grid systems. Villermaux et al. 1995 conducted experiments on a double grid system to observe intense vertical structures using a migrating bubble technique. This technique used 100 µm bubbles in water heated to 70°- 75°C so as to decrease the viscosity. The bubbles then migrate towards areas of low pressure, in this case the vertical structures. It was observed that the structures were short lived and occurred most often near the walls.

2.2.4. Mean Energy Input in Oscillating Grid Agitation

The mean energy input is a parameter which is often used in flotation literature and practice. In this section the determination of energy input in an oscillating grid cell is discussed. Various studies have been carried out in order to model energy input in oscillating grid mixers (c.f. Table 2.2). These studies have been supported by experimental techniques such as Computational Fluid Dynamics (CFD), Digital Particle Image Velocimetry (DPIV), Laser Doppler Velocimetry (LDV) and Laser Induced Fluorescence (LIF). The review presented here is derived from the work of Bache and Rasool 1996 and Guadayol et al. 2009. In an oscillating grid cell the energy input originates from the

oscillating motion of the grids through the fluid. This motion of the grid stack can be described, in terms of displacement (Y), velocity ($\dot{Y}$) and acceleration ($\ddot{Y}$), as follows:

$$Y(t) = -S/2 \cos(2\pi f t)$$
$$\dot{Y}(t) = S \pi f \sin(2\pi f t) \quad (2.10)$$
$$\ddot{Y}(t) = 2 S \pi^2 f^2 \cos(2\pi f t)$$

Table 2.2: Estimation of energy input in oscillating grid cells (summary of main equations and conditions)

Author	Conditions		Equation	Parameters
Taylor 1935	Outside the Grid		$£ = A\, u^3 l^{-1}$	A, , C,C_{HT} , k_g , α, γ ,C_1 , C_2 = are constants l = the size of the largest eddies (cm) L = integral length scale (cm) u = horizontal root mean squared (RMS) velocity(cm s^{-1}) D = diameter of oscillatory cage (cm) ΔP = the pressure drop across the oscillatory cage S = stroke length (cm) C_d = drag coefficient S_A = solid area of the grid (cm^2) f = frequency (Hz or s^{-1}) ρ_f = fluid density (g cm^{-3}) t_1 = time upwards (s) t_2 = time downwards (s) M = mesh size (cm) z = distance from the grid centre or between grids (cm) Y(t) = displacement(cm) $\dot{Y}$(t) = velocity(cm s^{-1}) $\ddot{Y}$(t) = acceleration(cm s^{-2}) F_D = classical drag force (N) P = instantaneous power input to the fluid (W) m_L = mass of fluid being agitated (kg) r = width of the bars in grid (cm) V = velocity of the grid (cm s^{-1}) $\bar{\epsilon}$ = average energy input or dissipation rate (W kg^{-1}) T = period of oscillation and is equal to f^{-1} (s) $\bar{P}$ = time-averaged cornet power input (W) ϵ = turbulent dissipation rate or turbulent energy input ε = turbulent kinetic energy (TKE) ($cm^2 s^{-3}$) E = turbulent kinetic or energy ($cm^2 s^{-3}$) E′ = kinetic energy input ($cm^2 s^{-3}$) $\phi(f)$= kinetic energy per unit frequency $u' = v'$ = horizontal RMS turbulent velocity (cm s^{-1}) $w' = w$ = vertical RMS turbulent velocity (cm s^{-1}) v = kinematic viscosity($cm^2 s^{-1}$ or Pa s) ε_D = rate of dissipation or turbulent kinetic energy P_s = power lost due to skin friction along shaft (Nm s^{-1}) P_g= power input to the grid (W) d = shaft diameter (cm) L_s = shaft length (cm) F = force in a cycle (N) ω_g = grid frequency ($\omega_g = 2\pi f_D$) (Hz or s^{-1}) ϕ = phase shift f_D = vibrator driving frequency (Hz or s^{-1}) C_s , C_p = calibration constants A_g = plan area of the grid or cross sectional area (cm^2) σ = corresponding solidarity Re = Reynolds number
Guadayol et al. 2009	Within the Grid Path	Sinusoidal Velocity	$Y(t) = -S/2 \cos(2\pi f t)$ $\dot{Y}(t) = S \pi f \sin(2\pi f t)$ $\ddot{Y}(t) = 2 S \pi^2 f^2 \cos(2\pi f t)$ $F_D(t) = \frac{1}{2} C_d \rho_f S_A \dot{Y}(t)$ $P(t) = F_D(t) \dot{Y}(t)$ $\bar{P}(t) = T^{-1} \int_0^T P(t)dt$ $\bar{P} = 2/3 C_d \rho_f S_A \pi^0 f^3 S^3$ $\bar{\epsilon} = \bar{P}/m_L$	
		Constant V	$P = \frac{1}{2} C_d S_A S^3 f (t_1^{-2} + t_2^{-2})$	
	Outside the Grid Path		$\varepsilon = A \quad C S^{9/2} M^{3/2} z^{-4} f^3$	
Brunk et al. 1996	Outside the Grid		$E = 3/2 C_{HT}^2 S^3 f^2 M z^{-2}$	
Sanchez and Redond 1998	Within the Grid Path		$P = k_g A_g \rho_f r^2 S^2 M^{-1} f^3 / 8\pi$	
Peters and Gross 1994	Energy Input comes from the Drag Force		$F_D(t) = \frac{1}{2} C_d \rho_f S_A V^2(t)$ $E' = 2 \int_0^{T/2} F_D(t) V(t) dt$	
Tennekes1975	Outside the Grid		$\phi(f) = \alpha \varepsilon^{2/3} u^{2/3} f^{-5/3}$	
Hopfinger,Toly 1976; Silva and Fernando1994	Outside the Grid Path		$u' = v' = C_1 M^{0.5} S^{1.5} f z^{-1}$ $w' = C_2 M^{0.5} S^{1.5} f z^{-1}$	
Orlins and Gulliver 2003	Within and Outside the Grid Path		$\varepsilon = TKE = \frac{1}{2}(u'^2 + v'^2 + w'^2)$ $TKE = \frac{1}{2}(2C_1^2 + C_2^2) M S^3 f^2 z^{-2}$	
Thompson and Turner 1975	Outside the Grid Path		$u' = 1.4 S^{2.5} f z^{-1.5}$	
Shy et al. 1997	Outside the Grid Path		$u' = 0.89 M^{0.5} S^{1.5} f z^{-1.5}$	
Bache and Rasool 1996	Within and Outside the Grid Path		$P = P_s + P_g$ $P_s = \pi^{P(R}\rho_f S^2 L_s d \nu^{0.5} f^{2.5}{}_D$ $P_s = C_s S^2 f^{2.5}{}_D$ $P_g = C_p \rho_f S^{2.5} \sigma A_g d^{-0.5} \nu^{0.5} f^{2.5}{}_D$ $P_g = C_p \rho_f Re^{-0.5} S^3 \sigma A_g f^3{}_D$ $F = F_{max} \cos \omega_g t$ $Re = f s d \nu^{-1}$ $\bar{P} = 0.5\pi S f_D F_{max} \sin\phi$ $\bar{\epsilon} = P_g / m_L$	
Stamenkovic´ et al. 2010	Within and Outside the Grid Path		$P = 2A_g \Delta P \pi S f \dot{Y}(t)[1-2Y(t)]$	

As the grid moves through and fluid it exerts a force due to the frictional drag of the plate (Guadayol et al., 2009), this frictional force transfers energy from the grids to the fluid. The frictional force is described by the classical drag force equation:

$$F_D(t) = \tfrac{1}{2} C_d \rho_f S_A \dot{Y}(t) \quad (2.11)$$

where C_d is the drag coefficient, ρ_f is the density of the fluid and S_A is the solids area of the grid. The drag coefficient (C_d) is assumed to be constant with time, making this a quasisteady state assumption. The instantaneous power input into a system can then be given as:

$$P(t) = F_D(t) \dot{Y}(t) \quad (2.12)$$

The net power input is given as the integral of power with time over a single oscillation:

$$\bar{P}(t) = T^{-1} \int_0^T P(t)dt \quad (2.13)$$

where T is the period of one oscillation and is equal to f^{-1}. Substitution of Equation 2.11 into Equation 2.13 and integration yields (Guadayol et al., 2009):

$$\bar{P} = 2/3 C_d \rho_f S_A \pi^3 f^3 S^3 \quad (2.14)$$

The mean energy input can be calculated by Equation 2.4. If it is assumed that energy input is additive for multiple grids, then for a system with n grids the mean energy input can be described by:

$$\bar{\varepsilon} = \frac{\bar{P}}{m_L} = \frac{2}{3} \frac{n C_d \rho_f S_A \pi^2 f^3 S^3}{m_L} \quad (2.15)$$

Energy input is therefore strongly dependent on the frequency and stroke of oscillation and these are the key operating variables in an oscillating grid system.

2.3. Effect of Energy Input on Flotation Kinetics

The effect of energy/power input on the subprocess of flotation still remains poorly understood despite all the improvements. This led to appreciation of the micro-environment and the effect of energy input on this environment. Energy input is thought to increase the rate of flotation by increasing the number of particle-bubble collisions, collision and attachment efficiencies. Furthermore effect of energy input on flotation is to decrease particle-bubble aggregates stability (increase detachment efficiency and bubble breakup). The overall effect that energy input has on flotation rate is therefore a balance of these two effects. However there are limits to which energy input can improve the flotation process and the extent and rate to which energy improves flotation is largely uncertain. This section provides a review of the theoretical and experimental findings of the effect of energy input on the flotation subprocess.

2.3.1. Theoretical Findings

Energy/power input is considered to influence all the subprocesses of flotation, either directly or indirectly through bubble break-up and gas dispersion. The majority of theoretical studies suggest that

energy input increases the particle-bubble collision frequency, which is especially important for fine particles (Julien Saint Amand, 1999; Schubert, 1999). It is unclear whether energy input improves particle-bubble attachment due to conflicting results as to the effect of energy input on particle-bubble contact time. However, studies suggest that energy input helps to overcome the 'energy barrier' to attachment. All studies conclude that energy input significantly increases particle-bubble detachment for coarser particles but has a lesser influence on fine particles. Several studies and flotation models demonstrate that energy input generally increases the rate of flotation (Julien Saint Amand, 1999; Koh and Schwarz, 2003; Pyke et al., 2003; Sherrell and Yoon, 2005). The particle-bubble collision mechanism and frequency of particle-bubble collisions are discussed in Section 2.3.1.1 and 2.3.1.2 respectively. The elements which make up the collection efficiency are discussed in Section 2.3.1.3. The summary of theoretical findings is reviewed in Section 2.3.1.4.

2.3.1.1. Particle - Bubble Collision Mechanism

Table 2.3 gives the different collision mechanisms concerning collision modelling according to scale of turbulence. Since energy input is thought to improve particle-bubble contacting by enhanced collision frequency and efficiency, the rest of this section reviews various collision models of relevance to turbulent collision.

Table 2.3: Collision mechanism in turbulence (Anderson, 2008)

Mechanism	Continuous phase flow regime	Applicability
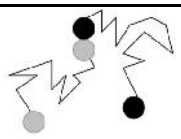 Brownian Motion	Laminar and very low Turbulence	Particles are small, Particles must be less than 1 μm
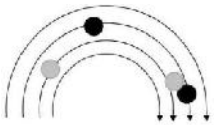 Shear Mechanism	Laminar and low Turbulence	Particle and bubble smaller than smallest eddies - $(d_p+d_b) << \eta$ - $St \leq 1$
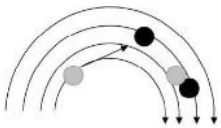 Accelerative Mechanism	Turbulent	Particle and bubble similar or smaller than smallest eddies - $(d_p+d_b) \leq \eta$ - $St \geq 1$
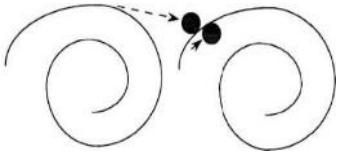 Pure Accelerative Collision	Highly Turbulent	Particles and bubbles are larger than smallest eddies - $(d_p+d_b) \geq \eta$ - $St \geq 10$ Particles and bubbles have independent velocities

Brownian motion in flotation corresponds to particles colliding with bubbles due to their random Brownian motion and long range hydrophobic forces. This is more applicable to random movement of particles due to random movement of molecules in the environment and is considered to only have an

effect on particle-bubble contacting for particles less than 1 μm. This is much smaller than the range of bubble sizes encountered in flotation. Nonetheless, the Brownian model has been developed for very small particles in a very low turbulent environment. The shear mechanism applies to laminar and low turbulence flow fields. Particles and bubbles follow streamlines within the viscous dissipation eddies range and collide due to their different positions within a shear flow field. The accelerative mechanism applies to collisions that occur in a low turbulence environment by accounting for the inertial effect of particles and bubbles. Collisions between particles and bubbles occur within a shear flow field, but they deviate from fluid streamlines due to particle inertia (see Table 2.3). Purely accelerative mechanism applies in cases where there are high turbulent flows or when large particles are encountered. Particles and bubbles are thrown randomly from eddy to eddy and collisions occur because of relative motion. Under these conditions, the viscous eddies become too small to contain particles and bubbles.

2.3.1.2. Particle - Bubble Collision Frequency

The rate of collision between particles and bubbles (Z_{pb}) is dependent on the hydrodynamics of the fluid in which they are contained. Different models apply depending on the turbulent regime that the particles and bubbles are contained in. For particles and bubbles which are contained within the smallest turbulent eddies, the collision rate is given as (Saffman and Turner, 1956) (Shear mechanism):

$$Z_{pb-\text{Shear}} = \sqrt{\frac{8\pi}{15}}\, N_p N_b \left(\frac{d_p + d_b}{2}\right)^3 \sqrt{\frac{\varepsilon}{\nu}} \tag{2.16}$$

In this equation the particles and bubbles must be small compared to the smallest eddies in the fluid as is mentioned in Table 2.3. It is therefore only applicable to low energy input and is generally not suitable for normal flotation systems. For example, consider a system with an average energy input of 1 kW/m^3, the smallest laminar eddy is approximately 130 μm (Schubert, 1999). In a typical flotation operation the fine particles would fall in this range, however the bubbles would be well above this size. This equation has been used to model the collision rates in the low dissipation regions of flotation cells (away from the impeller) in CFD modelling of flotation (Koh and Schwarz 2003, 2006; Evans et al., 2008). Abrahamson 1975 proposed the following equation for collision in turbulent fluids, where particles are randomly flung between turbulent eddies (Accelerative mechanism):

$$Z_{pb-\text{Accelerative}} = 5 N_p N_b \left(\frac{d_p + d_b}{2}\right)^2 \sqrt{u_p'^2 + u_b'^2} \tag{2.17}$$

where u_p' and u_b' are the RMS relative velocity for the particles and bubbles respectively. It is assumed that the colliding particles' velocities are independent, in magnitude and direction. This model has been used in many flotation studies in turbulent systems (Jordan and Spears, 1990; Schubert, 1999; Duan et al., 2003; Pyke et al., 2003; Sherrell, 2004; Koh and Schwarz, 2006; Evans et al., 2008). In order to calculate the collision rate from Equation 2.17 the particle and bubble root mean squared

velocity are required to be quantified. Various models have been proposed to calculate this. Abrahamson 1975 proposed the following equation:

$$u'^2_{p/b} = \frac{u'^2_f}{1 + \frac{1.5^2_{p/b}}{u'^2_f}} \tag{2.18}$$

where $\tau_{p/b}$ is the relaxation time of a particle/bubble and is a measure of the tendency of a particle or bubble to come to equilibrium in a fluid. Liepe and Mockel 1976 derived an equation empirically using data taken from many other researchers.

$$u'_{p/b} = 0.4 \frac{£^{4/9} d_{p/b}^{7/9}}{¬^{1/3}} \left(\frac{°_{p/b} - °_f}{°_f} \right)^{2/3} \tag{2.19}$$

Equation 2.19 was derived for particles, although it has been used in the literature for bubbles. Lee and Erickson 1987 derived a model for the RMS bubble fluctuating velocity:

$$u'^2 = C_0 (£\ d_b)^{2/3} \tag{2.20}$$

where C_0 is a constant equal to 2 (Batchelor, 1951). Brady et al. 2006 tested various models for determining the RMS velocity, for both particles and bubbles, in isotropic turbulence formed by fluid flowing through cylindrical grids. It was found that the Liepe and Mockel model predicted the velocity of 80 µm particles reasonably well, while the Abrahamson model was in good agreement with experimental data for 1.2 mm bubbles. The Abrahamson model did, however, also provide reasonable agreement for particles. Both the Liepe and Mockel model and the Lee and Erickson model over predicted the RMS velocity for bubbles. These results suggest that, when determining the RMS velocity, it may be useful to use the Abrahamson model to model bubble velocities, and the Liepe and Mockel model for particles.

In the flotation literature the Liepe and Mockel 1976 model is most commonly used, for both bubbles and particles (Jordan and Spears, 1990; Julien Saint Amand, 1999; Schubert, 1999; Duan et al., 2003; Pyke et al., 2003; Koh and Schwarz, 2006; Evans et al., 2008). In a standard flotation system $d_b >> d_p$, then u′ can be neglected, and substituting Equation 2.19 into 2.17 yields (Julien Saint Amand, 1999; Pyke et al., 2003) (Accelerative mechanism):

$$Z_{pb-\text{Accelerative}} = 5 N_p N_b d_b^2 \left(0.4 \frac{£^{4/9} d_{p/b}^{7/9}}{¬^{1/3}} \right) \left(\frac{°_f - °_b}{°_f} \right)^{2/3} \tag{2.21}$$

From the two models of collision rates (Equations 2.16 and 2.21) the following relationship between energy input and collision frequencies can be shown:

$$Z_{pb} \propto £^r \qquad \textit{where} \qquad 0.44 \le r \le 0.5 \tag{2.22}$$

Models for turbulent collision suggest that the rate of flotation is proportional to the energy input /power intensity. From the turbulent models the following relationship between energy input (ε) and collision frequencies can be derived (Equation 2.23) (Deglon, 2002):

$$Z_{pb} \propto £^{r} \qquad \textit{where} \qquad 0.44 \le r \le 0.75 \tag{2.23}$$

The major difficulty with validation of these models in the past was the localization of energy input and mean squared fluctuating velocity (RMS). Collision frequencies must therefore be calculated at each point in the fluid which makes this method a computationally expensive one.

2.3.1.3. Particle - Bubble Collection Efficiency

For a particle to be collected by a bubble in a flotation cell all the following subprocesses must be satisfied:

1. The particle must collide with the bubble (collision frequency and collision efficiency).
2. The disjoining film separating the particle and the bubble must thin, rupture and recede to form a stable contact angle (collection efficiency - attachment).
3. The particle-bubble aggregate must be sufficiently stable to withstand external stresses in the flotation cell caused by turbulence (collection efficiency - detachment).

These three subprocesses are termed collision, attachment and detachment respectively (Sutherland, 1948) and apply to collection zone kinetics. The collection efficiency is considered to be comprised of three subprocesses which describe the ability of a particle to be floated, and are discussed separately in this section. These subprocesses are the collision of a particle with a bubble, the attachment of a particle to a bubble and detachment of a particle from a bubble. The collection efficiency can then be expressed as (Derjaguin and Dukhin, 1961):

$$E_{coll} = E_c E_a E_S \tag{2.24}$$

where E_c is the collision efficiency, E_a is the attachment efficiency and E_s is the stability efficiency. The majority of the concepts stem from work done by Sutherland with a large body of work dedicated to it since then. This work has been thoroughly reviewed by many authors (Ralston et al., 1999; Pyke, 2004; Sherrell, 2004; Anderson, 2008; Miettinen et al., 2010).

2.3.1.3.1. Particle - Bubble Collision Efficiency

Over the past half century various attempts at modelling the probability of collision in terms of predominantly hydrodynamic forces have been undertaken. Initial attempts concentrated on including interceptional effects in well defined Stokes and potential flow fields while later attempts included interceptional, gravitational and inertial effects in Stokes, intermediate and potential flow fields. The challenge in this comparatively mature area of research is to develop a unified model for collision including both hydrodynamic and surface forces. Collision is the primary and arguably most important of the subprocesses of flotation and has received considerable theoretical attention for both quiescent and turbulent systems.

The collision efficiency between particles and bubbles has been modelled under highly idealised conditions: a spherical bubble rising in a quiescent solid/liquid suspension, which is a very dilute suspension of fine and spherical particles of uniform size. Thus, the collision efficiency between particles and a rising bubble is defined as the number of particles which can collide with or can be intercepted by the bubble. Only those particles that approach the bubble within a streaming tube of diameter d_c can collide with the rising bubble, as indicated in Figure 2.12. Fine particles will follow the fluid streamlines; it is usually assumed that the fluid streamlines come closest to the bubble at its equator. Hence a grazing trajectory is defined as the one that, at the bubble equator, passes within a distance of the particle radius from the bubble surface (Yoon and Mao, 1996; Heindel and Bloom, 1999). It can be inferred that only the particles located within the critical diameter d_c at an infinite distance from the bubble can collide with it. The particles outside the critical diameter d_c will sweep past the bubble. The dimension of d_c depends on the nature of the flow regime. The determination of an expression for d_c is largely dependent on the assumptions made about the dimensions of the bubble and particle. The collision efficiency (E_c) is then determined by (Heindel and Bloom, 1999):

$$E_c = \left(\frac{d_c}{d_p + d_b} \right)^2 \tag{2.25}$$

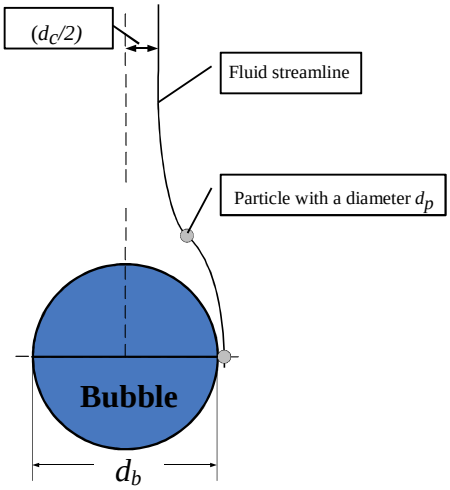

Figure 2.12: Particle colliding with a bubble at its equator

When a particle and bubble approach one another in a fluid they may not necessarily collide, but the particle may rather move with the fluid streamlines around the bubble. The collision efficiency is therefore dependent on the streamlines around a bubble, and the tendency of the particles to stay in the streamlines. The particle trajectory in the fluid flow and its tendency to stay in the streamlines can be characterized by the Stokes number:

$$St = \frac{\rho_p \, u_b \, d_p^2}{9 \, d_b \, \mu_f} \tag{2.26}$$

where d_b and u_b are the bubble size and rise velocity, ρ_p and d_p are the particle density and diameter and μ_f is the fluid viscosity. When St << 1 the particles are considered to have negligible inertia and will follow the fluid streamlines. When St >> 1 the particles will be relatively unaffected by the fluid streamlines. The flow of fluid around a bubble can be described by the bubble Reynolds number. The

bubble Reynolds number is calculated as indicated in Equation 2.27, where ρ_f the density of the fluid.

$$\mathrm{Re}_b = \frac{\rho_f \, u_b \, d_b}{\mu_f} \tag{2.27}$$

For $Re_b << 1$ the flow is considered to be in the Stokes regime, and potential flow when $100 < Re_b < 500$. Flow conditions which fall between the Stokes and potential flow regimes are known as the intermediate flow regime. Various models for the collision efficiency have been derived for the different flow regimes. Gaudin 1957 derived a model describing collision in the Stokes flow regime ($Re_b << 1$), neglecting particle inertia and assuming an immobile bubble surface.

$$E_c = \frac{3}{2}\left(\frac{d_p}{d_b}\right)^2 \tag{2.28}$$

For potential flow ($100 < Re_b < 500$), negligible particle inertia (follow streamlines) and an immobile bubble surface the following model derived by Sutherland 1948 holds.

$$E_c = 3\frac{d_p}{d_b} \tag{2.29}$$

Yoon and Luttrell 1989 derived a collision efficiency model for the intermediate flow regime, which assumed negligible particle inertia and an immobile bubble surface. This equation reduces to the expressions derived by both Sutherland and Gaudin for the Stokes and potential flow fields and predicts the probability of collision to be inversely proportional to the bubble size and the bubble size squared for very large and small bubbles respectively.

$$E_c = \left(\frac{3}{2} + \frac{4\mathrm{Re}_b^{0.72}}{15}\right)\left(\frac{d_p}{d_b}\right)^2 \tag{2.30}$$

Yoon and Luttrell 1989 summarized previous models for the collision efficiency, considering fine particles that follow the streamlines formed around a rising bubble in a quiescent liquid. The generalized form of the model for collision efficiency E_c is given in Equation 2.31, where the parameter B and the exponent n depend on the bubble Reynolds number. The model was developed for the intermediate range of bubble Reynolds numbers, and was validated using fine and very hydrophobic particles of coal. The bubble size ranged between 100 and 550 µm. The values of B and n for different flow regimes are shown in Table 2.4.

$$E_c = B\left(\frac{d_p}{d_b}\right)^n \tag{2.31}$$

Table 2.4: Values of the parameters B and n of Equation (2.31) (Yoon and Luttrell, 1989)

Flow Regime	***B***	***n***	***Reynolds***
Stokes	3/2	2	$Re \rightarrow 0$
Intermediate	$\left(\frac{3}{2} + \frac{4\mathrm{Re}^{0.72}}{15}\right)$	2	$0.2<Re<100$
Potential	3	1	$Re \rightarrow \infty$

Schimoller 1993 solved a dynamic force balance numerically for the particle-bubble system including both hydrodynamic and surface forces and found that collision could be improved by increasing the particle size, increasing the particle hydrophobicity, decreasing the bubble size and decreasing the particle zeta potential. This equation (Equation 2.31) was further modified for the bubble-particle interactions in the pulp zone by Do 2010 (Equation 2.32).

$$E_c = \tanh^2\left(\sqrt{\frac{3}{2}\left(1+\frac{0.187\,\mathrm{Re}}{1+0.249\,\mathrm{Re}^{0.56}}\right)}\left(\frac{d_p}{d_b}\right)\right) \tag{2.32}$$

Equation 2.32 has been used in various studies for flotation modelling (Koh and Schwarz, 2006; Evans et al., 2008; Jameson, 2010). This equation predicts increased collision efficiency with increasing particle size and decreasing bubble size.

2.3.1.3.2. Particle - Bubble Attachment Efficiency

Bubble-particle attachment processes have been less explored and modelled than those of bubble-particle collision. This is why there are only a limited number of attachment models available in the literature. Attachment between particles and bubbles is a complex interaction of both hydrodynamic and surface forces and, other than for certain deformation effects, is equivalent for both quiescent and turbulent systems. The attachment efficiency is defined as the fraction of particles which remain attached to bubbles after collision has occurred and is commonly modelled in terms of contact and induction times. The success of attachment depends largely on the hydrophobicity of the particle and is therefore the primary selective process in flotation. In order to model attachment two critical factors are considered, sliding time and induction time. If we consider a particle colliding with a bubble, the particle will make contact with the bubble and then slide around the circumference to a point, beyond which it will move away from the bubble. Sliding time is thus the time that a particle spends touching, or sliding along a bubble. Induction time is the time required for the particle to become attached to the bubble. If the sliding time is greater than the induction time then the particle can become attached to the bubble (Sutherland, 1948).

Dobby and Finch 1986 proposed a model based on two collision angles between a particle and bubble, measured from the vertical. The first is the adhesion angle (θ_a), which is the angle at which the sliding time will equal the induction time and the particle will attach. The second is the maximum possible collision angle, or angle of tangency (θ_t). The attachment efficiency (E_a) is then described by:

$$E_a = \frac{\sin^2 \theta_a}{\sin^2 \theta_t} \tag{2.33}$$

The adhesion angle (θ_a) can be calculated from (Dobby and Finch, 1986):

$$\theta_a = 2\arctan\left[\exp\left(-t_{ind}\,\frac{2(u_p+u_b)+(u_p+u_b)\left(\frac{d_b}{d_p+d_b}\right)^3}{d_p+d_b}\right)\right] \tag{2.34}$$

where u_p and u_b are the velocities of the particle and bubble respectively, and t_{ind} is the induction time, which can be calculated by the empirical equation (Dai et al., 1999):

$$t_{ind} = Ad_p^B \tag{2.35}$$

where B is a constant and A is inversely proportional to the contact angle of the particle and both determined from experimental data. The angle of tangency (θ_t) was given by Dobby and Finch 1986 as a set of equations, derived from experimental data, which are not reproduced here. In this case the model is known as the modified Dobby and Finch model and has been used by Pyke 2004 and Newell and Grano 2006 in general flotation models. This model predicts that attachment efficiency increases with decreasing particle size, decreasing bubble size and increasing contact angle. Dai et al. 1998 showed that the model was in agreement with experimental data from the flotation of quartz with particle sizes of 7.5-70 µm and contact angles between 33° and 74°. Yoon and Mao 1996 proposed a model based on the extended DLVO theory which includes surface properties of the particles and bubbles. This method focuses on the interaction of different forces and energies in the system. The attachment efficiency in this case is given as:

$$E_a = \exp\left(\frac{E_1}{E_{k-A}}\right) \tag{2.36}$$

where E_1 is the maximum energy that must be overcome in order for attachment to occur, and requires experimental data to calculate (Yoon and Mao, 1996). $E_{k\text{-}A}$ is the kinetic energy available in the system to overcome the energy barrier of attachment. Sherrell 2004 proposed that in turbulent systems the energy available to the particles/bubbles is the total turbulent kinetic energy ($TKE_{k\text{-}A}$) of the turbulent eddies which are of the same size, or smaller than the particles/bubbles. It is therefore taken to be the average energy between the eddies of the same scale of the particles/bubbles and the smallest possible eddies (Kolmogorov microscale). The energy available for attachment is given as:

$$E_{k-A} = \frac{1}{2}(m_p + m_b)TKE_{k-A} \tag{2.37}$$

where m_p and m_b are the mass of the particle and bubble respectively. Since all the energy available to the turbulent eddies originates from external agitation (the impeller in a stirred cell), the attachment efficiency is linked to the energy input in the system and would be expected to increase with increasing energy input. This model only takes thermodynamics effects into account and neglects the physical aspects. It can be shown (Pyke, 2004) that the equation contradicts theoretical and experimental data by predicting increased attachment efficiency with increased particle size. Despite this, the model has been used in flotation modelling (Sherrell, 2004).

2.3.1.3.3. Particle - Bubble Stability Efficiency

The analysis of detachment is primarily of relevance to turbulent systems as detachment is negligible in quiescent systems due to the appreciably lower external stresses in quiescent environments. The detachment efficiency (E_d) is defined as the fraction of attached particles which detach from bubbles in

the flotation cell and is equal to one minus the stability efficiency (E_s). Arbiter and Harris 1962 proposed that bubble oscillations and vibrations in turbulent systems promote both collision and detachment but did not validate this hypothesis experimentally. The stability efficiency can be described by the theory proposed by Schulze 1977, 1982 and is therefore often referred to as the Schulze model. Schulze derived an expression for the maximum floatable particle size by considering compressive, tensile and shear stresses acting on a particle-bubble aggregate in a turbulent field. This expression predicts a decrease in the maximum floatable particle size with decreasing bubble size, increasing energy input and decreasing contact angle. Jowett 1980 developed a model for the rupture of a particle-bubble aggregate in a turbulent eddy in terms of a centrifugal force or "g factor". The maximum floatable particle size was found to be dependent on the eddy rotation, contact angle and particle density and the detachment efficiency was shown to increase with increasing particle size.

Mika and Fuerstenau 1968 analysed detachment in an isotropic turbulent field and found the rate of detachment to be proportional to the particle size to the power of 7/3. Woodburn et al 1971 considered detachment to occur by sudden acceleration of a particle-bubble aggregate through eddy motion and found the probability of detachment to be proportional to the particle size to the power of 3/2. It has also been argued that once a stable three-phase contact is formed, the particle can only be pulled away by some external factor, such as the energy of the turbulent field. A particle-bubble aggregate caught in a turbulent eddy will rotate with a frequency appropriate to the eddy size, and if the kinetic energy of the particle exceeds the work of rupture, the particle will detach (Ahmed and Jameson, 1989). The efficiency of bubble-particle aggregate stability depends on the attachment force between the bubble and the particle in relation to the external stress forces, or detachment forces, in the environment. The description presented here follows the review in Nguyen and Schulze 2004. The stability of a particle-bubble aggregate is described by the combination of all the forces acting to detach the particle from the bubble (F_{det}) and the tenacity of the particle attachment (T). The stability efficiency is then described by the exponential relationship (Nguyen and Schulze, 2004):

$$E_s = 1 - \exp\left(\frac{T}{F_{\text{det}}}\right) \tag{2.38}$$

The Bond number is defined as the ratio of detachment to attachment forces. The corrected equation for the Bond number, simplified as the modified Bond number ($B_{O\text{-}m}$) by Goel and Jameson 2012. It can be expressed using Bond number (B_O) as follows (Schulze, 1993):

$$B_O = \left(\frac{T}{F_{\text{det}}}\right) \quad \Rightarrow \quad E_s = 1 - \exp\left(1 - \frac{1}{B_O}\right) \tag{2.39}$$

$$B_{O-m} = \frac{3.75\ d_p^2\ \circ_p\ £^{2/3} / d_b^{1/3}}{6\ \pm\ \sin^2(¯/2)}$$

The tenacity of particle attachment stems from the hydrophobicity of the particle and is given by:

$$T = 0.5®\ d_p \pm (1 - \cos¯) \tag{2.40}$$

where σ is the surface tension and θ is the contact angle. The detachment force in a turbulent environment can be considered to occur due to accelerative forces on the aggregate and is given as:

$$F_{\text{det}} = (\pi/6)(d_p^3(a+g)\Delta\rho) \tag{2.41}$$

where a is the acceleration of the aggregate due to the turbulence, g is the acceleration due to gravity and $\Delta\rho$ is the difference between the fluid density and particle density. The acceleration of the aggregate (a) due the movement of the fluid is calculated assuming that the aggregates have a centrifugal acceleration equivalent to the centrifugal acceleration of the turbulent eddies of similar size to the aggregate. In the inertial and viscous dissipation subrange of turbulence this is given as:

$$a = 1.9\frac{\varepsilon^{\frac{2}{3}}}{\left(\frac{d_p}{2}+\frac{d_b}{2}\right)^{\frac{1}{3}}} \quad \text{for inertial} \qquad a = 0.52\frac{\varepsilon^{\frac{3}{4}}}{\nu^{\frac{1}{4}}} \quad \text{for viscous} \tag{2.42}$$

In a typical flotation application the aggregate will likely be in the inertial subrange (see Table 2.1) and therefore Equation 2.42 will be applicable. Substitution of the tenacity (Equation 2.40) and the detachment forces (Equation 2.41) into Equation 2.38 gives the relationship:

$$E_s = 1 - E_d = 1 - \exp\left(1 - \frac{3\mu(1-\cos\theta)}{d_p^2(a+g)\Delta\rho}\right) \tag{2.43}$$

This model predicts increasing detachment with increasing energy input, increasing particle size, decreasing particle contact angle (hydrophobicity) and decreasing aggregate size. Another approach is to consider the energies associated with the aggregate. Sherrell 2004 used an Arrhenius type equation to describe the stability efficiency:

$$E_s = 1 - \exp\left(-\frac{W_A}{E_{k-D}}\right) \tag{2.44}$$

where W_A is the work of adhesion and $E_{k\text{-}D}$ is the kinetic energy of detachment. The work of adhesion is the energy required to separate a particle-bubble aggregate and as is given as (Mao and Yoon, 1997):

$$W_A = 0.25\pi\, d_P^2\, \mu\, (1-\cos\theta)^2 \tag{2.45}$$

$E_{k\text{-}D}$ has been calculated using the following relation (Do, 2010):

$$E_{k\text{-}D} = 0.5 m_p\left((d_p + d_b)\sqrt{\varepsilon/\nu}\right)^2 \tag{2.46}$$

where *v* is the kinematic viscosity. The energy available for detachment was considered to correspond to the kinetic energy of the largest eddies in the system, since all particles are subjected to these eddies and they contain the greatest amounts of energy for detachment. In the case of flotation of coarse particles, Tao 2004 deduced through a theoretical analysis that an increase in bubble size would produce an increase in the detachment efficiency of coarse particles. Therefore, the flotation of coarse particles can be enhanced using finer bubbles. On the other hand, if the bubbles are too small, they will not have enough buoyancy to levitate coarse particles. In general increasing detachment was observed with increasing particle size, energy input and with decreasing bubble size and contact angle.

2.3.1.4. Summary of Theoretical Findings

From the overview of this section it is evident that the particle size, bubble size, contact angle and the energy input are the most important physical and chemical factors affecting collection zone rate in flotation cells. Though many other chemical and physical factors appear in the various theories discussed in this section particle size, bubble size, contact angle and energy input consistently predominate in their influence on flotation rate. Consequently, theoretical findings applicable to the impact of these parameters on the subprocesses (Collision, Attachment and Detachment) of flotation are reviewed and are derived predominantly from the discussion in this section.

2.3.1.4.1. Effect of Particle Size

According to the fundamental flotation models the collision frequency is proportional to the sum of the particle size and bubble size (d_p is negligible) to the power of between 2.0 - 3.0. Models that have been derived suggest that collision efficiency reduces as particle size reduces, and that reduces the rate of flotation for the finest-size fraction. The analysis of collision in quiescent systems has shown the collision efficiency to be proportional to the particle sizes to the power of between 1.0 and 2.0 depending on the flow field. The analysis of collision in turbulent systems has focused on correlating the number of particle-bubble collisions to the sum of the particle and bubble sizes.

Attachment is considered to be more complex than collision and similar analyses have been applied to both quiescent and turbulent systems. The induction time has been shown to either remain constant or decrease with decreasing particle size. The contact time has been shown to increase with decreasing particle size for quiescent systems but has yielded conflicting results in turbulent systems. Some researchers have shown the contact time to decrease with decreasing particle size, others have calculated the contact time to be too short for attachment to occur while still others concluded that turbulence does not influence the contact time significantly. The attachment efficiency has been shown to increase with decreasing particle in both quiescent and turbulent systems.

The analysis of detachment is of relevance to turbulent systems only as buoyancy of the particle-bubble aggregate is of more relevance to quiescent systems than detachment effects. Initial research focused on particle size effects and found the detachment efficiency to be proportional to the particle size to the power of between 1.5 and 2.0. Subsequent research focused on predicting the stability of particle-bubble aggregates in terms of parameters such as particle size and density. From this analysis the detachment efficiency has been shown to increase with increasing particle size and density.

2.3.1.4.2. Effect of Bubble Size

According to the fundamental flotation models the collision frequency appears to suggest that the collision rate increases indefinitely with an increase in bubble size. However, because there is an upper limit of the bubble size, for a given local energy input, there is a maximum in the size of bubbles. Moreover, the equations for collision efficiency were proportional to the particle to bubble

size ratio to the power of 1.5 to 2.0. The analysis of collision in quiescent systems has shown the collision efficiency to be inversely proportional to of the bubble size to the power of between 1.0 and 2.0 depending on the flow field. This power was between 2.0 and 3.0 for analysis of collision efficiency in turbulent systems which the number of collisions was proportional to the sum of the particle and bubble sizes. Altogether with the complexity of the theoretical expressions for the effect of bubble size on the rate of flotation, it is not possible to present a simple relationship. The contact time has been shown to increase with decreasing bubble size for quiescent systems but has yielded conflicting results in turbulent systems. The attachment efficiency has been shown to increase with decreasing bubble size in both quiescent and turbulent systems. Some studies focused on predicting the stability of particle-bubble aggregates in terms of bubble size and contact angle. From these studies the detachment efficiency has been shown to increase with decreasing bubble size and decreasing contact angle.

2.3.1.4.3. Effect of Contact Angle

According to the fundamental flotation models contact angle has no effect on collision frequency and collision efficiency due to collision is mainly controlled by hydrodynamic properties (e.g., bubble size, energy input) in the flotation cell. Then under constant hydrodynamic conditions, the collision efficiency may be regarded as constant so that changes in the collection efficiency may be attributed to interfacial properties, nominally represented by the contact angle. Therefore attachment and detachment efficiency are influenced and dominated by contact angle between bubble and particle.

The stability of particle-bubble aggregates increases with the contact angle of particles in the pulp, reaching a peak at the maximum attainable contact angle of the collector-mineral system, characteristic of the collector hydrocarbon chain length and maximum adsorption density. The detachment efficiency is sensitive to both particle size and contact angle, with very fine particles (<10 µm) and coarse particles (>100 µm) floating poorly, but for different reasons. Coarse particles have low flotation rate due to detachment problems associated with disruptive forces in the flotation cell (Pyke et al., 2003), whereas fine particles' poor floatability emanates from low collision efficiency between bubbles and particles.

The energy barrier manifests as a critical contact angle, which represents the amount of activation energy that must be overcome before bubble–particle attachment can occur. For every particle size theoretical considerations published to date support the existence of a critical contact angle below which flotation does not occur (Blake and Ralston, 1985; Crawford and Ralston, 1988; Miettinen, 2007). The existence of a critical contact angle below which flotation recovery does not exist has been studied extensively by researchers such as Blake and Ralston 1985, Crawford and Ralston 1988, and Chipfunhu et al. 2011, using quartz particles in a mechanically agitated flotation cell. The critical contact angle increases as the particle size increases (Gontijo et al., 2007; Chipfunhu et al., 2011 and 2012; Awatey et al., 2013), or decreases as particle size decreases (Miettinen et al., 2010).

2.3.1.4.4. Effect of Energy Input

The variable which is considered to influence all of the subprocesses of flotation is energy/power input. At higher levels of the energy input velocity of suspended particles may increase due to the increased fluid velocity, which influences the adhesion angle. According to the fundamental flotation models the collision frequency is proportional to the energy input to the power of between 0.44 and 0.75. Models that have been derived suggest that particle-bubble collision increases as energy input increases, and that increases the rate of flotation at higher energy input. Furthermore, the attachment efficiency between bubbles and particles increases at higher energy input. However, there is an optimum for the energy input as it may have a negative impact on the particle-bubble stability efficiency of the coarse particles at the higher energy input. Some studies focused on detachment efficiency in terms of level of turbulence. This analysis has been shown detachment to increase with increasing energy input. The detachment efficiency has been shown to be proportional to the energy input to the power of between 0.66 and 1.0. It can be surmised that the rate of collision and attachment between bubbles and particles increases with increasing energy input; however, intense energy input causes bubble-particle detachment, which appears to control the collection process.

2.3.2. Experimental Findings

Over the past few decades there have been numerous studies where flotation rates/recoveries have been investigated as a function of energy/power input, particle size, bubble size and contact angle. In this section the findings from experimental studies on flotation kinetics are reviewed. This review is limited to those studies which investigated the effects of particle size, bubble size, contact angle and energy input on single mineral flotation rates, since these are relevant to this investigation.

2.3.2.1. Effect of Particle Size

The relationship between particle size and the flotation rate is well established in the flotation literature (Jameson et al., 1977; Deglon, 1998; Pyke et al., 2003). The general form of the relationship between particle size (d_p) and flotation rate (k) for fine particles (below the optimum size for flotation) can be described by the power equation $k \propto d_p^n$.

In an agitated cell, Gaudin et al. 1942 found that, for the flotation of galena with particle sizes above 4 µm, the value of n was 1. For particles below 4 µm, the flotation rate was independent of particle size. Bruyn and Modi 1956 found n to be between 1.0 and 3.2 for quartz flotation for the -65 µm and 79-254 µm size ranges respectively. An exception to the general trend of a strong dependence of the flotation rate on particle size was evidenced by the work of Cameron 1962 who found this to be independent of particle size. Tomlinson and Fleming 1963 conducted flotation tests on apatite, haematite, galena and quartz in a Hallimond tube and found n to be 1 for quartz it was 2 for the other minerals. Reay and Ratcliff 1975 found n to be 0.44 for flotation of -5 µm latex particles in a stirred cell with very small bubbles. Jameson et al. 1977 reviewed various literature studies (Reay and

Ratcliff, 1975; Collins and Jameson, 1976; Anfruns and Kitchener, 1977) on the effect of particle size on flotation rates in quiescent systems. It was concluded that, for fine particles (4 µm < d_p <30 µm) floated with sub 100 µm bubbles, the value of n was 1.5. However n was 2 for larger bubbles (600 µm < d_b <1000 µm) and intermediate particles (10 µm < d_p <50 µm).

Trahar 1981 investigated the batch flotation of several sulphide minerals, and found a roughly linear relationship between the flotation rate and particle size, for -20 µm particles floated with excess collector. Ahmed and Jameson 1985 floated latex, quartz and zircon in a stirred cell, and found that there is a weaker relationship between particle size and the flotation rate (n < 1) than previous Jameson work (Jameson et al., 1977). Similar findings were reported by Luttrell 1986 in the flotation of -8 µm quartz, Spears and Jordan 1989 in the flotation of -40 µm galena and Jordan and Spears 1990 in the flotation of -20 µm chalcopyrite. Crawford and Ralston 1988 used methylation techniques to render 15 to 125 µm quartz particles hydrophobic to various contact angles. A linear relationship between flotation rate and particle size was found, for particles with contact angles from 50° to 88°. Deglon 1998 found n to be 0.15 and 0.38, for the flotation of -32 µm and -100 µm quartz, respectively. Pyke et al. 2003 found that, for quartz flotation at low energy inputs, the relationship is approximately linear. Changunda et al. 2008 found that n = 1 for all bubble sizes for -100 µm quartz at an energy input of 0.44 kW/m^3. After Changunda, Massey et al. 2012 also used an OGC for quartz flotation and he found a value of approximately 0.7 for n, at an energy input of 0.5 kW/m^3.

2.3.2.2. Effect of Bubble Size

It is well established in the flotation literature that flotation rates increase with decreasing bubble size. The relationship between the flotation rate (k) and the bubble size (d_b) is commonly expressed as the inverse power equation $k \propto d_b^{-m}$ (Jameson et al., 1977; Gorain et al. 1997, 1998; Deglon, 1998).

In two of the first studies on bubble size, Bennet et al. 1958 and Brown 1965 found that decreasing the bubble size led to an increase in the flotation rate for coal particles. Reay and Ratcliff 1975 found m to be 0.44 and 1.5 for latex and quartz respectively while Anfruns and Kitchener 1977 found m to be 2.69 for the flotation of glass beads and quartz. Jameson et al. 1977 reviewed the literature (Reay and Ratcliff, 1975; Collins and Jameson, 1976; Anfruns and Kitchener, 1977) and found a value for m of 3, for flotation in quiescent systems with sub 100 µm bubbles. However m was 2.67 for larger bubbles (600 µm < d_b < 1000 µm) and intermediate particles (10 µm < d_p < 50 µm). It is likely that for each type of ore treated in a flotation machine there exists an optimum bubble size distribution that will produce the optimum recovery at the highest flotation rate. The ability to control the generation of bubbles in order to produce an optimum size range in a flotation cell appears to be highly attractive, since it may enhance flotation efficiency. Schubert and Bischofberger 1978 found that decreasing the bubble size led to an increase in the flotation rate of tin in both laboratory and industrial mechanical flotation cells. Ralston 1983 based on industrial results concluded that the value for m is close to 1.

Ahmed and Jameson 1985 concluded from batch flotation tests conducted in a small flotation cell that the flotation rate of fine particles is never as strongly dependent on the bubble size as in quiescent conditions. They found a value for m of 1.67, for fine quartz particles (25 µm < d_p < 40 µm) at a low agitation speed, while at a higher energy input, the effect of the bubble size appears to become weaker (m=1.46). They determined that in a stirred cell the relationship between flotation rate and bubble size is never as strong as in quiescent systems. Nevertheless, higher flotation rate observed at bubble sizes below 200 µm. When decreasing bubble size from 650 µm to 75 µm at low agitation speeds, a thirty fold increase in the flotation rate was observed. Yoon and Luttrell 1986 found the value of m to be 2.1-2.3, for fine coal flotation with 300 to 450 µm bubbles. In a later study Yoon and Luttrell 1989 found a dramatic increase in the flotation rate when using -100 µm bubbles in a quiescent system. Diaz-Penafiel and Dobby 1994 found the value for m was between 1.15 and 2.08 for the 5 to 40 µm silica particles in a column cell when m was 1.54 for -50 µm particles with bubble sizes from 800 µm to 2000 µm.

Gorain et al. 1997, 1998 found that the collection zone flotation rate is linearly correlated with S_b, the average bubble surface area flux in a flotation cell, This model has been criticized by Heiskanen 2000 due to the fact that a very fine zinc rougher concentrate was used in the tests. Nevertheless, Gorain found a value of 1 for m which indicated that the rate of flotation in industrial flotation cells varies as d_b^{-1}, which is a weaker dependency than the one predicted using the interceptional collision models. Deglon 1998 floated -32 µm quartz particles in a stirred cell, and found a value for m of 2.2, at low energy input. Later Deglon et al. 1999 found a value of 1.6 for m. In deinking flotation, Julien Saint Amand 1999 observed a value for m of 1.5, for the flotation of -50 µm ink particles. Changunda et al. 2008 floated -100 µm quartz particles in an oscillating grid cell and found a value of 0.75 for m, at an energy input of 0.44 kW/m^3. After Changunda, Massey et al. 2012 also used an OGC for quartz flotation and he found a value of approximately 0.9 for m, at an energy input of 0.5 kW/m^3.

2.3.2.3. Effect of Contact Angle

There is a considerable body of experimental evidence to suggest that contact angle plays an important role in flotation kinetics. The rate of flotation is dependent on the contact angle range and particle size fraction when the hydrodynamics are constant. For each particle size fraction and contact angle range, there is a nonfloating component which decreases with an increase in the contact angle. It would appear that the nonfloating component in each size fraction has a contact angle at or less than the critical required for stable bubble-particle attachment. A critical contact angle appears for all size fractions, with the fine and coarse size fractions having apparently greater values than intermediate size fractions (Crawford, 1986; Miettinen et al., 2000; Gontijo et al., 2007). Generally flotation rate of the mineral particles increases with an increase in the contact angle. The magnitude of the increase in flotation rate with unit increase in contact angle is particle size dependent (Muganda et al., 2008).

2.3.2.4. Effect of Energy Input

Many experimental studies have been performed in order to gain knowledge on the effect of energy /power input on flotation kinetics. A selection of these studies is summarized in Table 2.5. In some of these studies the bubble size is controlled independently of the energy input, so as to decouple the effect of energy input and bubble size. The majority of these studies have been conducted in stirred cells. Two studies have used oscillating grid flotation cells. Changunda et al. 2008 used an OGC flotation cell but was limited to an energy input of 0.6 kW/m^3 which is lower than typical energy input used in both the flotation literature and industrial mechanical cells. The energy input could vary for different minerals or different particle size distributions. The typical range of the energy input for copper flotation is between 1.2 and 1.5 kW/m^3, and for platinum flotation is 3 kW/m^3 (Nelson et al., 2002). Massey et al. 2012 used a laboratory OGC at energy inputs of up to 5 kW/m^3.

Table 2.5: Experimental studies on the effect of energy input on flotation kinetics

Author	Ore	Flotation Cell	Hydrophobicity	Av. Energy Input(kW/m^3)	Particle Size (µm)
Ahmed and Jameson1985	Quartz-Zircon	Stirred Cell	Moderate collector dosage	0.01 - 2.5*	< 50
Breytenbach 1995	Quartz	Agitated Column	Moderate collector dosage	0 - 7.2	< 150
Deglon 1998	Quartz	Stirred Cell	Low collector dosage	0.1 - 1.9	<100
Ityokumbul et al. 2000	Pyrite	Agitated Column	Moderate collector dosage	0 - 3	< 25
Pyke 2004	Quartz-Galena	Stirred Cell	Contact angle of 53 ˚- 80 ˚	0.45 - 1.8	< 75
Newell and Grano 2006	Quartz	Stirred Cell	Contact angle of 80 ˚	0.15 - 1.8*	< 100
Changunda et al. 2008	Quartz	OGC	Contact angle of 65 ˚	0.015 - 0.6	< 120
Anderson et al. 2009	Quartz	OBC	Low and moderate collector dosage	0 - 0.225	< 104
Jameson 2010	PGM	Concorde Cell	Moderate collector dosage	100	< 53
Jameson 2010	Galena	Fluidized Bed	Moderate collector dosage	0.09	<1400
Tabosa 2012	Copper	Stirred Cell	Moderate collector dosage	1 - 7.5	< 300
Massey et al. 2012	Quartz	OGC	Low and moderate collector dosage	0.5 - 5	< 74
Amini 2012	Copper	Stirred Cell	Moderate collector dosage	1 - 5	< 90
Safari et al. 2016	Three Sulphide Three Oxide	OGC	Low, moderate and high collector dosage	0.5 - 3 0.1 - 2	< 150 < 650

*** From Anderson (2008), assuming a power number of 5.5 for a six bladed Rushton turbine.**

2.3.2.4.1. Stirred Cells

In one of the first studies on effect of energy, Sun and Zimmerman 1950 investigated the effects of impeller speed on the flotation of coal and galena. An optimum in recovery as a function of both impeller speed and particle size was found and observed to move to lower impeller speeds with increasing particle size. Mackenzie and Matheson 1963 found an increase in the rate of flotation with increasing impeller speed for individual particle size fractions. Kirchberg and Topfer 1965 confirmed this finding but also observed an optimum in impeller speed after which the rate of flotation began to decrease. Harris and Raja 1970 concluded that high energy inputs lead to high rates of flotation. Schubert and Bischofberger 1978 found an increase in the recovery of tin with increasing impeller speed and established optimum energy inputs for different particle size fractions. Bogdanov et al. 1980 found an optimum in the flotation rate constant as a function of both impeller speed and bubble size

for -10 µm martite. The optimum was found to occur at the highest impeller speed used in the study for 200 µm bubbles while increasing impeller speed resulted in a continual decrease in the flotation rate constant for 800 µm bubbles. Malhotra et al 1980 performed flotation tests on molybdenite in a mechanical flotation cell and found an increase in the rate of flotation with increasing impeller speed for fast floating particles but observed no response for slow floating particles. Schubert et al. 1982 postulated that the flotation of fine particles is primarily limited by collision and concluded that fine particle recovery could be improved by energy input. Schubert considered fine particles to damp turbulence at high percent solids thus limiting the collision process further. Varbanov 1984 performed flotation tests on 63 to 500 µm glass spheres in a mechanical flotation cell and found a distinct optimum in recovery as a function of both impeller speed and particle size. Ahmed and Jameson 1985 found an optimum in the flotation rate constant as a function of impeller speed, particle size, bubble size and particle density. An increase in energy input was found to lead to a decrease in flotation rate for large or dense particles and small bubbles. They hypothesised that the decrease in the flotation rate constant was due to increased particle-bubble detachment through small bubbles being subject to rapid rotation on being caught up in small, high frequency eddies.

Schulze et al. 1989 suggested that improved flotation performance could be obtained in quiescent environments as the collision in mechanical flotation cells was considered to result in insufficient contact time for attachment. Scheiner and Jordan 1989, Jordan and Spears 1990 investigated the effects of turbulence on flotation kinetics in a batch flotation cell agitated by a standard impeller and a spinning disc impeller. The flotation rate constant was found to increase with increasing energy input for both impellers. Jordan and Susko 1992 studied the flotation of coal and proposed that turbulence should lead to improved flotation performance in mechanical cells. Li et al 1993 found an increase in the flotation rate of both quartz and galena with increasing impeller speed in a batch flotation cell.

Most of these studies have demonstrated that increasing energy input improves the flotation rate of fine particles (Schubert and Bischofberger, 1978; Ahmed and Jameson, 1985; Jordan and Spears, 1990; Deglon, 2002; Pyke et al., 2003; Newell and Grano, 2006; Schubert, 2008; Tabosa et al., 2010, 2012, 2016). The majority of these studies have been for normal flotation bubbles and the few studies on microbubbles have found that far lower levels of energy input are required for optimum flotation (Ahmed and Jameson, 1985; Deglon, 2002). Some studies have attempted to quantify the increase in the rate of flotation with increasing energy input. Ahmed and Jameson 1985, 1989 were the first to use a system where small bubble generation was decoupled from the impeller speed. This was achieved by sparging a stirred cell with bubbles of a known size. In the study, -50 µm latex, zircon and quartz particles were floated using bubble sizes ranging from 0.07 mm to 0.65 mm. It was found that the flotation rate increased with increased impeller speed, for all particle and bubble sizes used. The dependence of flotation rate on impeller speed was found to be higher when floating with larger bubbles. The results for quartz flotation, using cetyl trimethyl ammonium bromide (CTAB - 2.5 ppm) as the collector, are reproduced in Figure 2.13, for three impeller speeds and three bubble sizes.

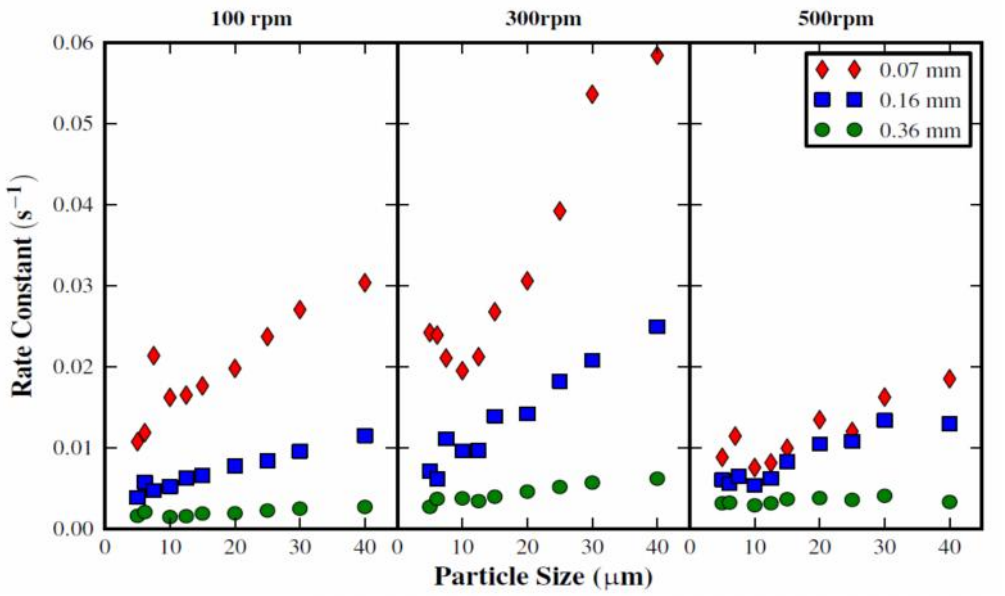

Figure 2.13: Flotation rate constant versus particle size for the flotation of quartz (2.5 ppm CTAB) in a stirred cell, at three agitation rates and bubble sizes (adapted from Ahmed and Jameson, 1985)

Figure 2.13 illustrates that the flotation rate when using sub 0.36 mm bubbles increases with increasing agitation, until an optimum agitation rate (approximately 300 rpm), after which the flotation rate decreases. The flotation rate decreases, when the agitation rate is increased from 300 rpm to 500 rpm and increases with decreasing bubble size. Flotation with large bubbles (0.65 mm) resulted in increasing flotation rates with increased agitation, for all agitation rates used. Similar trends were noted for the flotation of zircon. These trends were attributed to increased detachment rates with increased energy input and decreased bubble size. It was recommended that the optimum conditions for flotation involves small bubbles and the minimum impeller speed required for particle suspension (Barbery, 1984; Schubert, 1985; Weiss and Schubert, 1989; Westhuizen and Deglon, 2007).

Deglon 1998 investigated the effect of energy input on flotation, in a stirred cell similar to that used by Ahmed and Jameson 1985, and sparged with discrete bubble sizes of 0.13 mm, 0.24 mm and 0.82 mm. Quartz (-32 µm and -100 µm) was floated using hexadecyl pyridinium chloride (HPYC) (1.6×10^{-5} mol/L) as a collector. The results for flotation of -100 µm quartz, using 0.13 and 0.82 mm bubbles, are reproduced in Figure 2.14. Deglon showed that the flotation rate increases with increasing energy input to an optimum, after which the flotation rate decreases. These optimum flotation conditions are dependent on the bubble size used, with optimum energy inputs of 0.65 and 1.5 kW/m^3 observed, for flotation with 0.13 mm and 0.82 mm bubbles respectively. It is clear from Figure 2.14 that the optimum flotation conditions are small bubbles and low energy inputs. Further analysis of the data showed that the relationship between flotation rate and energy input followed the form $k \propto \varepsilon^{0.91}$ (Deglon, 2002). Rodrigues et al. 2001 and Leal et al. 2002 and recently Tabosa et al. 2016 also obtained a strong relationship between recovery and energy input in their studies. They showed that the overall recovery increases with an increase of mean energy input until a maximum is reached above which any excess in energy input decreased the flotation recovery.

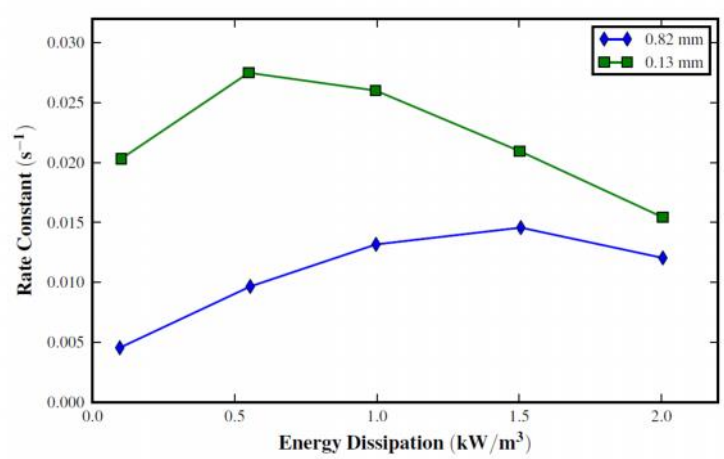

Figure 2.14: Flotation rate constant versus energy input for the flotation of quartz -100 µm in a stirred cell, for 0.13 mm and 0.82 mm bubbles (adapted from Deglon, 1998)

Pyke 2004 investigated the effect of energy input on flotation of quartz, chalcopyrite and galena in a stirred cell and sparged with bubbles of approximately 1.2 mm. The flotation of methylated quartz (-75 µm), with a contact angle of 73°, resulted in decreasing flotation rates for all particle sizes, when the energy input was increased from 0.45-1.45 kW/m^3. However quartz with a contact angle of 80° resulted in flotation rates for fine particles which remained relatively constant, when the energy input was increased from 0.45-1.8 kW/m^3. The flotation rates for coarse particles decreased with increasing energy input over the same range. These results indicated that the effect that energy input on flotation kinetics was dependent on both the particle size and particle hydrophobicity. Flotation rates decreased, or stayed constant, with increased energy input above 0.45 kW/m^3, this indicates that the optimum energy input for flotation in the system was less than 0.45 kW/m^3. This is low compared to the optimum energy input of 1.5 kW/m^3 found by Deglon 1998 for similar conditions. Pyke showed that galena flotation rate for coarse and intermediate particle size is substantially higher than that of chalcopyrite or quartz particles (Figure 2.15a). Figure 2.15b shows the influence of energy input at the same contact angle, bubble size and velocity for three minerals.

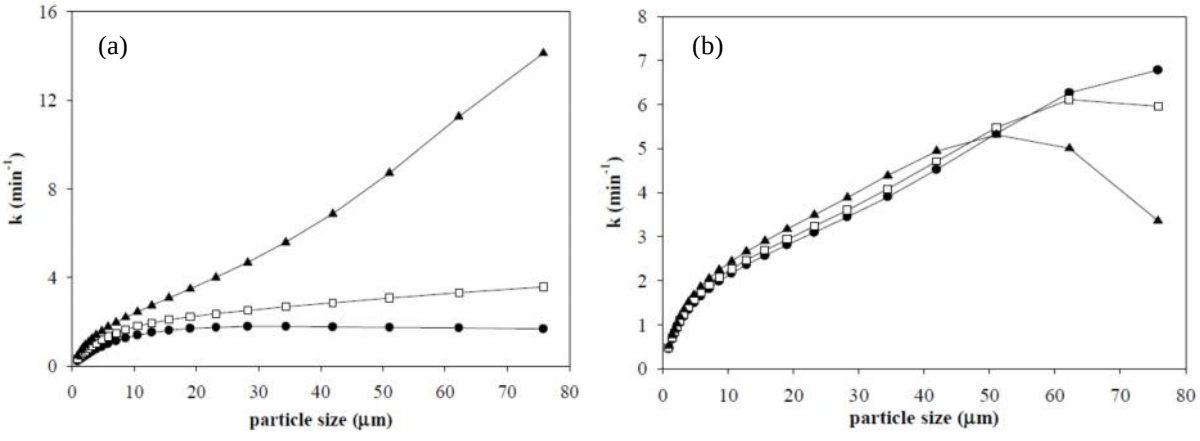

Figure 2.15: (a) Effect of density on flotation rate constant (õ quartz : 2.65 g/cm^3, □ chalcopyrite :4.1 g/cm^3, ▲ galena :7.4 g/cm^3), (b) Effect of turbulence on flotation rate constant (õ 2 m^2/s^3, □ 3 m^2/s^3, ▲ 6 m^2/s^3) Parameters: $\bar{}_a$ = 60 °, Gas flow rate = 5.5 dm^3/min, d_b = 0.12 cm, v_b = 18 cm/s (Pyke, 2004)

Chalcopyrite (density of 4100 kg/m^3) was floated using 100 g/t SEX, which produced particle advancing contact angles of 67°. It was found that the flotation rates for -75 µm particles increased when the energy input was increased from 0.6-1.7 kW/m^3. Galena (density of 7400 kg/m^3) was floated using 10 g/t DBPhos, which resulted in particle advancing contact angle of 72°. It was observed that flotation rates for -75 µm particles increased as the energy input was increased from 1.2-1.7 kW/m^3, however the magnitude of the increase was significantly smaller for coarse particles. Subsequent increases in the energy input resulted in decreased flotation rates for all particle sizes due to increases of detachment forces. It was concluded that the greater density of the galena particles results in a decreased stability of the galena particle bubble aggregates and increased detachment rates compared with quartz particles at similar turbulence levels. The decrease in flotation rate constant of coarse particles observed in Figure 2.15b is due to a decrease in bubble-particle aggregate stability.

Some studies have attempted to quantify the increase in the rate of flotation with increasing energy input. Nonaka et al. 1982, Saint Amand 1999 and Deglon 2002 found that the rate of flotation increases with the energy input to the power of 0.75, 0.50 and 0.91 respectively; while Newell and Grano 2006 found that this is approximately proportional to the level of agitation. They measured the flotation rates of methylated quartz particles, in geometrically similar stirred cells with volumes ranging from 2.25-50 dm^3, in order to assess scale-up parameters for flotation cells. In the experiments, 0.65 mm bubbles were used to float quartz with an advancing contact angle of 80°. It was found that increasing the energy input led to a linear increase in flotation rate (i.e. $k \propto \varepsilon^1$), to an optimum at 4.1 kW/m^3. After this optimum the flotation constant was independent of the energy input.

2.3.2.4.2. Oscillatory Baffled Column

The oscillatory baffled column (OBC) is a novel cell developed by Anderson 2008, who investigated its use both as a research tool and as a potential industrial cell. The oscillatory baffled column is composed of many circular baffles, which are oscillated vertically in a column in order to produce the agitation. In his study, -100 µm quartz was floated using a fixed bubble size of 0.6 mm. Energy inputs of 0.004-0.22 kW/m^3 were investigated. These were controlled by changing the oscillating frequency and amplitude of the baffle cage. Particle hydrophobicity was varied by using HPYC (1.6×10^{-5} mol/L) and dodecylamine (1×10^{-4} mol/L) as collectors, to produce low and moderately hydrophobic particles respectively. When using low hydrophobicity quartz, the flotation rates for -36 µm particles increased with increasing energy input to an optimum at approximately 0.01 kW/m^3. This optimum energy input was an order of magnitude lower than the value of 0.65 kW/m^3 observed by Deglon 1998 in a stirred cell using identical collector surface coverage conditions. The flotation rates for particles greater than 36 µm decreased for all energy inputs used. The results for the flotation of moderately hydrophobic quartz are reproduced in Figure 2.16.

It is illustrated in Figure 2.16 that the flotation rate constant for -36 µm particles increases with increasing energy input, up to approximately 0.05 kW/m^3, beyond which the flotation rate is

independent of energy input. Particles greater than 36 µm display optimum flotation rates at an energy input of approximately 0.05 kW/m^3, after which the flotation rate decreases with increasing energy input. This optimum energy input was higher than observed for low hydrophobicity quartz, although it was still an order of magnitude lower than those found using stirred cells. The large difference between the optimum energy input found in the oscillatory baffled column and in stirred cells was proposed by Anderson 2008 to be due to the oscillatory flow imparted on the fluid by the baffles, resulting in an additional fluctuating velocity in the system. This was thought to result in high root mean squared (RMS) velocities in the fluid, leading to high RMS velocities for particles and bubbles at relatively low energy inputs. It was shown that increasing the RMS velocities of particles and bubbles results in increased flotation rates. The OBC was therefore speculated to increase particle-bubble contacting at considerably lower energy inputs than in conventional cells.

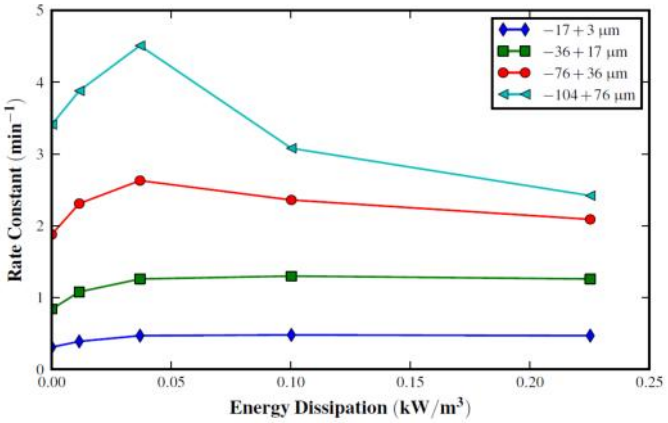

Figure 2.16: Flotation rate constant versus energy input for the flotation of moderately hydrophobic quartz in an oscillatory baffled column, for four particle size classes (adapted from Anderson, 2008)

2.3.2.4.3. Oscillating Grid Cell

Changunda et al. 2008 investigated the effect of energy input on the flotation of quartz in a laboratory OGC. Flotation experiments were performed using quartz (P_{80} = 100 µm) which was methylated to an advancing contact angle of 65°. Bubble sizes of 0.13 mm, 0.24 mm and 0.82 mm, and energy inputs of 0.015-0.60 kW/m^3, were used in the investigation. Flotation results for the -48 +26 µm particle size class are shown in Figure 2.17. This Figure illustrates that the flotation rate increased approximately linearly with increased energy input (i.e. $k \propto \varepsilon^1$), for the three bubble sizes used. Similar trends were observed for all particle sizes used in the study. This linear relationship was higher than many theoretical studies have indicated (Nonaka et al., 1982; Julien Saint Amand, 1999). However, Newell and Grano 2006 noted a similar linear relationship between energy input and flotation rate in an experimental study. Anderson et al. 2009 presented similar linear correlation for lower energy input values. By increasing the energy input the flotation rate constant remained constant for finer particles but dropped for the coarser fraction.

It was observed by Changunda et al. 2008 that increase in the flotation rate with increasing energy input was approximately equal for the three bubble sizes used. Similar trends, with regard to changing

bubble size, were noted for all particle sizes used. In order to discuss the role of particle size on the effect that energy input has on flotation kinetics, the results for the flotation of three particle sizes with 0.24 mm bubbles are reproduced in Figure 2.18. This figure illustrates that increase in the flotation rate with increasing energy input (the slope of the line) increases with increasing particle size. The effect that energy input has on the flotation kinetics is therefore dependent on the particle size being floated. An exception to this trend was the flotation rates for coarse particles floated with small (0.13 mm) bubbles, where increasing energy input resulted in flotation rates remaining relatively constant. This effect was attributed to a combination of buoyancy and detachment effects. From these results, Changunda proposed that the effect of energy input on flotation rate was dependent on the particle size, but was less dependent on the bubble size.

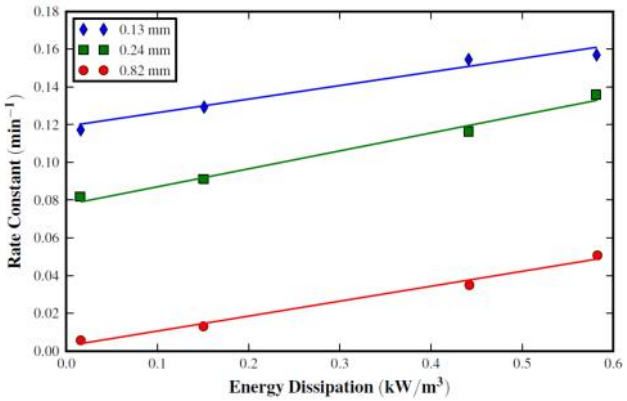

Figure 2.17: Flotation rate constant versus energy input for the flotation of -48 +26 µm quartz in an oscillating grid cell, for three bubble sizes (adapted from Changunda et al., 2008)

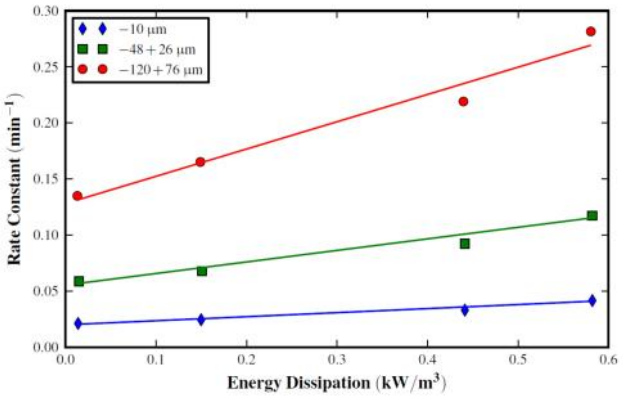

Figure 2.18: Flotation rate constant versus energy input for the flotation of quartz in an oscillating grid cell, for 0.24 mm bubbles and three particle size classes (adapted from Changunda et al., 2008)

Experiments conducted in stirred cells and the OBC have shown that increasing energy input results in increased flotation rates to an optimum, beyond which the flotation rate decreases with increasing energy input. This optimum is thought to be the point where the rate of detachment becomes greater than the rate of increased particle-bubble collisions. It is clear from Figures 2.17 and 2.18 that this optimum is not observed in OGC, indicating that there is negligible detachment occurring due to the low energy inputs used in Changunda study. The effects of detachment clearly observed in Massey et al. 2012 study, with increasing energy input. Massey et al. 2012 investigated the relationship between

the flotation rate constant and energy input up to 5 kW/m^3, in a laboratory OGC. The results for quartz flotation and for three different bubble and particle sizes are shown in Figure 2.19. The highest flotation rates are obtained using small bubbles at low power intensities. With larger bubbles, flotation rates generally increase with increasing energy input, up to around 2-3 kW/m^3. The deviation from the near linear increase in the flotation rate with energy input is attributed to particle–bubble detachment. Detachment rates increase significantly with increasing energy input. These results are different to the linear trends in the flotation rate with increasing power observed by Changunda. However, there power intensities were limited to 0.60 kW/m^3, which fit to the start of Massey's results in Figure 2.19. Massey et al. 2012 showed that the effect of energy input on flotation kinetics is strongly dependent on both particle and bubble size. He showed the flotation rate for fine particles increases with energy input to the power of 0.9 and 0.7, for flotation with 0.24 and 0.82 mm bubbles respectively.

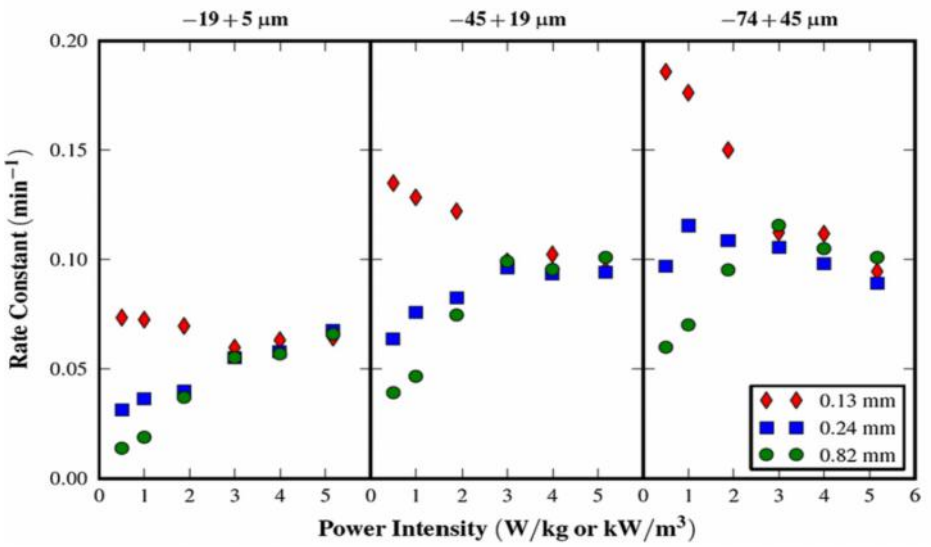

Figure 2.19: Flotation rate constant versus power intensity for all bubble and particle sizes (Massey et al., 2012)

2.3.2.5. Summary of Experimental Findings

Over the past few decades there have been numerous studies where flotation rates/recoveries have been investigated as a function of particle size, bubble size, contact angle, particle density and energy/power input. The relationship between the flotation rate and particle size can be described by $k \propto d_p^n$, where n is 1.0-1.5 in quiescent systems, and 0.3-1.0 in turbulent systems. The relationship between the flotation rate and bubble size is commonly described by $k \propto d_b^{-m}$, where m is 1.1-3.0 in quiescent systems, and in the range of 0.4-2.2 for turbulent systems.

The effect of increasing energy input is generally to increase the flotation rate to an optimum, beyond which increasing the energy input results in decreasing flotation rates. At energy inputs below the optimum, the relationship between energy input and flotation rate can be described by $k \propto \varepsilon^N$, where N is in the range 0.7-1.0. The optimum energy input is in the range of 0.05-5 kW/m^3, and appears to be a function of particle size, bubble size, particle hydrophobicity and contacting environment. In general the highest flotation rates are achieved when floating with fine bubbles at low energy inputs.

2.4. Flotation Modelling

Researchers for many decades have attempted to model the flotation process in an effort to better understand, control and improve the performance. Numerous research studies have been performed to find an appropriate model to predict performance in flotation circuits (Gaudin, 1957; Bascur et al., 1983; Deng et al., 1996; Dobby and Savassi, 2005; Barnwal, 2006; Zheng et al., 2006). The challenge in this field is to develop more comprehensive kinetic expressions which include parameters such as particle size, bubble size, particle hydrophobicity (contact angle), particle density and energy input etc. These models have ranged from fully empirical through to the more fundamental investigations of single bubble-particle interactions. King 1973 categorised the flotation models into three groups of empirical, phenomenological and fundamental. In this literature study, the methodologies to extend the flotation modelling are categorised into four groups of fundamental, kinetic, phenomenological and empirical models.

Fundamental models incorporate physical understanding of the process and often predict the performance reasonably accurately, but it is generally difficult to obtain all the parameters necessary, and often some are fitted by empirical relationships. Kinetic models, as the name suggests are models, which are based on flotation kinetics. Kinetic models are suitable for flotation modelling, because they are capable of representing the complex subprocess of flotation in a more complete way compared to most other types of models. The phenomenological models links parameters such as flotation rate constant to properties of the flotation micro environment and is between empirical and fundamental models. Phenomenological models are expected to show higher extrapolation capability in comparison with empirical models, which can be an important advantage for process optimization and product development. The more simplified, empirical models are purely mathematical curve fitting and generally easy to generate the necessary data, but the capability of predicting performance when some part of the process has changed is often lacking.

2.4.1. Fundamental Models

Historically, a large number of fundamental models have been developed to describe the flotation process. Fundamental studies which utilise the relevant models describing particle-bubble collision frequency and collection efficiency have been conducted, to derive general flotation models for turbulent systems. In general, the role of energy input (power/agitation) investigations in order to promote particle-bubble contacting, have been restricted to the development of fundamental models which are difficult to validate experimentally. A variety of fundamental flotation models have been developed over a long time to model the flotation rate constant by considering flotation subprocesses in a flotation process such as particle size, bubble velocity and size, gas flow rate, contact angle/particle hydrophobicity, viscosity, turbulence, energy input and other parameters, which some of them discussed in previous sections (Sutherland, 1948; Gaudin, 1957; Reay and Ratcliff, 1973; Yoon and Luttrell, 1989; Schulze, 1989; Nguyen, 1997). Ahmed and Jameson noted that most of these

studies reported their data for idealised conditions. Numerous equations have been developed to explain the flotation subprocesses (Dobby and Finch, 1990; Nguyen and Schulze, 2004; Pyke, 2004; Newell, 2005; Koh and Schwarz, 2006; Miettinen, 2007). Some of these models are applied in very low bubble Reynolds number conditions, which is not always the case in a flotation cell. Reynolds number changes in a wide range between 0.5 to 400 depending on how far the bubble is from the impeller (Nguyen and Schulze, 2004).

Bloom and Heindel (2002 and 2003) developed a population balance model to include both attachment and detachment phenomena that can be considered as the equivalents of forward and reverse reactions. They give kinetic rate of attachment ($Z_1P_cP_aP_s$) and the kinetic rate of detachment as the product of a frequency (Z_2), and a probability of destabilization ($1 - P_s$). The frequency originates from theoretical analysis of floc break-up, which assumes that it is only turbulent eddies of the size of the floc (or in this case bubble–particle aggregate) that can result in breakage. Unfortunately, the two factors (Z_2 and $1 - P_s$) involve some of the same considerations related to breakage of the aggregate by turbulence eddies, so it is unclear whether some effects may be accounted for twice in simply multiplying the two factors as done by Bloom and Heindel. Clearly, there is need for an integrated theoretical analysis, complemented by numerical simulations and experimental investigations. Also, particle collision and detachment frequencies in flotation have been related to the turbulent energy density (Bloom and Heindel, 2002; 2003).

A general flotation model for bubble-particle capture occurring within a turbulent environment was reported by Pyke et al. 2003, which was based on the Abrahamson model (Equation 2.17) for collision frequency, along with the Liepe and Mockel model (Equation 2.19) for the particle RMS velocity, and the Lee and Erickson model (Equation 2.20) for bubble RMS velocity. The collision efficiency was described by the generalised Sutherland equation, the attachment efficiency by the modified Dobby and Finch model (Equation 2.33), and the stability efficiency by the Schulze model (Equation 2.38). The general flotation model was used to calculate the theoretical flotation rate. The results showed good agreement between the experimental and calculated flotation rates, when the values for the bubble velocity and energy input used in the calculation corresponded to those measured away from the impeller zone of the flotation cell.

Another flotation model was derived by Sherrell 2004. It was found that the model predictions showed reasonable agreement with experimental data from the flotation of glass beads with varied contact angles, percent solids and energy inputs. The greatest discrepancies between the experimental and theoretical flotation rate constants occurred when the flotation experiments were conducted at a high percent solid, using large particles with low contact angles. Newell and Grano 2006 fitted the fundamental model derived by Pyke et al. 2003 to quartz experimental data, in different sized batch cells, operating at various energy inputs. It was found that using the measured bubble rise velocity in the model calculations resulted in the model underestimating the experimental flotation rates. The model was therefore fitted to the experimental data using the bubble velocity as a variable.

The fundamental flotation models are developed based on fundamental physical methodologies and laws, which are their most considerable advantage. The majority of the models are physically meaningful and the dimensions of the models are balanced at both sides of the equation. The models contain parameters that represent the physical properties of the flotation micro environment. However, a large number of data points are required to produce statistically significant parameters. The assumptions that have been made to generate the models may not be realistic. For instance, all the particles are assumed to be perfectly spherical, liberated and the surfaces equally hydrophobic. Bubble overloading and the competition between particles with different mineralogy and size are neglected. Most of the equations contain a large number of variables that cannot be easily measured. Even the measurable parameters cannot be measured with an acceptable level of precision in an industrial environment. Thus, the final error on the calculated flotation rate constant may be large due to accumulation of error for the various parameters. Therefore, these models have not been widely applied for the design or optimization of industrial flotation circuits due to the difficulty of making the necessary measurements and complexity of their application to industrial circuits. Compared to other type of models (kinetic, phenomenological and empirical models), these models have more parameters to calculate the flotation rate constant, which are often difficult to measure. They require detailed information about the turbulence and proper estimation of contact angle or hydrophobicity which is difficult to obtain in a three-phase industrial flotation cell. In spite of these shortcomings, well-developed fundamental models make an important contribution to the understanding of flotation from first principles.

2.4.2. Kinetic Models

Several approaches have been developed to predict the rate of flotation using kinetic models. Early attempts focused on developing an understanding of the subprocess of flotation, but as far back as the 1930's, researchers realised the importance of the kinetics of flotation. The representation of the flotation process as a kinetic reaction began when a number of researchers observed a strong similarity between the rate of flotation and a first-order chemical process. Since then, the recovery of particles in the pulp of a flotation cell is calculated as a function of a first order rate constant and the mean residence time. Kinetic models, as the name suggests are models, which are based on flotation kinetics. The first attempt at modelling flotation kinetics was by Zuninga 1935 who found that experimental flotation data could be accurately represented by a simple first-order kinetic model. Jameson et al. 1977 assumed that the rate of removal of particles in the vessel was a direct function of the number concentration of particles N_p, as given in Equation 2.47 which is the most commonly described first order flotation kinetic model (n=1) in literature.

$$\frac{dN_p}{dt} = -kN_p^n \tag{2.47}$$

where k is the flotation rate constant and N_p is the number of particles per unit volume. Subsequently, numerous researchers have modelled flotation using the types of kinetic expressions represented by Equation 2.47. The order of the rate equation (n) has been a subject of active debate over the years and has been found to vary between 0 and 2.8 depending on the system being studied. The arguments for non first order expressions have been found to be largely empirical and have generally been rejected in favour of the first order expression (Fichera and Chudacek, 1992).

However, it is not realistic to only have one flotation rate constant because the particles in a stream are different in terms of size and their association with other minerals, and they transfer at different rates. Kelsal 1961 took a new approach and put the floatable materials into two major categories of slow and fast floating. To incorporate the physical characteristics of the particles, King categorised the particles in the feed into different size and liberation classes (King 1973, 1976 and 1978). Most of the kinetic models have been developed for the forward rate process (i.e. collision-attachment), however Deglon developed a kinetic expression for a forward and reverse rate process (i.e. collision-attachment and detachment). He developed a model to include both attachment and detachment phenomena that can be considered as the equivalents of forward and reverse reactions (Deglon et al., 1999; Deglon, 2002; 2003). He showed that the flotation rate can actually be interpreted as the net effect of two competing rates, one of attachment and the other of detachment, and proposed that the rate expression for flotation take into account both the pulp and gas phases. The model is given in Equations 2.48 and 2.49.

$$\frac{d(CV)}{dt} = -k_a CV + k_d C_s SV \tag{2.48}$$

$$\frac{d(C_s SV)}{dt} = k_a CV - k_d C_s SV - S_b C_s A \tag{2.49}$$

The process of particle-bubble attachment is assumed to be first-order with respect to the concentration of particles in the pulp phase (C) and controlled by an attachment rate constant (k_a). This is directly analogous to the definition of the flotation rate constant and the two are equivalent in the absence of significant detachment effects. The process of particle-bubble detachment is assumed to be first-order with respect to the concentration of particles on bubble surfaces (C_s) and controlled by a detachment rate constant (k_d). The argument for the use of first-order kinetics is equivalent to that for the flotation rate constant i.e. elementary “reaction kinetics” in the absence of complex interactions. The specific bubble surface area (*S*) is used to convert the term to a volumetric basis as a surface concentration (C_s) is employed in the expression.

2.4.3. Phenomenological Models

Flotation kinetic models are useful as it has practical application in the design of flotation cells and circuits. Flotation fundamental models are intrinsically more powerful as it provides real information

on the subprocesses of flotation. The most suitable method of analysing flotation rates should, therefore, combine the kinetic and fundamental models. The combination of kinetic models with fundamental models, containing information on the flotation micro environment is referred to as phenomenological models.

A series of research studies have been conducted to investigate relationships between the hydrodynamic parameters of a flotation cell and the flotation rate constant. The flotation rate constant in King model (King, 1973) was proportional to froth transmission co-efficient, bubble surface area per unit volume of pulp, particle size, hydrodynamic parameter, which is related to the degree of agitation, gas rate, gas hold up, cell volume and water recovery. Yoon and Mao 1976 and Jameson et al. 1977 showed one of the first expressions which kinetic and fundamental flotation models are linked in the collection zone and, consequently, allows for comparison of flotation kinetics between cells with similar flotation micro-environments but different dimensions and gas flowrates. According to the model suggested by Jameson et al. 1977 in a quiescent system, the rate constant can be calculated from:

$$k = \frac{3\ G_{fr}\ E_{coll}\ H}{2\ d_b\ V_c} \tag{2.50}$$

where G_{fr} is the gas volumetric flowrate, H is the height of the cell, V_c is the cell volume and E_{coll} is the bubble-particle collection efficiency (Equation 2.24), which can be defined as the fraction of particles in the path of a bubble, that successfully attach to the bubble and rise to the froth. This expression (Equation 2.50) can be recast in terms of superficial gas velocity (J_g), yielding Equation 2.51. This equation has been used by numerous researchers (Yoon, 1991; Ralston, 1992).

$$k = \frac{3}{2}\frac{J_g E_{coll}}{d_b} \tag{2.51}$$

Assuming bubbles are uniform and spherical, bubble surface area flux (S_b) can be introduced to the model (Jameson et al., 1977; Laplante et al. 1989a, 1989b; Yoon and Mao, 1996). That is the bubble surface area moving out of the cell per unit time per unit cross-sectional area of the flotation cell.

$$k = \frac{1}{4} S_b E_{coll} \tag{2.52}$$

Gorain (Gorain et al., 1996; 1997; 2000) developed based on experimental studies which only used air parameters as the hydrodynamic parameter influencing the flotation rate constant. In this model, flotation is decoupled into the pulp or collection zone and the froth zone. Gorain found that plotting k as a function of S_b yielded a straight line over the range of the data collected for several flotation cells. According to Gorain 2006, flotation rate (k) can be calculated from the following equation:

$$k_i = P_i \times S_b \times R_{fi} \tag{2.53}$$

where P_i is floatability component of *i*th fraction, S_b is bubble surface area flux and R_{fi} is froth recovery. However some studies showed that the linear relationship is within a range and out of that the relationship is not linear.

Operating conditions such as air rate in a small cell were manipulated to obtain the k-S_b relationship for a given ore type and system chemistry. Gorain assumed that the hydrodynamics and level of turbulence in the cell influences S_b only regardless of the cell's characteristics and level of energy input. Comparing this model to the fundamental models indicates that more hydrodynamic parameters are required. This model does not account for energy input or turbulence in the flotation cells. It has been acknowledged by several authors (Deglon, 2000; Pyke 2004, 2006; Newell and Grano, 2006) that turbulence could be a major contributor to flotation modelling.

Jameson and Gorain models (Equations 2.50 and 2.53) are first-order flotation kinetic models and do not take energy input into account and therefore studies have been conducted to model flotation in turbulent systems. For flotation in turbulent systems the rate equation can be written as (Julien Saint Amand, 1999; Koh and Schwarz, 2003; Pyke, 2004; Sherrell, 2004; Newell and Grano, 2006):

$$\frac{dN_p}{dt} = -kN_p = -Z_{pb}E_{coll} \qquad \Rightarrow \qquad k = \frac{Z_{pb}E_{coll}}{N_p} \tag{2.54}$$

where Z_{pb} is the rate or frequency of particle-bubble collisions per unit volume and is dependent on the energy input in the system. The flotation rate constant in Equation 2.54 can be expressed in terms of both the hydrodynamic parameters including energy input and fundamental parameters (Pyke et al., 2003):

$$k = \left(\frac{2.39\ G_{fr}}{d_b\ V_c}\right)\left(\frac{0.33\ £^{4/9} d_b^{\,7/9}}{¬^{1/3}}\right)\left(\frac{°_p - °_f}{°_f}\right)^{2/3} E_{coll} \tag{2.55}$$

2.4.4. Empirical Models

Empirical modelling refers to any kind of modelling based on empirical observations rather than on mathematically describable relationships of the system modelled. Typically, empirical models are used in the design and feedback controllers in flotation plants. These empirical models are usually linear and only valid in narrow operating zones, thus making them inaccurate in larger operating ranges. However, empirical models require less investment in modelling but need larger experimental data sets to generate models of good predictive capability. Furthermore, since they do not provide any physical insight into the process and its behaviour, they do not have any diagnostic utility outside of their use in control. There are several empirical and semi-empirical methodologies to extend the flotation rate constant. Development of an empirical input-output model entails a series of steps, which

include the collection of appropriate data, selection of a model structure, estimation of model parameters and checking of the model. The models developed by experimental design methods (i.e. DOE, SOE) fall into the category of empirical models. They are arguably the most widely used type of empirical models due their relative simplicity to develop, in spite of their noted limitations.

2.5. Summary of Literature Review

The literature relevant to this thesis has been reviewed in this chapter. The review of flotation cells included common industrial cells, and novel flotation cells which have been developed. It was observed that both operate using turbulent environments, and therefore knowledge of the effects of energy input on flotation may be relevant to both current flotation technologies and future developments. Background information was given on turbulence fundamentals in order to highlight the areas important in flotation. Oscillating grid turbulence was then reviewed, demonstrating why they may be considered to provide a near ideal environment for the investigation of turbulent systems. From theoretical findings, it was observed that energy/power input affects flotation in two ways. Firstly, increased energy input is thought to increase particle-bubble collision frequencies, resulting in increased flotation rates (k). This relationship can be expressed as $k \propto \varepsilon^N$ (Table 2.6). The second effect of energy input on flotation is to decrease the stability of particle-bubble aggregates. The overall effect that energy/power input has on flotation kinetics is therefore a balance of these two counteracting effects.

The majority of experimental studies on the effect of energy input on flotation kinetics have been conducted in stirred cells, with some research conducted in an oscillatory baffled column and an oscillating grid cell. It is evident from the experimental literature that flotation kinetics is a function of many factors, including the particle size, bubble size, particle hydrophobicity and energy input. In general, increasing energy input results in increased flotation rates to an optimum, after which the flotation rate decreases with increasing energy input. This optimum is thought to be the point where the rate of detachment becomes greater than the rate of increased particle-bubble collisions, as proposed in the theory. Table 2.6 showed different values for the constant N in the relationship between energy input and flotation rate, as found in theoretical and experimental studies.

Table 2.6: Values for the constant N in the relationship $k \propto \varepsilon^N$

Theoretical		Experimental	
Nonaka et al. 1982	0.75	Nonaka et al. 1982	0.75
Julien Saint Amand 1999	0.44 - 0.5	Deglon 2002	0.91
Pyke 2004	0.44	Newell and Grano 2006	1
Schubert 2008	0.5	Changunda et al. 2008	1
Jameson 2010	0.75	Massey et al. 2012	0.7 - 0.9

Chapter 3:
Materials and Methods

This chapter describes the materials and methods used in the investigation to achieve the objectives of this study. A detailed description of the design, operation, measurements, materials, reagents, conditions and procedures with details of the experimental program for the investigation for the laboratory oscillating grid flotation cell (OGC) is given in Section 3.1. Similar information is given for pilot scale OGC in Section 3.2.

3.1. Laboratory OGC

The oscillating grid cell design was based on the oscillatory multi-grid mixer as used by Bache and Rasool 2001. However, in this study an OGC with a more robust design such that higher energy dissipations could be achieved (up to 5 kW/m^3) was used. A schematic of the oscillating grid cell is shown in Figure 3.1. The dimensions of the oscillating grid cell and grids are given in Table 3.1.

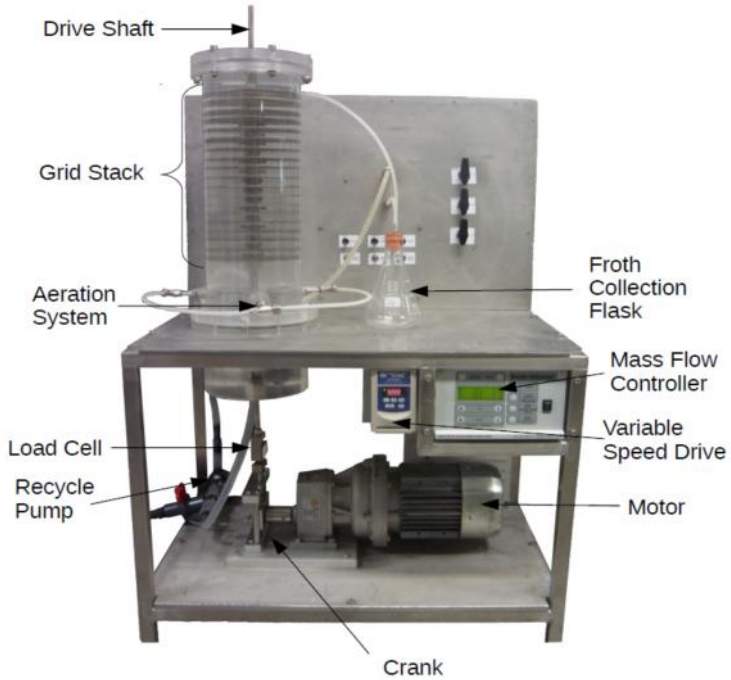

Figure 3.1: The laboratory oscillating grid flotation cell

Table 3.1: Physical specifications for the laboratory scale oscillating grid flotation cell

Lab. Scale OGC	Dimensions
Volume (L)	10
Tank Height (mm)	380
Tank Width (mm)	180
Number of Grids	19
Grid Spacing (mm)	18
Grid Hole Shape	Square
Grid Hole Size (mm)	6.8
Grids Solids Size (mm)	1.6

The oscillating grid cell was operated by oscillating the grid stack vertically in a PVC column. The grids had the same dimensions as used by Changunda et al. 2008 and Massey et al. 2012. The grids were cut from a single sheet of 1.5 mm stainless steel for added strength. Nineteen grids were mounted horizontally on the drive shaft to make up the grid stack. Turbulence was generated in the system by oscillating the grid stack at a set stroke length of 18 mm, which corresponds to the spacing between the grids. The energy input/dissipation was altered through changing the oscillating frequency of the grid stack which was manipulated by changing the rotational speed of the motor. The shaft was oscillated vertically through the use of a crank, which was driven by a variable speed 750 Watt AC Bonfigilioli electric motor.

3.1.1. Aeration System

The aeration system consisted of a nitrogen cylinder from which gas was regulated and fed to the system at a constant pressure of 200 kPa. Nitrogen was chosen as the aeration gas because of its homogeneity (very pure >99.999%) and for consistency with similar flotation energy studies (Ahmed and Jameson, 1985; Deglon, 2002). The nitrogen was passed through a saturator then accurately metered through a Brooks™ Smart (TMF) mass flow controller before being sparged into the cell through three sintered glass discs (Duran sintered discs supplied by Glasstech (Pty) Ltd) situated below the plate stack. Discs (frits) with porosity 1, 2 and 4 were used to produce different bubble sizes. A flow diagram of the aeration system is shown in Figure 3.2. The frits were mounted in stainless steel pipes which could be rotated through 180 degrees, as shown in Figure 3.3. When in the “down” position the frits were protected from being clogged with settling particles, and when the gas was turned on it was trapped in the pipe. When rotated to the “up” position the air was allowed to escape.

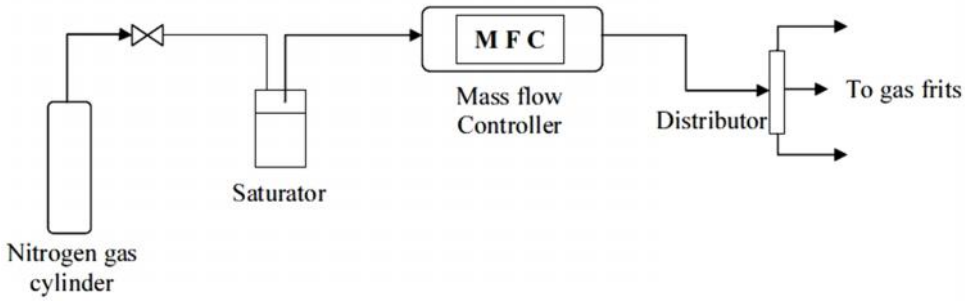

Figure 3.2: Flow diagram of OGC aeration system

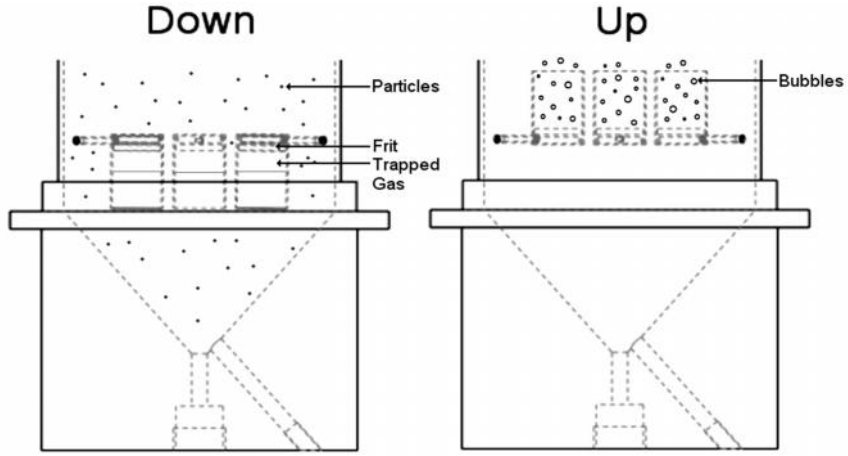

Figure 3.3: Schematic of sintered glass discs placement with detail of rotation

3.1.2. Recycle System

The flotation experiments were run in batch mode, and a recycle was therefore required to keep the particles sufficiently dispersed. The column was fitted with a conical base so that slurry could be collected and continuously reintroduced to the top of the cell. A peristaltic pump was used so as to maintain a constant recycle flow of 5 L/min. The piping had few obstructions and had a suitably large diameter to ensure laminar flow.

3.1.3. Froth Removal System

In order to minimise froth recovery effects a very low froth was maintained, which was removed by skimming a vacuum nozzle, attached to a conical flask, across the liquid surface. This method has been used by many previous researchers (Ahmed and Jameson, 1985; Deglon, 1998; Changunda et al., 2008; Massey et al., 2012). Six separate concentrates were collected using this method (Figure 3.4).

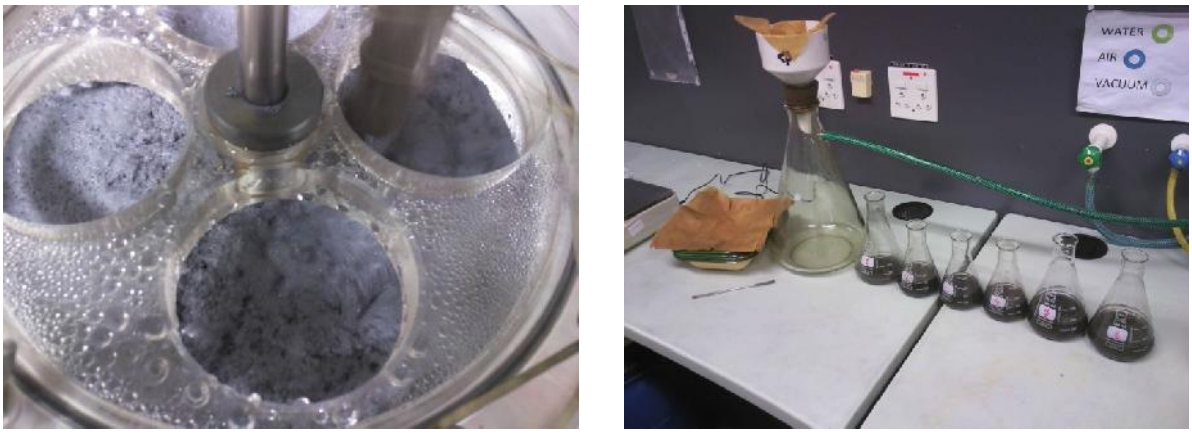

Figure 3.4: OGC froth removal system (galena concentrates)

3.1.4. Energy Input Measurements

The average energy/power input was determined by measuring the force which was supplied to the system using a load cell (Loadcell Services S-type) mounted in line with the drive shaft, so as to

directly measure the forces exerted on the drive shaft. A small flag mounted on the crank cut an optical switch once a cycle in order to determine the frequency and phase of the crank. Electrical signals were captured using a National Instruments data acquisition card, and sent to a computer where they were saved using LabVIEW© for signal analysis (Figure 3.5). The measured force was then used to calculate energy input. The method described in this section, to determine the energy input in the oscillating grid cell, follows that of Bache and Rasool 1996.

Figure 3.5: Energy input measurement and calibration testing with galena sample

The force measured by the load cell was composed of a combination of forces, namely, the force required to accelerate the grids, frictional force in the mechanism and the force exerted by the grids on the fluid. In order to determine the force exerted by the grids on the fluid, the force was measured with no fluid in the cell (F_{dry}) and then with fluid (F_{wet}), as described by Tojo et al. 1979. The force exerted on the fluid was then calculated by Equation 3.1:

$$F(t) = F(t)_{wet} - F(t)_{dry} \quad (3.1)$$

The instantaneous power supplied to the fluid at time (t) was then calculated by Equation 3.2:

$$P(t) = F(t)V(t) \quad (3.2)$$

where the instantaneous velocity V(t) was given by Equation 3.3:

$$V(t) = \pi S f \sin(2 \pi f t) \quad (3.3)$$

where S is the stroke length and f is the frequency of oscillation. The average power input was calculated from the integral of the power over one oscillation (Tojo et al., 1979) (Equation 3.4):

$$\bar{P} = \int_0^{1/f} F_D(t)V(t)dt \quad (3.4)$$

where F is the instantaneous measured force, V is velocity of the grid stack, and f is the oscillating frequency. The average energy input was calculated as shown in Equation 3.5 (Schubert, 1999):

$$£ = \frac{\bar{P}}{m_L} \quad (3.5)$$

where m_L is the mass of fluid in the agitated zone. The average energy input/power intensity in the OGC is equivalent to the local turbulent energy dissipation rate as turbulence in the OGC is relatively homogeneous and isotropic. The RMS turbulent velocity can be calculated from the turbulent energy dissipation rate, or inferred directly from the data of Bache and Rasool 2001 who conducted a detailed analysis of turbulence in the OGC. However, the turbulent energy dissipation rate is used in most models for particle-bubble contacting. It should be noted that under the conditions used in the investigation: energy input, power intensity (kW/m^3), specific power input (W/kg) or turbulent energy dissipation rate (W/kg or m^2/s^3) are equivalent (Massey et al., 2012).

3.1.5. Bubble Size Measurements

In this study, bubbles were generated using sintered glass discs with three different porosities under identical conditions (gas rates, frits, frother type, frother dosage) to those of Deglon 1998, Changunda et al. 2008 and Massey et al. 2012. Bubble size in laboratory scale was measured photographically and confirmed for the large bubble size (0.82 mm) using the UCT bubble analyser in this study at the same conditions to the previous studies. Table 3.2 shows the maximum pore size of the different sintered glass discs (porosity 1, 2 and 4 discs), with the mean bubble size produced. Bubble size was measured at different level of energy input (0.5 - 3 W/kg) for porosity 1 and results confirmed that bubble size was reasonably constant in all conditions. Therefore at the energy inputs used in this study bubble break up was negligible. Furthermore bubbles were too small to be broken up by the grids.

Table 3.2: Sintered glass frit pore sizes and corresponding mean bubbles sizes produced (laboratory scale OGC)

Porosity	Max Pore Size (µm)	Mean Bubble Size (mm)
1	100 - 160	0.82
2	40 - 100	0.58
4	10 - 16	0.13

3.1.6. Contact Angle Measurements

The contact angle is generally determined by sessile bubble or sessile drop techniques. Contact angle is normally measured through the liquid or vapour phase of a bubble or water drop on a polished single mineral surface (Subrahmanyam et al., 1999). Liquid penetration techniques such as equilibrium pressure and wetting rate measurements are reliable and rapid for determining the contact angle of minerals. The Washburn technique was used in this study to determine the contact angle (Figure 3.6). Contact angle measurements were carried out on heterogeneous mixtures of particles. This method makes use of capillary pressure to drive a liquid at an observable rate through particles packed bed in a capillary tube to measure the contact angle.

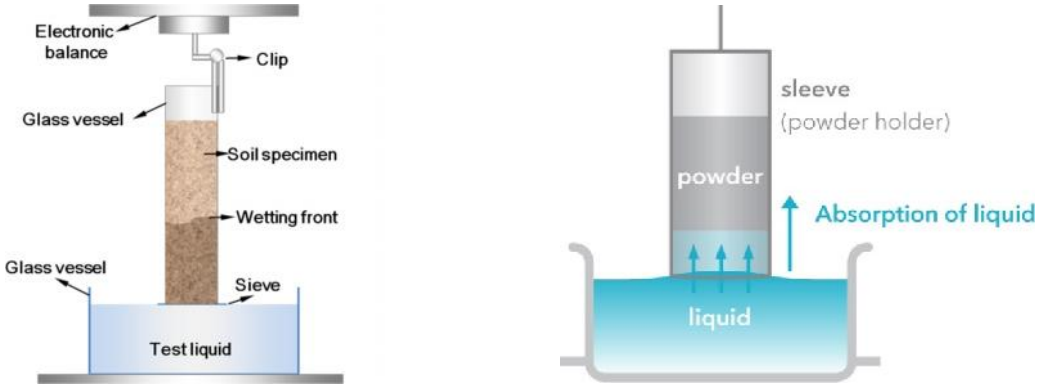

Figure 3.6: Schematic of Washburn technique, as described by Washburn 1921

In this study KRUSS Force Tensiometer was used for measuring contact angle as shown in Figure 3.7. An 8 mm glass tube with a filter base was packed with mineral powder. The filled glass tube was attached to a suspended force sensor. The glass tube was brought into contact with the test liquid and the powder start wetting because of capillary action forces the liquid to be drawn up. The increase in mass of the tube was measured with respect to time with a force sensor. The bulk powder can be looked upon as a bundle of capillaries, and then the process can be described by Equation 3.6:

$$\frac{m^2}{t} = \frac{c \circ_l^2 \pm \cos^{-}}{\ll} \tag{3.6}$$

where m = Mass; t = Flow time; c = Capillary constant of the powder; ρ_l = Density of the liquid; σ = Surface tension of the liquid; θ = Contact angle and μ = Viscosity of the liquid.

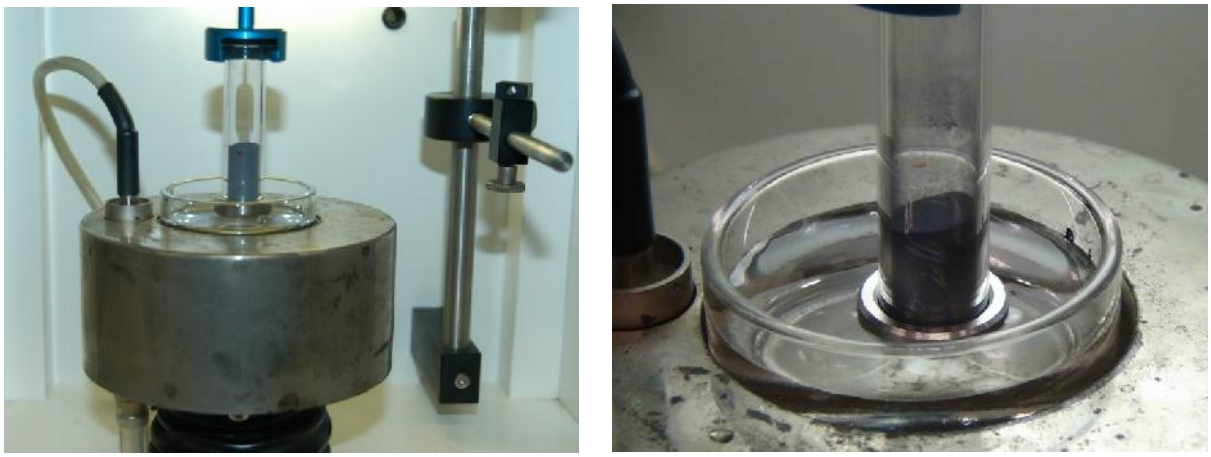

Figure 3.7: Capillary penetration method for galena contact angle measurement using KRUSS Force Tensiometer

The constant c depends on the nature of the powder, measuring tube and packing. Plotting mass square (m^2) against time (t) showed a linear region, the slope of which, for known liquid properties (σ, ρ and η), only contains the two unknowns c and θ. To determine the constant c, a measurement was carried out with n-Hexane as a perfectly wetting liquid, with which the contact angle θ was 0°. Once c was known, a second experiment was conducted using water for contact angle measurement. A constant packing method with a fixed powder column height of 60 mm was used to achieve best

reproducibility. The packing of the powder inside of the tube was done in several stages, each time adding the same weight of powder into the tube over the same height to ensure homogeneous densities and penetrability throughout the whole length of the sample. Thus, by maintaining the same ratio of mass vs. height of packing in the column, the repeatability of the packing was ensured in such a way that powders of the same material and particle size distribution had the same bulk density. In this study pulp surface tension was measured accurately by using KRUSS Force Tensiometer (Figure 3.8).

Figure 3.8: Surface tension measurements using KRUSS Force Tensiometer (K12 and K100)

A plot of the rise of the water Mass Square (m^2) versus time (t) gives the gradient of the non-wetting liquid (water) and that of n-Hexane gives the gradient of the wetting liquid. Substituting surface tension and viscosity as 72.80 mN/m and 1.0 cP for water and 24.95 mN/m and 0.98 cP for n-Hexane in Equation 3.6 lead to Equation 3.7 which was used to determine the contact angles.

$$\text{Cos}\,\theta = [(\text{gradient of non-wetting liquid}) \;/\; (\text{gradient of wetting liquid})\,] \times 0.345 \qquad (3.7)$$

In the case of galena sample, the gradients of the non-wetting and wetting liquids were obtained directly from data are shown in Figure 3.9. The contact angle for the galena powder at low collector dosage is found to be 53˚.

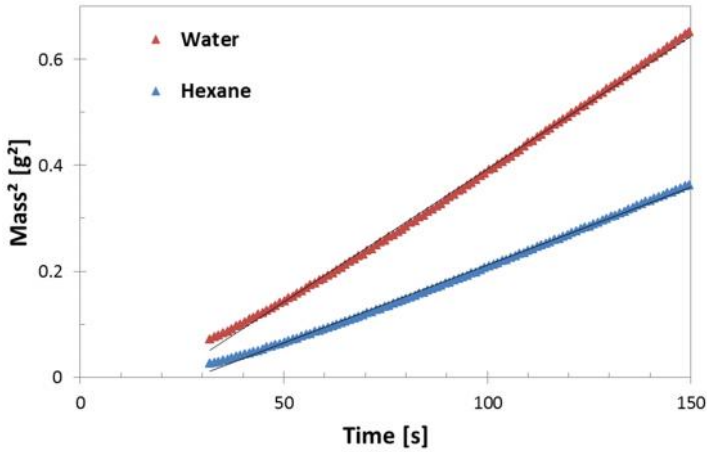

Figure 3.9: Wetting kinetics for galena powder in water (red line) and hexane (blue line) (CA = 53˚)

3.1.7. Materials and Reagents

The flotation experiments were performed in the oscillating grid cell using three sulphide minerals (galena, pyrite and pentlandite) and two oxide minerals (apatite and hematite). Galena (PbS) originated from the Touissit mine, Morocco. Pyrite (FeS_2) was obtained from the Huanzala mine, Peru. Pentlandite ($(Fe,Ni)_9S_8$) was obtained from the Frood-Stobie mine, Canada. Apatite ($Ca_5(PO_4)_3F$) was obtained from the Ipirá mine, Brazil. Hematite (Fe_2O_3) was obtained from the Timbopeba mine, Brazil. Minerals were received in pieces up to 100 mm in size. Minerals were crushed through a Jaw crusher and screened to collect the -5 mm particle size fraction as shown in Figure 3.10 and then pulverized. Ten kilograms of minerals powder was generated using this method. To ensure that samples were representative, pulverized minerals were blended and divided into individual feed samples for the flotation tests using two different rotary sample dividers in two different steps (Figure 3.11). Prepared feed samples were sealed in plastic bottles and polyethylene bags and stored under nitrogen at -30℃ to minimize oxidation. This procedure was applied for all minerals individually. Mineralogical and X-ray powder diffraction data indicated that all the samples were of high purity with no impurity peaks detected. The elemental composition of the minerals was determined by ICP analysis. The specific gravity of the minerals was determined using a pycnometer. BET analysis was used to determine the specific surface area of the samples using a Micromeritics TriStar II 3020. The bulk elemental composition, specific gravity and BET of samples are shown in Table 3.3.

Figure 3.10: Pentlandite sample preparation

Figure 3.11: Rotary dividers used to randomly split mineral particles

Table 3.3: Specific gravity, specific surface area and bulk elemental composition of mineral samples

Mineral	Specific Gravity	BET	Elements Present (Mass Percentage)									
Unit/Elements	g/cm^3	m^2/g	S	Fe	Pb	Cu	Zn	Ca	Mg	Si	P	Ni
Galena	7.60	0.21	13.12	0.07	86.11	0.05	0.01	0.02	0.23	0.09	0.15	0.01
Hematite	5.30	2.47	0.00	49.16	0.00	0.00	0.00	0.01	0.00	13.95	0.00	0.00
Pyrite	5.07	0.51	53.52	45.61	0.04	0.12	0.20	0.07	0.01	0.16	0.10	0.01
Pentlandite	4.42	1.07	32.5	34.56	0.04	0.84	0.05	0.41	0.52	2.07	0.12	27.32
Apatite	3.19	0.11	0.00	0.01	0.00	0.00	0.00	39.36	0.00	0.02	18.25	0.00

Particle size analysis was done using the Malvern Mastersizer™ as shown in Figure 3.12, which is capable of detecting particles as small as 0.2 µm to 2000 µm. This method uses laser diffraction to determine the particle size and therefore gives a slightly larger reading than that obtained from a screen. The particle size distributions of the flotation concentrates, tailings and feeds were determined using this method. Reproducibility of the size measurements was tested by doing three repeated tests on all the samples. The PSD results of the galena feed sample are presented in Table 3.4. This table shows that the reproducibility of the Malvern Mastersizer™ measurements was good.

Figure 3.12: Malvern Mastersizer™

The particle size distributions (PSD) of sulphide and oxide minerals after sample preparation are shown in Figure 3.13. An appropriate pulverizing time in combination of stage screening for each mineral was chosen to generate a similar PSD for all sulphide minerals. However oxide minerals were prepared differently, therefore different PSD's were produced due to the nature of oxide mineral flotation e.g. apatite was a coarser float than hematite. It is illustrated in this figure that all sulphide minerals have similar PSD with a d_{80} of approximately 90 µm whereas hematite and apatite have different PSD with a d_{80} of around 20 µm and 250 µm respectively.

Table 3.4: Particle size analysis of galena feed sample, as given by the Malvern Mastersizer

Particle Size (µm)	% Passing		
	Run 1	Run 2	Run 3
10	18.02	18.17	17.89
25	35.01	35.62	34.77
50	55.21	56.07	54.87
100	84.77	85.47	84.29

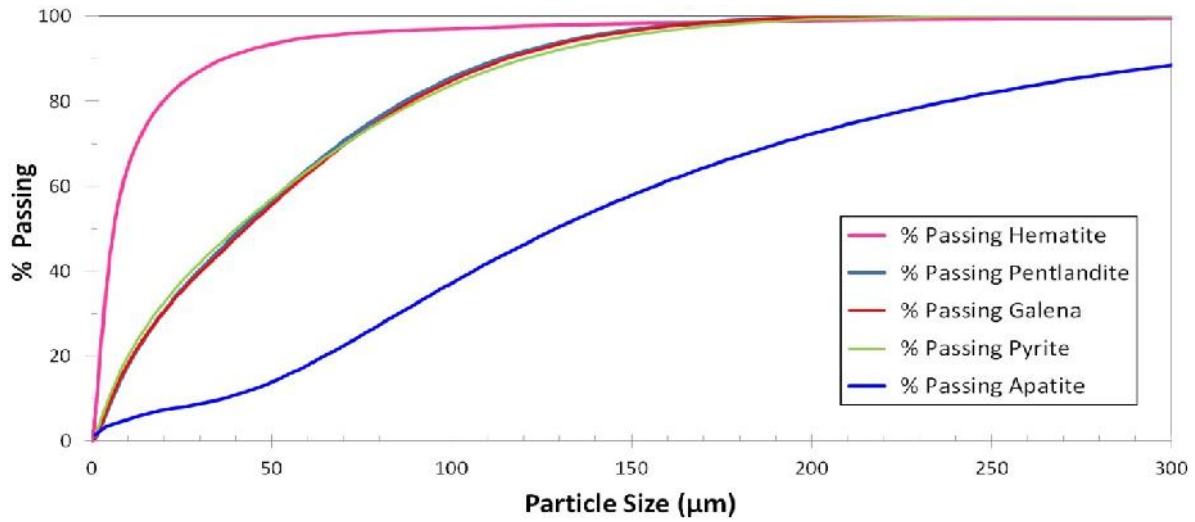

Figure 3.13: Particle size distribution (PSD) of sulphide and oxide minerals

Mineralogical studies were performed on sulphide minerals due to their complexity compared to oxide minerals. In this study vertical sections in different size fractions were generated as shown in Figure 3.14. Normally for dense samples vertical sections give more accurate results compared to normal disc sections. Samples were screened in four different size fractions. Milled graphite was added to each sample. Graphite was added to minimise touching particles and also to help with electron conductivity. The mixed graphite and sample was added into the mould and then resin carefully added to the mould. It was kept in a pressure pot overnight to cure. Eventually the blocks were removed from the mould and sliced into smaller sections and remounted into 30 mm round mounts (typically 3 blocks per fraction) to create new vertical block. Finally all blocks were polished and carbon-coated. The carbon coat was needed to diffuse electrons off the surface of the sample when they were in the QEMSCAN. These vertical sections were prepared for each size fraction of each mineral.

Figure 3.14: Vertical sections of sulphide minerals for mineralogical study using QEMSCAN

QEMSCAN is the name for an integrated automated mineralogy and petrography solution providing quantitative analysis of minerals. QEMSCAN is an abbreviation standing for Quantitative Evaluation of Minerals by SCANning electron microscopy. Mineralogical studies based on QEMSCAN images

showed that particles were angular and of irregular shape. Furthermore this result indicated that all the samples were of high purity and more than 97 % of the particles were fully liberated, as shown in Figure 3.15. Mineralogical results were tied to chemical analyses shown in Table 3.3. It is clearly observed from this figure that pyrite particles had more irregular shapes compared to galena particles and due to this pyrite had a higher BET compare to galena at the same PSD.

Xanthates (SEX - sodium ethyl xanthate, PAX - potassium ethyl xanthate, SIBX - sodium isobutyl xanthate) were received in powder form and used as collectors for sulphide minerals. MIBC (methyl isobutyl carbinol) was used as a frother. Fatty acid or amine (OA - Oleic acid, DAC - dodecyl amine chloride) were received in liquid form and used as collectors for oxide minerals. Reagents were prepared on a daily basis and adjusted to the correct pH using NaOH and HCl, if required. All reagents were of the analytical grade quality. All solutions were made with deionized water.

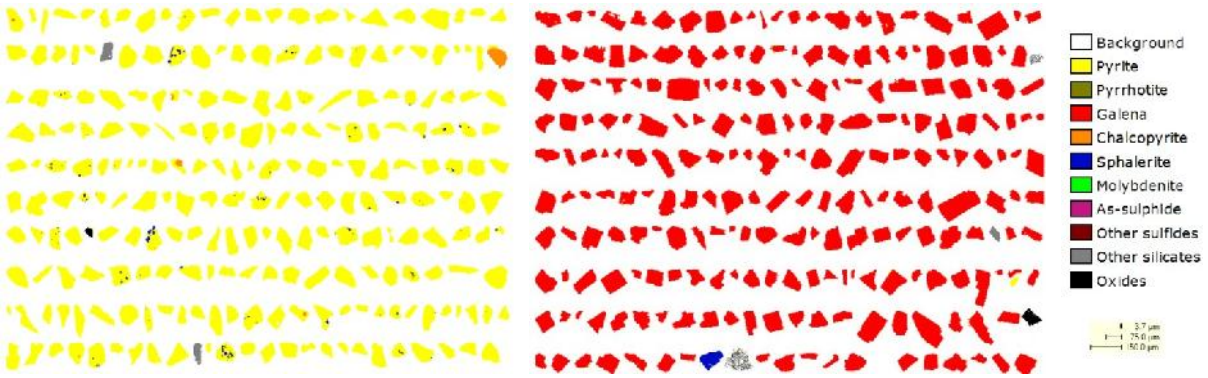

Figure 3.15: QEMSCAN results for galena and pyrite feed samples

3.1.8. Experimental Conditions and Procedures

The flotation experiments were conducted in batch mode, using constant flotation conditions for all experiments. These operating conditions are given in Table 3.5. These conditions are similar to those used by Massey et al. 2012. Energy inputs were chosen to cover the range of energy inputs typically found in industrial mechanical flotation cells. A low gas flow rate and mass percentage solids were used to have minimal influence on turbulence and to minimise bubble loading in the oscillating grid cell. Bubble sizes were fairly small in terms of industry use; however they correspond to the range typically used in the literature (Ahmed and Jameson, 1985; Deglon, 2002; Anderson, 2008; Changunda et al., 2008; Massey et al., 2012). Furthermore, small bubbles (0.13 mm) have more influence on flotation kinetics in the pulp zone. In addition, the largest bubble size (0.82 mm) was comparable to the average bubble size found in industrial mechanical flotation cells. A high frother dosage was used to minimise bubble coalescence in the system. A range of short chain collectors (SEX, PAX, SIBX) and long chain collectors (OA, DAC) were used for sulphide and oxide minerals respectively. Three collector dosages were used to produce different contact angles. Collector dosages were calculated to approximate 25, 50 and 100% of a pseudo-monolayer surface coverage. The calculation was based on the surface area which measured by BET method. At high collector dosage (%100 surface coverage) a

maximum recovery of up to 90 % was achieved over the 9 minute flotation time period for the best condition in terms of bubble size and energy input.

Before the experiment began, the oscillating frequency corresponding to the desired energy input to be used was set on the motor. To begin with, the spargers were set up facing downwards and with no gas flow, and the cell was filled with water. Frother and collector were pre-dispersed in beakers of water, and added to the cell. The oscillating grid and recycle pump were then started, and allowed to operate for 2 min in order to mix the reagents throughout the cell. The sample was then introduced as slurry from the glass beaker at the top of the cell. After 7 min of conditioning time the nitrogen gas was started, and allowed to run for 15 seconds to reach steady state. Since the spargers were facing down this nitrogen gas was trapped, as shown in Figure 3.3. After 15 seconds the spargers were turned to face upwards, and once the slugs of nitrogen gas had risen to the surface the timer was started for the flotation tests. Six concentrates were collected during experiments at the times specified in Table 3.5.

The concentrates and tails were filtered, dried and weighed before sizing using a Malvern Mastersizer™ 2000. Based on feed, concentrate and tail data the mass of each particle size class, in the concentrate and tail, was calculated. The mass recovery of each size class was used to determine the flotation rate constant using the standard first-order expression ($R(t) = 1 - e^{-kt}$) for a batch flotation cell. The recovery (R) is the fraction of the feed that is recovered at time t. Entrainment was negligible due to the low percentage solids, low percentage of ultrafine particles in feed and low water recovery.

Table 3.5: Experimental conditions

Condition/Parameter	Value (Sulphide minerals)	Value (Oxide minerals)
Scale	Lab. Scale	Lab. Scale
Solids	Galena, Pyrite, Pentlandite	Apatite, Hematite
Solids concentration (mass %)	0.5	0.5
Gas	Nitrogen	Nitrogen
Superficial gas velocity (cm/s)	0.0065	0.0065
Bubble size (mm)	0.13, 0.58, 0.82	0.13, 0.24, 0.58, 0.82
Particle size (micron)	-150	-650, -75
Energy input (W/kg or kW/m^3)	0.5, 1, 2, 3	0.1, 0.5, 1, 2, 3, 4, 5
Sampling time (min)	1, 2, 3, 4, 6, 9	1, 2, 3, 4, 6, 9
Tests condition	Batch	Batch
Frother	MIBC	MIBC
Frother concentration (ppm)	100	100
Collector	SEX, PAX, SIBX	OA, DAC
Collector dosage	Low , Moderate, High	Low , Moderate, High
Surface coverage (%)	25, 50, 100	25 , 50, 100
Contact angle (°)	40-50, 60-70, 80-90	40-50, 60-70, 80-90

3.1.9. Experimental Program

The experimental program for this study was composed of two major parts. The preliminary experiments in order to find best flotation conditions in the oscillating grid cell, and the main flotation experiments conducted in order to investigate the effect of energy/power input on flotation kinetics. In

this study a comprehensive data set was collected (around 450 flotation tests). A summary of the experimental flotation test for all samples is given in Table 3.6. The focus of the study was on the flotation of sulphide minerals. Repeatability was determined by performing multiple flotation experiments for all conditions. The average relative error (coefficient of variation) on the flotation rate constant was found to be around 6.21% in laboratory OGC. Similar errors have been reported by Massey et al. 2012, where errors of approximately 5.6 % were found for flotation rate constant in a similar system. These errors were considered to be in a reasonable range for these experiments, and are used as a standard throughout the study.

Table 3.6: Summary of flotation tests

Summary	Sulphide Minerals			Oxide Minerals	
	Galena	Pyrite	Pentlandite	Apatite	Hematite
Number of tests	137	85	122	71	21
Number of repeats	3.81	2.36	3.39	1.97	1.50
Relative error (k) %	6.73	5.93	6.31	8.47	3.60
Number of mass balance analysis	959	595	854	497	84
Number of BET tests	25	19	17	7	3

3.2. Pilot Scale OGC

A pilot-scale oscillating grid flotation cell was designed and constructed, as shown in Figure 3.16. Physical specifications for the cell are given in Table 3.7. The pilot scale OGC was operated as an entirely self-contained unit, using variable speed feed, recycle and tailing mono-pumps. The cell had a stack of 19 grids which were oscillated at various frequencies using a variable speed drive. The energy input was altered by changing the oscillating frequency which was manipulated by changing the rotational speed of the motor. Froth was removed from OGC using a conventional froth launder.

Figure 3.16: Pilot scale oscillating grid flotation cell

Table 3.7: Physical specifications for the pilot scale oscillating grid flotation cell

Pilot Scale OGC	Dimensions
Volume	0.4 m^3
Tank height	2.50 m
Tank diameter	0.39 m
Number of grids	19
Mesh size	0.02 m
Grid spacing	0.05 m
Bar diameter	0.003 m
Grid solidity	25 %

3.2.1. Aeration System

The aeration system consisted of air regulator, rotameter, distributor and spargers. Air (clean compressed air) flow rate was measured by using a rotameter and regulated at a constant pressure before being distributed to the spargers. In pilot scale OGC bubble sizes were generated using different sparging systems. Porous Metal (PM) and Cavitation Tube (CT) spargers supplied by Canadian Process Technologies (CPT) were used. The bubble sizes generated by these spargers were in the range typically found in industrial flotation cells. Aeration was performed by feeding air into the cell either directly through porous metal spargers situated at the bottom of the column or indirectly through a cavitation tube sparger situated at the side of the column. The CPT PM and CT spargers are shown in Figure 3.17.

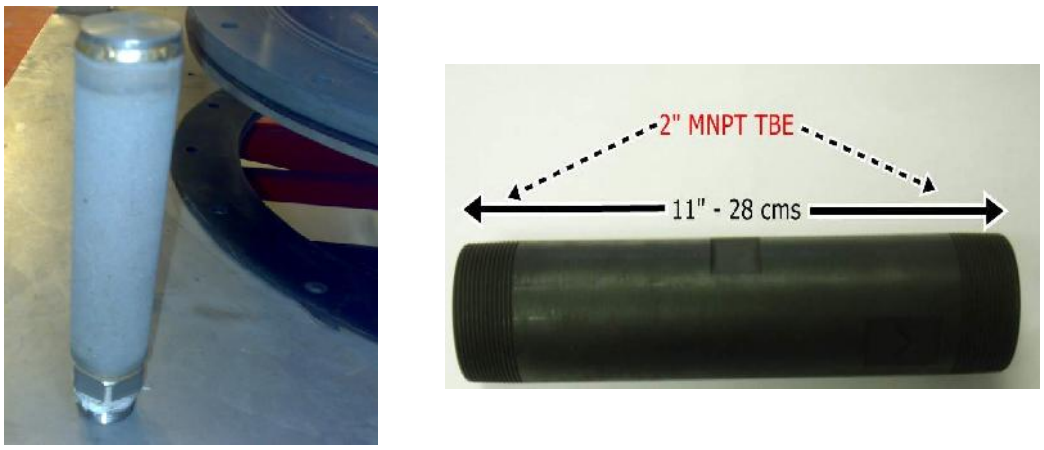

Figure 3.17: CPT porous metal and CPT cavitation tube

3.2.2. Recycle System

The flotation experiments were run in continuous mode, therefore a recycle was not required to keep the particles sufficiently dispersed. However, it was necessary for the cavitation tube sparger. The column was fitted with a conical base with a recycle pipe so that the slurry could be collected and continuously introduced to the cavitation tube for generating small bubbles in the cell. A helical pump was used so as to maintain a constant flow at high pressure. Recycle flow rate was controlled by using variable speed drive and magnetic flow meter.

3.2.3. Froth Removal System

Froth depth was measured manually and controlled using the tailings pump. The froth was removed continuously from the cell using a conventional froth launder, fitted with a small froth crowder. A fixed amount of wash water was used to clean the froth launder during tests. A pilot scale OGC during operation is shown in Figure 3.18.

Figure 3.18: Pilot-scale oscillating grid flotation cell during operation at the Baobab Concentrator

3.2.4. Energy Input Measurements

The energy input measurements for the pilot scale OGC was measured with the same method as discussed in section 3.1.5.

3.2.5. Bubble Size Measurement

In this study, bubble size was measured photographically with the Anglo Platinum Bubble Sizer (APBS). The device consisted of a collection pipe, a measurement box with a mounted waterproof camera case, a measuring reservoir and valves as shown in Figure 3.19. The APBS was installed at the top of the cell and the collection pipe was located inside the pulp close to the pulp-froth interface. This pipe was immersed into the pulp to direct bubbles into the viewing box, which consisted of a viewing pane where images of the bubbles were captured by the digital camera. There was a valve at the bottom of the viewing box (the top of the collection pipe) which was first closed while the reservoir was filled with solution (water + frother). A lighting array was located inside the viewing box to deliver back light at the viewing pane for capturing clear pictures of the bubbles. The funnel valve was closed and converts the APBS into a sealed chamber. The bottom valve was opened and the collection pipe filled with the solution in the reservoir. Bubbles rose up the collection pipe through the viewing box and the digital camera used to capture pictures for image analysis with the Stone Three software

(Figure 3.20). The flotation cell was adjusted to the appropriate experimental conditions and the system was allowed to equilibrate after 5 minutes. Around 10 to 30 snapshot images of bubbles were taken at intervals of 15 seconds over a period of 5 minutes by the digital camera of the APBS device for each set of test conditions. An average of 7000 bubbles was measured per condition but the number of bubbles evaluated for each experimental condition depended on the spread of the bubble size distribution.

Figure 3.19: Anglo Platinum Bubble Sizer used for pilot scale OGC

The software output consisted of bubbles that were analysed, the arithmetic mean diameter (d_{10}) and the Sauter mean diameter (d_{32}) of the bubbles. During the bubble counting, the variations of the mean bubble size parameters were monitored. The arithmetic mean bubbles size (d_{10}) produced by CPT Porous Metal and CPT Cavitation Tube spargers are given in Table 3.8.

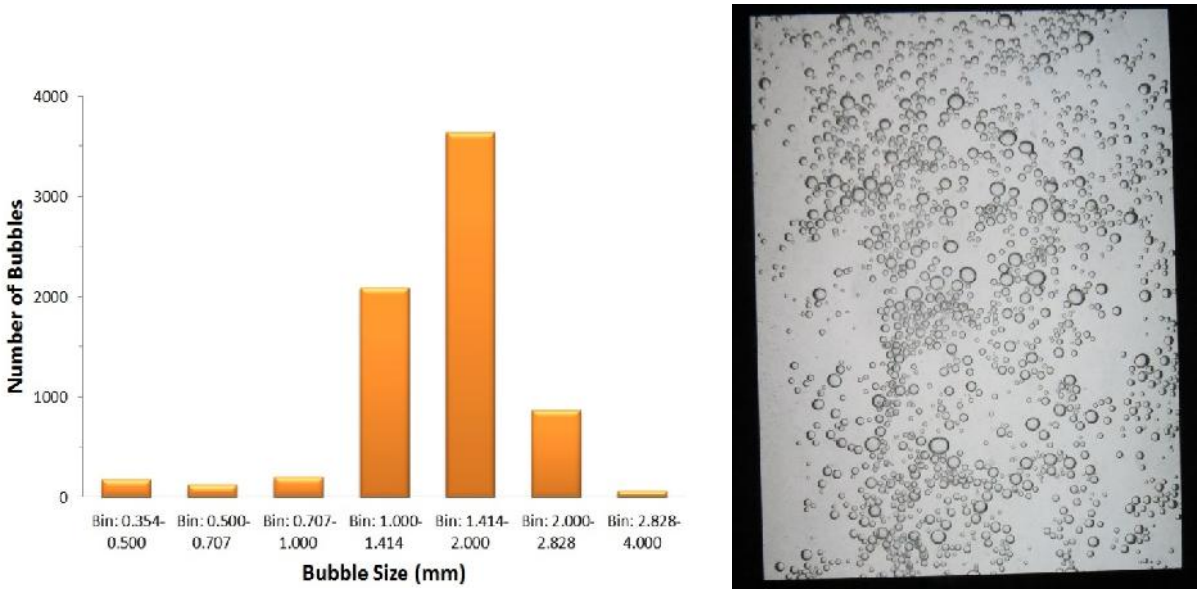

Figure 3.20: Bubble size distribution in pilot scale OGC using Anglo Platinum Bubble Sizer

Table 3.8: Mean bubbles sizes produced by CPT Porous Metal and Cavitation Tube spargers (pilot scale OGC)

Sparger	Mean Bubble Size (mm)
CPT Cavitation Tube	0.71
CPT Porous Metal	1.47

3.2.6. Materials and Reagents

The flotation experiments were performed in the oscillating grid cell using feed taken directly from the Baobab Concentrator in the Limpopo province of South Africa. The feed to the Baobab Concentrator was Platreef Ore (PGM) from the nearby Mogalakwena Concentrator belonging to Anglo American Platinum. Feed to the OGC was obtained from different streams. Secondary rougher feed (SRF), primary cleaner tail (PCT) and secondary cleaner tail (SCT) streams were used as a feed for the OGC flotation experiments. The feed SG varied depending on plant operation but on average was 1.13 t/m^3 for primary and secondary cleaner tail and 1.26 t/m^3 for secondary rougher feed. No additional reagents were added to the OGC. Sample preparation was conducted at the Baobab plant laboratory and CMR laboratory at the University of Cape Town. In the PGM study, the concentrates, feeds and tails were filtered, dried and weighed before the classification process. All samples were screened into three size fractions (-25, +25 to -53 and +53 µm) as are shown in Figure 3.21 and were sent to Anglo Research for assay analysis (Platinum and Palladium).

Figure 3.21: PGM samples preparation

3.2.7. Experimental Conditions and Procedures

The flotation experiments were conducted in continuous mode, using constant flotation conditions for all experiments. Operation of the OGC flotation cell was stable. The conditions for the flotation experiments are given in Table 3.9. Energy input were chosen to cover the range of power intensities typically found in industrial mechanical flotation cells. A typical flotation column superficial gas velocity of 1 cm/s was used. Two bubble sizes were used depending on the method of sparging. Bubble sizes from the porous sintered metal and cavitation tube spargers are towards the upper and lower ends of the range typically found in industrial flotation cells respectively.

To minimise froth recovery effects, a shallow froth depth of around 10 cm was maintained. The standard plant reagent scheme and dosages were used at the Baobab Concentrator. Feed was obtained directly from the plant and pumped through a 2 inch hose to a 1.5 m^3 agitated surge tank. Flotation tests were conducted over a period of 30 to 60 minutes to allow for steady state. Concentrate was collected continuously for 7 to 10 minutes. Increments of feed and tails were taken every 1 minute for 7 to 10 minutes. Tails flow rates and SG's were measured at the start and end of each test. OGC operating conditions were monitored continuously during the test. The flotation rate was calculated using the standard first-order expression for a continuous flotation cell. Entrainment was negligible due to the low water recovery, relatively low percentage solids and the low percentage of ultrafine particles in the feed stream.

Table 3.9: Experimental conditions

Condition/Parameter	Value
Scale	Pilot Scale
Solid	PGM (Platinum Ore)
Solids concentration (mass %)	15-30 %
Gas	Air
Superficial gas velocity (cm/s)	1
Bubble size (mm)	0.71, 1.47
Particle size (micron)	-75
Energy input (W/kg or kW/m^3)	0, 0.1, 0.25, 0.4, 0.5, 0.75 ,1 ,1.5 ,2, 2.5
Sampling time (min)	Continuous
Tests condition	Continuous
Frother	Plant reagents
Frother concentration (ppm)	Plant dosage
Collector	Plant reagents
Collector dosage	Plant dosage

3.2.8. Experimental Program

The experimental programme consisted of 27 tests on the effect of energy/power input on flotation kinetics of which the majority (17) were with normal bubble size (1.47 mm) and the remaining 10 tests were with fine bubble size (0.71 mm). The flotation experiments conducted in the pilot scale oscillating grid cell are summarized in Table 3.10. The flotation experimental programme is given in Table 3.11.

Table 3.10: Table of summarized experiments conducted in the pilot scale oscillating grid cell

Experiment	Ore	Energy input (kW/m^3)	Bubble Size (mm)
Flotation Experiments	Platinum ore (PGM)	0, 0.1, 0.25, 0.4, 0.5, 0.75, 1, 1.5, 2, 2.5	0.71, 1.47

Table 3.11: Experimental programme for the pilot scale oscillating grid cell

Parameter	Stream	Test Number	Conditions[1]
Energy/ Power Normal Bubble	Primary Cleaner Tail (Close Circuit)	Tests 1 to 7	0.11, 1.14, 0.46, 0.86, 0.12, 1.73, 0.87 kW/m^3
Energy/ Power Normal Bubble Fine Bubble	Primary Cleaner Tail (Open Circuit)	Tests 8 to 10 Tests 11 to 14	0.84, 0.11, 1.67 kW/m^3 0.11, 0.44, 0.83, 0.11 kW/m^3
Energy/ Power Normal Bubble	Secondary Rougher Feed	Tests 15 to 21	0.13, 1.28, 0.35, 1.88, 0.96, 0.13, 2.57 kW/m^3
Energy/ Power Fine Bubble	Secondary Cleaner Tail (Open Circuit)	Tests 22 to 23	0.11, 0.28 kW/m^3
Energy/ Power Fine Bubble	Secondary Rougher Feed	Tests 24 to 27	0.12, 0.31, 0.00, 0.12 kW/m^3

[1]Experimental conditions are listed in the order in which tests were conducted (i.e. sequentially).

The OGC flotation cell operated stably/consistently. However, there was variability in the nature of the feed to the cell. Variability was most significant between test campaign days, but occurred during the course of a day. The coefficient of variation (relative precision) for the variability in feed rate (due to changes in % solids) and feed grade (due to changes in quality) over the full test campaign was 7.03% and 10.72% respectively. Repeatability was determined from 5 repeat tests (same conditions) conducted over different days and in different streams. The coefficient of variation for recovery and grade were 19.47% and 12.85% respectively. These high values were primarily due to the variability in feed rate (solid %) and grade. However, a full set of tests evaluating a particular condition (e.g. energy input or bubble size) was i) always completed in a single day and ii) conducted randomly with large changes between sequential test conditions (see Table 3.11). In addition, changes in metallurgical results (e.g. recovery, grade and mass pull) were very large (300% recovery, 200% grade and 300% mass pull), exceeding even the high experimental error occurring between test campaign days.

3.3. Error Analysis

As indicated in Sections 3.1.9 and 3.2.8, experimental error was determined by performing repeat flotation tests and calculating the coefficient of variation. The coefficient of variation, also termed the relative error/precision or relative standard deviation, is the ratio of the standard deviation to the mean expressed as a percentage (cf. Equations 3.8 to 3.10). This is commonly used in the field of probability & statistics to measure the relative variability of data sets on a ratio scale. The coefficient of variation can be used for plotting relative error bars on graphs which allows one to determine whether trends in data are significant or are merely within the range of experimental error. The coefficient of variation can also be used for estimating the standard deviation for experiments without repeat tests. This quantity can be used within areas such as inferential statistics (e.g. t-test) or more advanced statistical techniques (e.g. ANOVA) for more rigour statistical data analysis.

$$« = \frac{\sum x}{n} \tag{3.8}$$

$$± = \sqrt{\frac{\sum (x - «)^2}{n - 1}} \tag{3.9}$$

$$CV = 100\frac{±}{«} \tag{3.10}$$

where μ is average value and σ is standard deviation, and n is the number of repeats.

The coefficient of variation for the flotation rate constant was found to be in the range of 4-8% with an average of 6.2% for the laboratory OGC. This quantity varied from 14-27% with an average of 20% for the pilot scale OGC. The error in the pilot scale OGC results is much higher due to variability in the plant feed. These values were used to plot error bars on graphs for both the laboratory and pilot scale OGC results. However, it was decided to remove error bars from the laboratory OGC graphs as these were too small to be seen, given the order of magnitude variation in the flotation results between the various test conditions. Error bars are plotted on the pilot scale OGC graphs, but again they are not overly significant given the large variation in flotation results. More advanced error analysis was not considered necessary given the magnitude of the trends in flotation results, relative to experimental error.

Chapter 4:
Results and Discussion

This chapter presents and discusses flotation results for both the laboratory and pilot scale oscillating grid flotation cells (OGC). Results for the laboratory and pilot scale OGC are given in Section 4.1 and Section 4.2 respectively. A phenomenological attachment-detachment kinetic model is developed in Section 4.3 based on the flotation data from the laboratory OGC. Finally, the overall effect of energy/power input on flotation kinetics is summarized in Section 4.4.

4.1. Laboratory Oscillating Grid Cell

The effect of principal parameters on flotation kinetics is presented in Section 4.1.1. The purpose of this section is to demonstrate that trends in the flotation rate with principle flotation parameters such as particle & bubble size are consistent with literature findings i.e. to establish the integrity of the data. The effect of energy input on flotation kinetics is given in Section 4.1.2. The purpose of this section is to present and interpret the detailed flotation results for all mineral types and to compare these with literature findings. The relative effect of energy input on flotation kinetics is given in Section 4.1.3. The purpose of this section is to compare results for all mineral types on a relative basis by normalizing flotation data as rate constants for the various minerals differ substantially in overall magnitude. The simulated effect of energy input on flotation kinetics is presented in Section 4.1.4. The purpose of this section is to both augment and interrogate the interpretation of results in Sections 4.1.1 to 4.1.3 through simulation of the flotation rate constant using the best available fundamental models from the flotation literature. Flotation rate constant data for all the flotation tests can be found in the Appendix A.

4.1.1. The Effect of Principal Parameters on Flotation Kinetics

This section presents and discusses the effect of the principle flotation parameters particle size, bubble size and contact angle (collector dosage) on the flotation rate of sulphide minerals at low energy input (0.5 W/kg) as most fundamental studies in the literature are for quiescent systems. Flotation results for the effect of particle size are presented for the -30 µm (finer) size class where bubble-particle detachment is minimal. Flotation results for the effect of bubble size and contact angle are presented for three particle size classes for comparative purposes, namely, -19 µm (fine), +19-38 µm (intermediate) and +38-150 µm (coarse). Galena, pyrite and pentlandite flotation results are indicated as "A", "B" and "C", respectively on all figures.

4.1.1.1. Effect of Particle Size

Figure 4.1 shows the relationship between the flotation rate constant and particle size for three bubble sizes and a high collector dosage at low energy input (0.5 W/kg). This figure demonstrates that the flotation rate constant increases proportionately with increasing particle size over the range of particle and bubble sizes presented in this figure. For example, the flotation rate constant increases by around 250% when particle size is increased from 5 to 30 µm for most conditions.

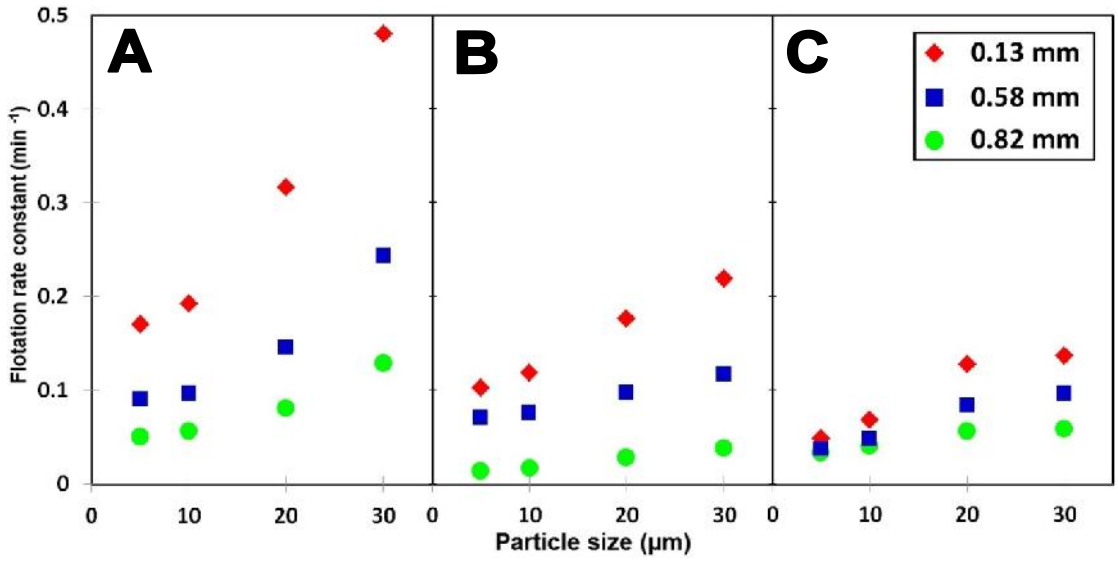

Figure 4.1: Flotation rate constant (min^{-1}) versus particle size (µm) for three bubble sizes and high collector dosage at low energy input (0.5 W/kg), A: Galena, B: Pyrite, C: Pentlandite

Particle size is one of the most influential physical parameters affecting flotation kinetics. Fundamental studies have shown that particle-bubble collision, attachment and detachment are all dependent on particle size. The low flotation rate of fine particles is often attributed to their small size & inertia which leads to a low probability of the particle colliding with bubbles as they tend to follow bubble fluid streamlines (Schulze et al., 1989). The increase in the flotation rate with increasing

particle size is primarily due to increased bubble-particle collision, which is well established in the flotation literature (Deglon, 2002; Pyke et al., 2003; Changunda et al., 2008; Anderson et al., 2009; Massey et al., 2012).

The relationship between the flotation rate constant and the particle size is commonly expressed as $k \propto d_p^n$. The value of n is typically in the range of 1 - 1.5 for quiescent systems. Literature studies for turbulent systems have shown that this value decreases with agitation. In this study, the value of n was found to be around 1 which is in the range of values found in the flotation literature. Massey et al. 2012 likewise found a similar relationship between the flotation rate constant and particle size at low energy input.

4.1.1.2. Effect of Bubble Size

Figure 4.2 shows the relationship between the flotation rate constant and bubble size for all particle sizes and collector dosages at low energy input (0.5 W/kg). This figure indicates that the flotation rate constant increases in inverse proportionality with decreasing bubble size over the range of particle and bubble sizes presented in this figure. For example, the flotation rate constant increases by around 350%, 250% and 200% for galena, pyrite and pentlandite respectively with a decrease in bubble size from 0.82 to 0.13 mm and at a high collector dosage and coarse particle size. The highest flotation rates are obtained using small bubbles.

Bubble size is also one of the most influential physical parameters affecting flotation kinetics. Fundamental studies have shown that particle-bubble collision, attachment and detachment are all dependent on bubble size. The increase in the flotation rate with decreasing bubble size is primarily due to an increase in the bubble-particle collision efficiency as reported in the flotation literature for both quiescent systems (Yoon and Luttrell, 1986; Diaz and Dobby, 1994; Nguyen et al., 2006) and turbulent systems (Ahmed and Jameson, 1985; Deglon, 2002; Changunda et al., 2008; Massey et al., 2012). However, decreasing bubble size is also thought to increase bubble-particle sliding times, decrease tangential velocities of particles sliding on bubble surfaces and increase attachment efficiencies (Ralston and Dukhin, 1999; Yoon, 2000; Attalla et al., 2000; Krasowska et al., 2007; Diaz, 2007; Sayed Ahmed, 2013).

The relationship between the flotation rate constant and the bubble size is commonly expressed as $k \propto d_b^{-m}$. The value of m is typically in the range of 1 - 3 for quiescent systems. In this study, the value of m was found to be around 1 which is in the range of values found in the flotation literature.

Despite the fact that in general the flotation rate constant increases with decreasing bubble size, the influence of bubble size on flotation kinetics is also dependent on particle size and energy input. Figure 4.2 demonstrates that the increase in the flotation rate caused by decreasing bubble size is more pronounced for smaller particles than for larger particles. For example, the flotation rate constant increases by around 950% with decreasing bubble size from 0.82 to 0.13 mm for fine pyrite particles

at a low collector dosage. Whilst, for intermediate and coarse particles the flotation rate constant increases by around 450% and 200% respectively. However, the magnitude of these changes decreases at a high collector dosage.

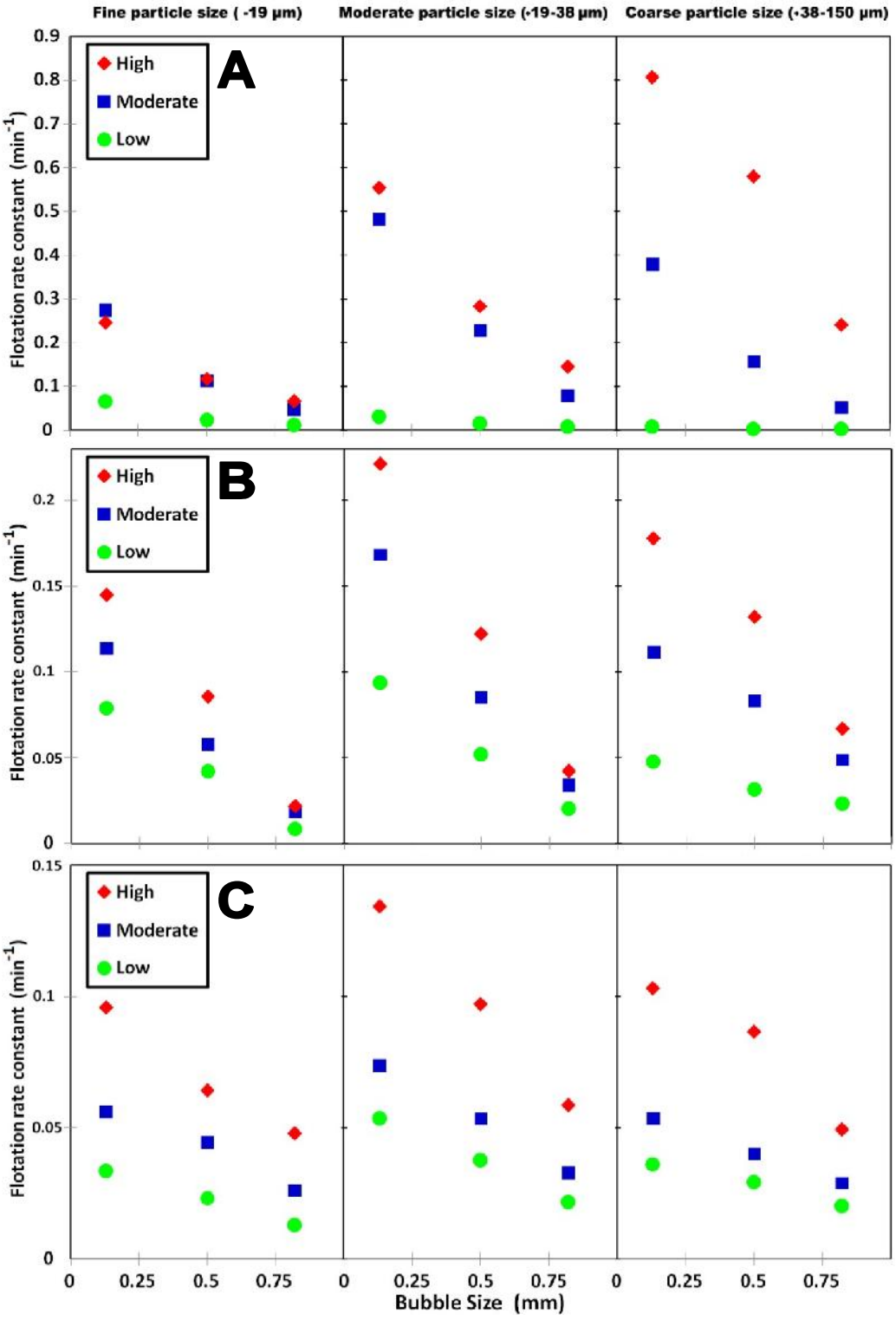

Figure 4.2: Flotation rate constant (min^{-1}) versus bubble size (mm) for the flotation of all particle sizes and all collector dosages at low energy input (0.5 W/kg), A: Galena, B: Pyrite, C: Pentlandite

4.1.1.3. Effect of Contact Angle

Figure 4.3 shows the relationship between the flotation rate constant and the contact angle for all particle sizes and bubble sizes at low energy input (0.5 W/kg). The three different contact angles for each mineral indicated in this figure refer to the three different collector dosages. Average contact angles of 50±5, 70±5 and 90±5 degrees were measured for low, moderate and high collector dosages respectively. This figure demonstrates that the flotation rate constant increases proportionately with increasing contact angle for all particle and bubble sizes. For example, the flotation rate constant increases by around 600%, 400% and 300% for galena, pentlandite and pyrite respectively with increasing collector dosage from low to high for fine particles and small bubbles. A notable exception is the result for galena at a low collector dosage, where the flotation rate is initially very low for all particle and bubble sizes. This is due to the contact angle at a low collector dosage being less than the critical contact angle, below which flotation will not occur. The flotation rate increases rapidly with subsequent increases in the contact angle.

The contact angle is one of the most influential chemical parameters affecting flotation kinetics. Fundamental studies have shown that particle-bubble attachment and detachment are determined by the interfacial properties, and therefore are strongly dependent on the contact angle. However, bubble-particle collision is primarily determined by hydrodynamics and is therefore independent of the contact angle. The increase in the flotation rate with increasing contact angle is due to an increase in the particle-bubble attachment and stability efficiencies. Higher contact angles increase the interaction energy between particles and bubbles and decrease induction times, resulting in higher attachment efficiencies. The success of attachment depends largely on the hydrophobicity of the particle as reported by Pushkarova 2008 and shown in Equation 2.33. Higher contact angles also improve the bubble-particle stability efficiency resulting in less detachment of particles.

As indicated previously, there is a critical contact angle below which flotation will not occur. The critical contact angle for flotation of sulphide minerals is due to their mineral characteristics. Therefore minerals with higher particle density, such as galena, need a higher initial contact angle for flotation to occur. For example, at a low collector dosage pyrite and pentlandite have a higher flotation rate than galena but at all other conditions galena has higher flotation rate. Furthermore, particle size plays an important role for the critical contact angle at which flotation commences. The minimum contact angle needed for flotation to commence increases with increasing particle size (Bellson Awatey, 2014).

Despite the fact that in general the flotation rate constant increases with increasing contact angle, the influence of contact angle on flotation kinetics is also dependent on particle size and bubble size. Figure 4.3 shows that the increase in flotation rate caused by increasing contact angle is more pronounced for larger particles than for smaller particles. Therefore, the effect of contact angle on the flotation rate increases with increasing particle size i.e. for a given bubble size an increase in contact angle has a greater effect on the flotation rate of coarse particles compared to fine particles. For

example, by increasing collector dosage from low to high the flotation rate constant increased by around 200% for fine pyrite particles with small bubbles. Whilst for intermediate and coarse particles the flotation rate increased by around 250% and 350%, respectively. Similar trends are observed for the other minerals. The flotation rate constant for coarse particles is very sensitive to changes in particle hydrophobicity.

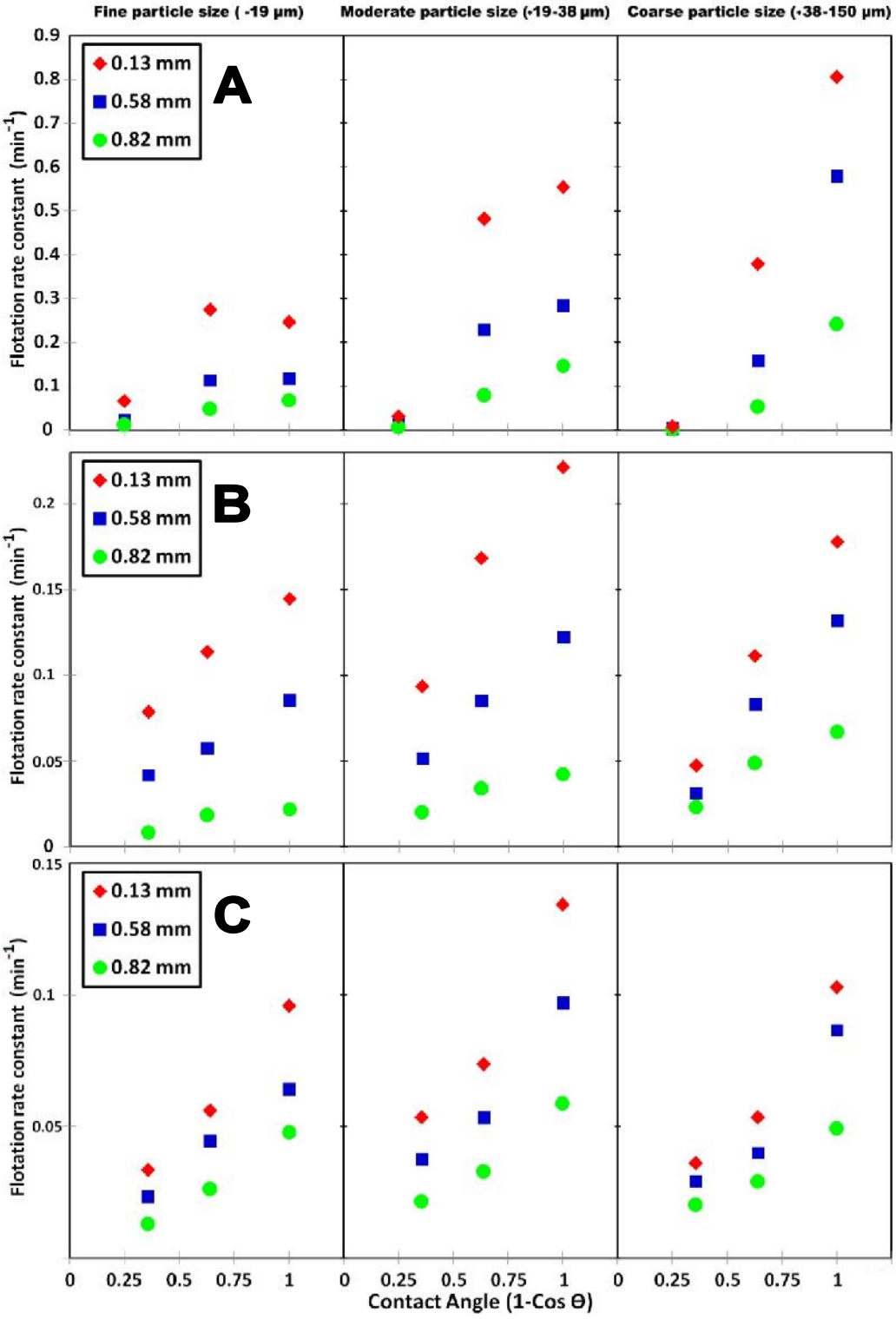

Figure 4.3: Flotation rate constant (min^{-1}) versus contact angle for the flotation of all particle sizes and all bubble sizes at low energy input (0.5 W/kg), A: Galena, B: Pyrite, C: Pentlandite

In addition, the increase in flotation rate caused by contact angle is more pronounced for larger bubbles than for smaller bubbles. Therefore, the effect of contact angle on flotation rate increases with increasing bubble size i.e. for a given particle size an increase in contact angle has a greater effect on the flotation rate with larger bubbles compared to smaller bubbles. For example, by increasing collector dosage from low to high the flotation rate constant for fine galena particles increased by around 600% with 0.82 mm bubble size and 350% with 0.13 mm bubble size.

4.1.2. The Effect of Energy Input on Flotation Kinetics

This section presents and discusses results for the effect of energy input on the flotation rate constant for the sulphide minerals (galena, pyrite and pentlandite) in Section 4.1.2.1 and the oxide minerals (apatite and hematite) in Section 4.1.2.2. Flotation of sulphide minerals is the main focus of this study and the same flotation conditions for all minerals were used.

4.1.2.1. Sulphide Minerals

This section presents and discusses flotation results for galena, pyrite and pentlandite. Flotation results are presented for three particle size classes for comparative purposes, namely fine (-19 μm), intermediate (+19 -38 μm) and coarse (+38 -150 μm). Galena, pyrite and pentlandite flotation results are indicated as “A”, “B” and “C” respectively on all figures. It should be noted that the relative magnitude of the flotation rate constant depends quite strongly on the mineral type. So for example, in general, galena has significantly higher flotation rate constants than pentlandite. Thus results are discussed in terms of trends in the flotation rate constant, rather than the overall magnitude.

4.1.2.1.1. Fine Particles

Figure 4.4 shows the relationship between the flotation rate constant and the energy/power input for the fine particles (-19 μm) and for all bubble sizes and collector dosages. The flotation rate constant increases with increasing collector dosage due to an increase in the probability of bubble-particle attachment, as discussed previously. The flotation rate constant also increases significantly with decreasing bubble size due an increase in the probability of bubble-particle collision, as noted previously. The flotation rate constant increases steadily with increasing energy input for all bubble sizes and collector dosages. Here, increases of up to 300% are observed when increasing energy input from 0.5 to 3 W/kg. This significant increase suggests that energy input improves the flotation of fine particles, as observed in numerous theoretical and experimental studies (Schubert and Bischofberger, 1978; Ahmed and Jameson, 1985; Jordan and Spears, 1990; Deglon, 2002; Pyke et al., 2003; Newell and Grano, 2006; Schubert, 2008; Massey et al., 2012). This is primarily attributed to an increase in the number of bubble-particle collisions as noted by Schubert and indicated in Equation 2.55 (Pyke et al., 2003). This increase could also be partly due to an increase in attachment efficiency, as discussed

in Section 2.3.1.3.2. Here, increasing energy input increases the kinetic energy of particles which helps overcome the energy barrier to attachment, as shown in Equation 2.36 and suggested by Jameson 2010. However, the effect of increasing energy input on the flotation rate is not strongly dependent on the bubble size and collector dosage, which will be explained further in Section 4.1.2.3.

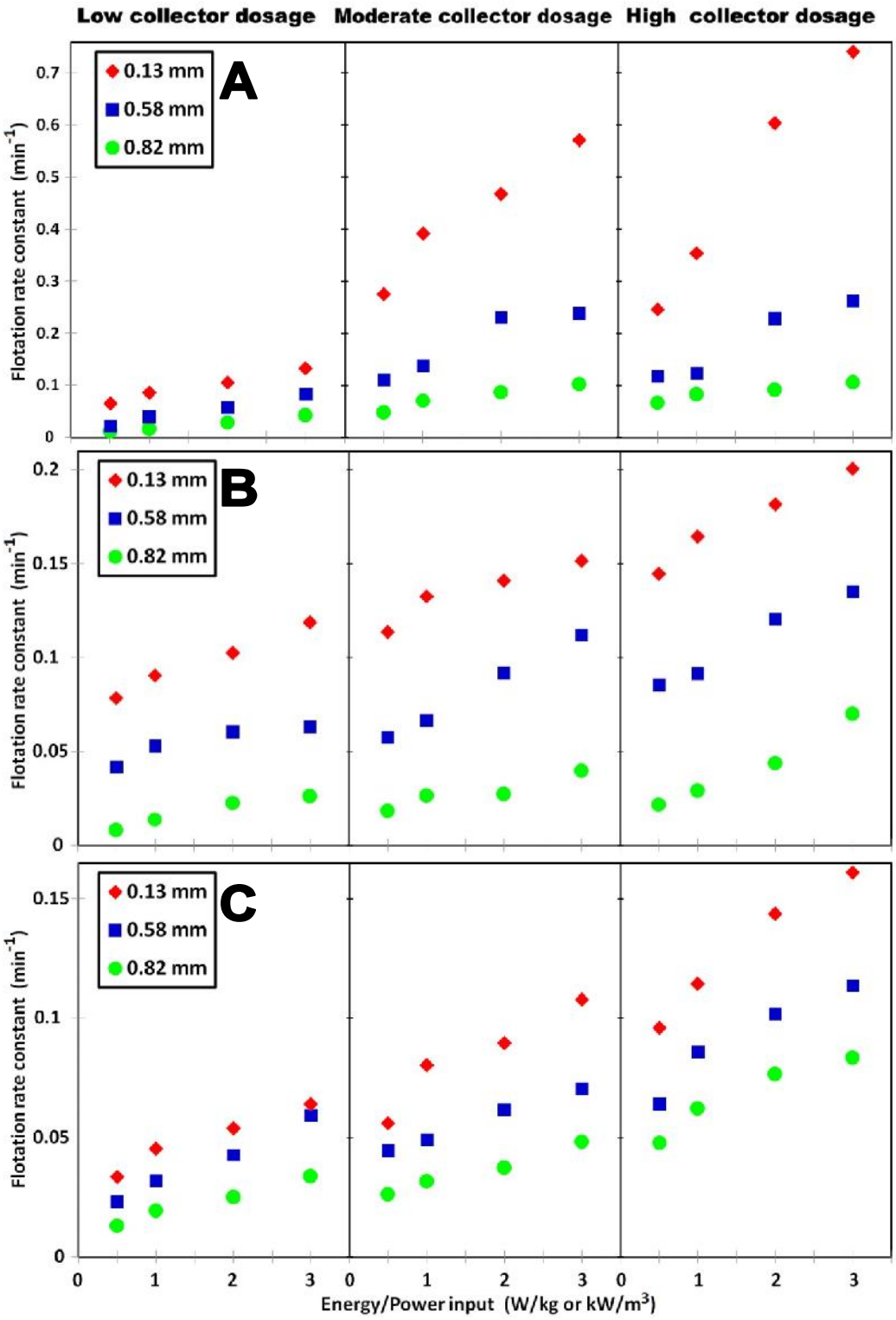

Figure 4.4: Flotation rate constant (min^{-1}) versus energy input (W/kg) for the flotation of fine particles (-19 µm), all bubble sizes and collector dosages, A: Galena, B: Pyrite, C: Pentlandite

4.1.2.1.2. Intermediate Particles

Figure 4.5 shows the relationship between the flotation rate constant and the energy/power input for the intermediate particles (+19-38 µm) and for all bubble sizes and collector dosages. The intermediate particles have flotation rates which are larger than those for fine particles, at the lower energy inputs, due to an increase in the probability of bubble-particle collision.

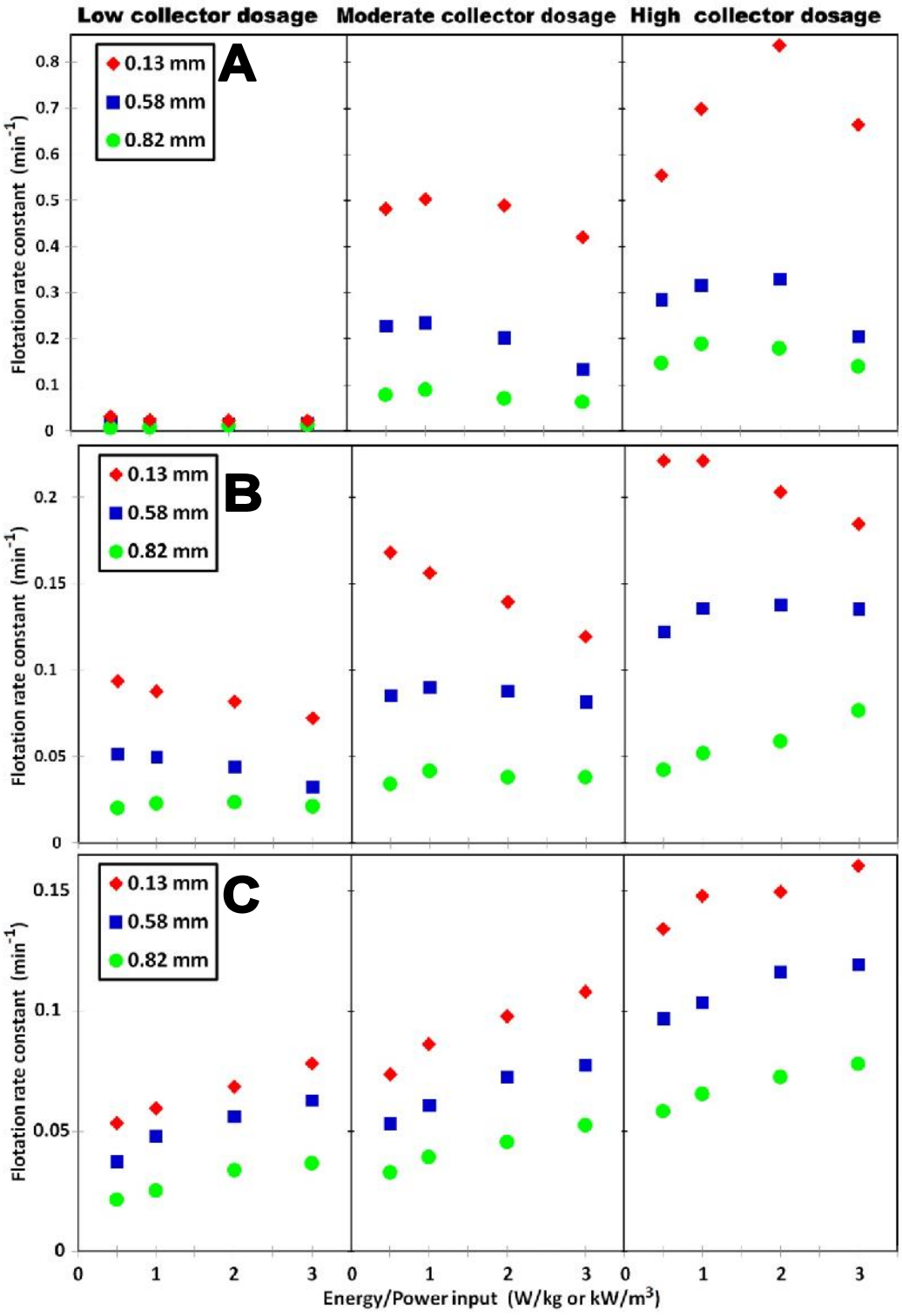

Figure 4.5: Flotation rate constant (min^{-1}) versus energy input (W/kg) input for the flotation of intermediate particles (+19-38 µm), all bubble sizes and collector dosages, A: Galena, B: Pyrite, C: Pentlandite

Again the flotation rate constant increases with increasing collector dosage and decreasing bubble size. For intermediate galena particles, increasing energy input has no effect on the flotation rate constant at the low collector dosages but leads to an optimum in the flotation rate constant at both moderate and high collector dosages. This optimum is at around 1 W/kg for the moderate collector dosage and 2 W/kg for the high collector dosage, with subsequent increases in the energy input resulting in large decreases in flotation rates for all bubble sizes. For intermediate pyrite particles, increasing energy input generally leads to a decrease in the flotation rate constant for small bubble sizes and a slight increase, or a shallow optimum, for intermediate and large bubble sizes. For intermediate pentlandite particles, increasing energy input generally leads to an increase in the flotation rate constant, although results tend towards a shallow optimum at the higher energy inputs. The trends shown in Figure 4.5 suggests that energy input generally improves the flotation of intermediate particles up to an optimum. This is attributed to an increase in the number of bubble-particle collisions and increasing attachment efficiency. However, further increases in energy input result in increased bubble-particle detachment due to reduced stability of bubble-particle aggregates. This results in an optimum energy input which depends on the mineral type and their particle hydrophobicity and density. The intermediate galena particles have a much sharper optimum at lower energy inputs due to the higher particle density. A similar argument could apply when comparing the pyrite and pentlandite results, although the density difference is much smaller.

4.1.2.1.3. Coarse Particles

Figure 4.6 shows the relationship between the flotation rate constant and the energy/power input for the coarse particles (+38-150 µm) and for all bubble sizes and collector dosages. It is clear from this figure that increasing energy input leads to large decreases in the flotation rate constant for all bubble sizes and collector dosages. For example, for galena at a high collector dosage and small bubble size, the flotation rate constant decreases by over 400% as the energy input increases from 0.5 to 3 W/kg. The comparative decrease is around 300% for pyrite and 200% for pentlandite, which is significantly smaller than that for galena, due to the higher particle density. The decrease in the flotation rate constant is due to an increase in the probability of bubble-particle detachment for larger particles, as a result of increased turbulence, which reduces the stability of coarse bubble-particle aggregates (Schulze, 1993; Oteyaka and Soto, 1995; Ralston et al., 1999; Cowburn et al., 2006; Goel and Jameson, 2012). Here, particles detach when detachment forces exceed the maximum attachment forces as shown in Equation 2.38 (Nguyen and Schulze, 2004). The detachment force is directly proportional to the particle size and particle density suggesting that coarse or dense particles are more likely to detach from the bubbles than fine particles, as observed experimentally in several studies (Soto and Barbery, 1991; Ralston et al., 1999). It is also clear from this figure that detachment increases with decreasing bubble size.

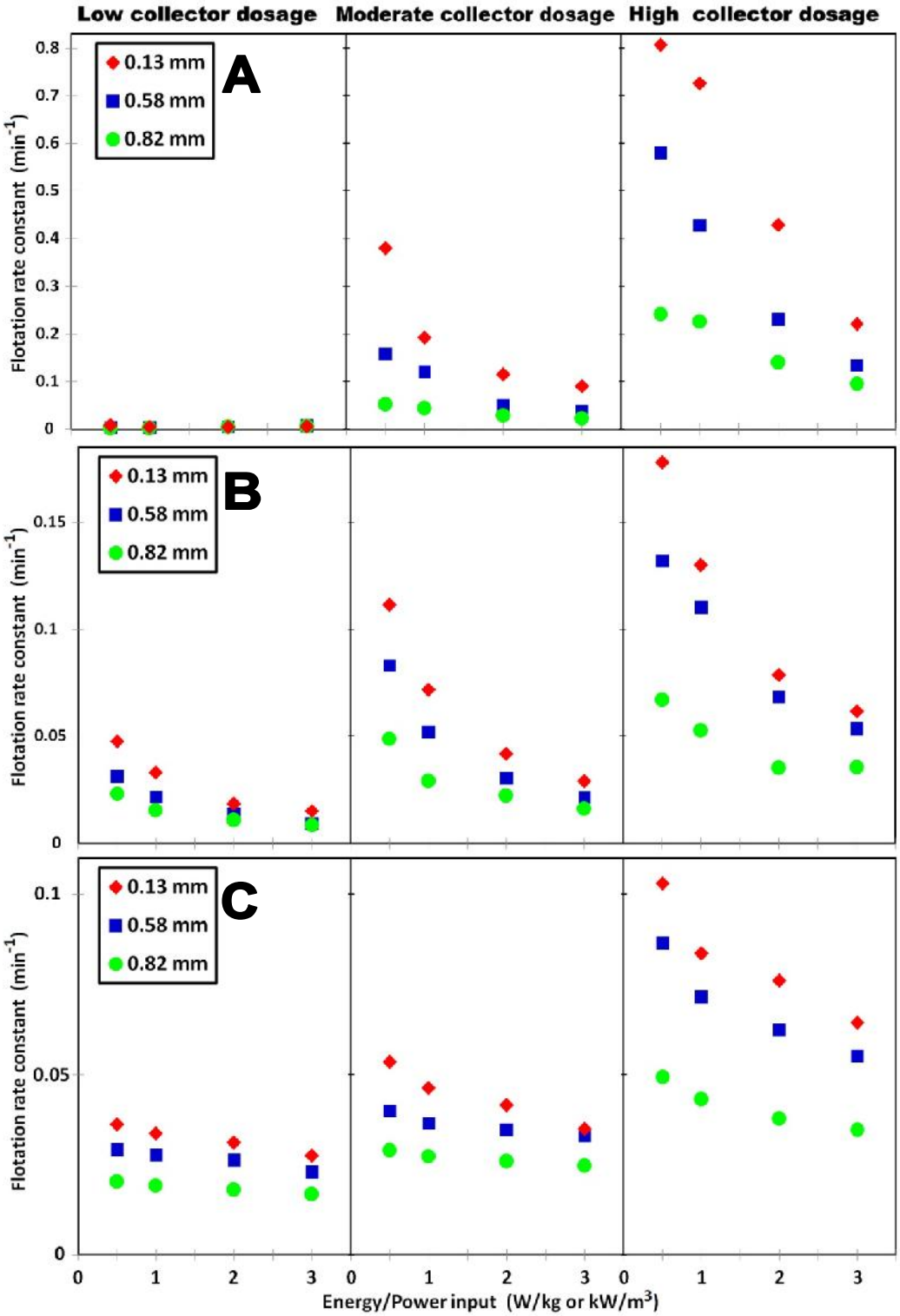

Figure 4.6: Flotation rate constant (min^{-1}) versus energy input (W/kg) for the flotation of coarse particles (+38-150 µm), all bubble sizes and collector dosages, A: Galena, B: Pyrite, C: Pentlandite

For example, at a high collector dosage and 0.5 W/kg energy input, the flotation rate constant for the small bubble size is 230% greater than that for the large bubble size. However, this difference decreases to only 150% greater when the energy input is increased to 3 W/kg. This increase in bubble-particle detachment with decreasing bubble size has been observed by a number of researchers (Ahmed and Jameson, 1985; Tao, 2004; Deglon, 2002; Do, 2010; Massey et al., 2012). This is

sometimes attributed to increased acceleration of bubble-particle aggregates in the more vigorous smaller turbulent eddies, as shown in Equations 2.41 & 2.42. It is clear from this figure that the highest detachment rates are for small bubbles and coarser particles, which is expected.

4.1.2.2. Oxide Minerals

This section presents and discusses results for the apatite and hematite flotation tests. For oxide minerals, results are presented by mineral type as different size distributions and test conditions were used due to the nature of oxide flotation. Apatite and hematite were floated at selected conditions from those given in Table 3.4. Here, results are presented according to size classes appropriate to the mineral e.g. apatite is coarser than hematite. For particle size class comparison purposes, the flotation results are divided into four classes, viz. fine (-19 µm), intermediate (+19 -38 (-45) µm), coarse (+38 -150 µm) and very-coarse (+150 -650 µm).It should be noted that the majority of trends observed in the oxide mineral results are entirely consistent with those for the sulphide minerals. Hence this section presents a brief overview of key features, rather than a detailed description of the variation of the flotation rate constant with energy input, particle size, bubble size and collector dosage.

4.1.2.2.1. Apatite

Figure 4.7 shows the relationship between the flotation rate constant and the energy/power input for three particle size classes, 0.58 mm bubbles and two collector dosages. Here, the apatite flotation results are for coarser particles at lower energy inputs. The flotation rate constant for fine & intermediate particles (-38 µm) increases by around 200% with an increase in energy input from 0.1 to 2 W/kg at both low and moderate collector dosages. However, the flotation rate constant for the very coarse particles (+150-650 µm) decreases by over 900% over the same energy input range at a moderate collector dosage.

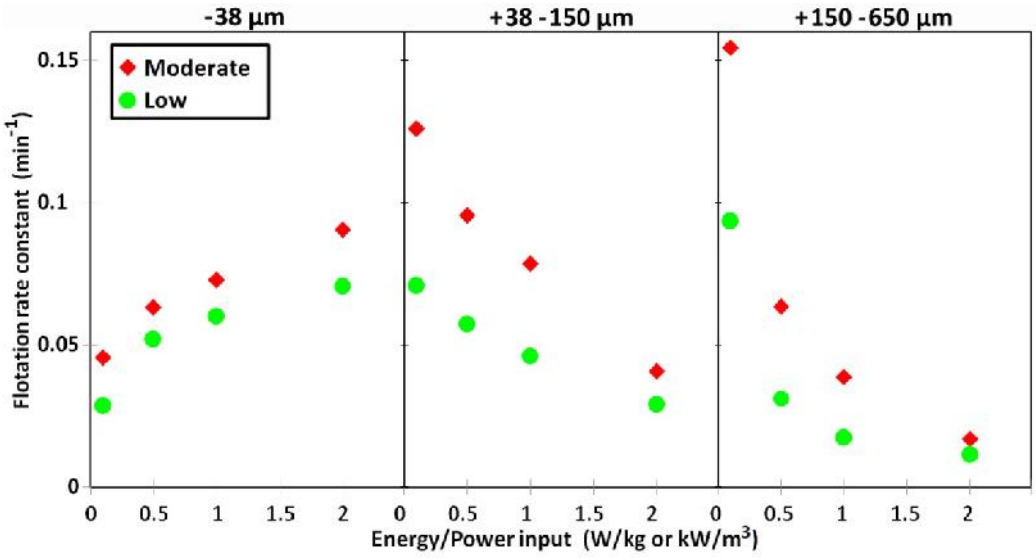

Figure 4.7: Flotation rate constant (min^{-1}) versus energy input (W/kg) for three particle sizes and two collector dosages

The highest flotation rate is obtained for the very coarse particles at the lowest energy input and a moderate collector dosage. These results clearly demonstrate that optimal energy inputs for the flotation of fine and coarse apatite differ significantly, due to the wide particle size range found in most industrial flotation applications. Fine particles require high energy inputs to promote bubble-particle collision but these results in high detachment rates for very coarse particles. These high detachment rates may be reduced by increasing collector dosage to improve hydrophobicity and bubble-particle aggregate stability i.e. to decrease the probability of bubble-particle detachment. The positive impact of reagent dosage on the flotation rate of coarse apatite particles has been observed by Senior et al. 1994 and Matiolo et al. 2015.

4.1.2.2.2. Hematite

Figure 4.8 shows the relationship between the flotation rate constant and the energy/power input for two particle size classes, all bubble sizes and a moderate collector dosage. Here, the flotation rate constant increases steadily with increasing energy input for fine particles (-19 µm), but generally decreases for intermediate particles (+19-45 µm). The flotation rate constant for fine particles increases by around 350% with increasing energy input from 0.5 to 5 W/kg for the large bubbles. However, the flotation rate constant for intermediate particles decreases by over 450% for the same conditions. These results suggest that higher energy inputs are beneficial for the flotation of hematite, which consists predominantly of finer particles in most industrial flotation applications.

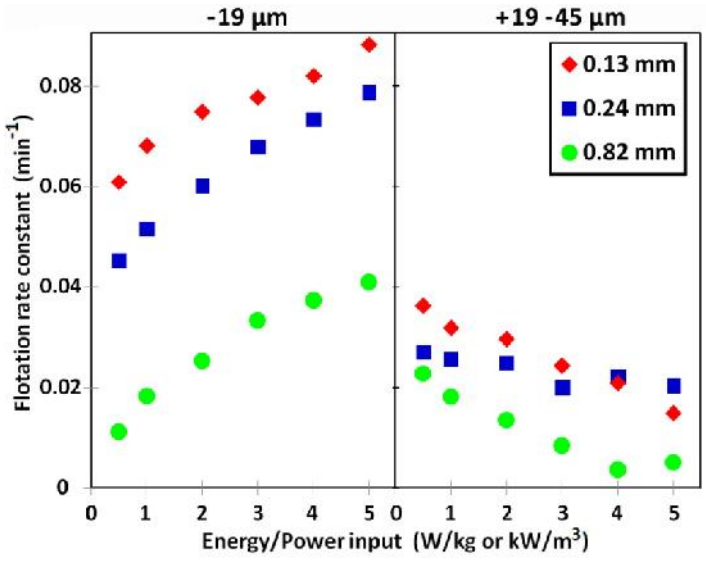

Figure 4.8: Flotation rate constant (min^{-1}) versus energy input (W/kg) for two particle sizes and three bubble sizes

4.1.3. Relative Effect of Energy Input on Flotation Kinetics

This section presents and discusses results for the relative effect of energy input on the flotation rate constant for all minerals. It is difficult to discern from Figures 4.4 to 4.8 what the effect of

energy/power input on flotation kinetics is in terms of magnitude for the various particle sizes, bubble sizes and particle densities. As observed in these figures, the flotation rate changes (increases or decreases) significantly with increasing energy input. Figure 4.9 illustrated the percentage increases or decreases in flotation rate relative to the flotation rate at low energy input (0.5 W/kg) for all particle sizes, all bubble sizes, a moderate collector dosage and all mineral types. For comparative purposes, the minerals in this figure are sorted based on their density from high to low.

Figure 4.9 shows that the flotation rate constant increases almost linearly with increasing energy input for fine particles under most conditions. Here, the flotation rate constant increases by around 220%, 200%, 180%, 170% and 150% with increasing energy input up to 3 W/kg for galena, hematite, pyrite, pentlandite and apatite respectively. Hence increasing energy input has a more significant effect on bubble-particle collision and attachment for minerals with higher density, such as galena. This figure shows that the increase in the flotation rate of fine particles with increasing energy input is a function of particle density, but is less dependent on bubble size, as observed by Changunda et al. 2008.

The flotation rate constant also increases (or decreases) almost linearly with increasing energy input for intermediate particles under most conditions. Here, the flotation rate constants for galena and hematite decrease by a maximum of 200% with increasing energy input up to 3 W/kg. The flotation rate constant is relatively unchanged for pyrite, whilst it increases by a maximum of 160 % for pentlandite and apatite. Notable exceptions are the results for the intermediate galena and pyrite particles, where increasing energy input leads to an initial increase in the flotation rate constant followed by a decrease. The magnitude of the decrease for galena is higher than that for pyrite due to a higher density and therefore a higher detachment rate.

The flotation rate constant decreases almost linearly with increasing energy input for coarse particles under all conditions. This decrease is around 400 %, 300%, 150% and 200% with increasing energy input up to 3 W/kg for galena, pyrite, pentlandite and apatite respectively. Hence, increasing energy input has a more significant effect on bubble-particle detachment for minerals with higher density, such as galena. It is clear from this figure, that coarse particles do not benefit from agitation. Here, the optimum condition for the flotation rate of coarse particles is when the energy input is just enough to keep the particles in suspension (Westhuizen and Deglon, 2007).

The majority of theoretical and experimental studies have found energy input to have less of an effect on the increase in the flotation rate constant than the linear dependence observed in this study. However, some more recent studies have also noted this linear dependence (Newell and Grano, 2006; Changunda et al., 2008; Tabosa et al., 2016). Results in this figure indicate that increases in the flotation rate with increasing energy input are more dependent on particle size and particle density than on bubble size and contact angle. This suggests that energy input and bubble size may respectively play more and less of a role in promoting particle-bubble contacting in turbulent environments than noted in the flotation literature.

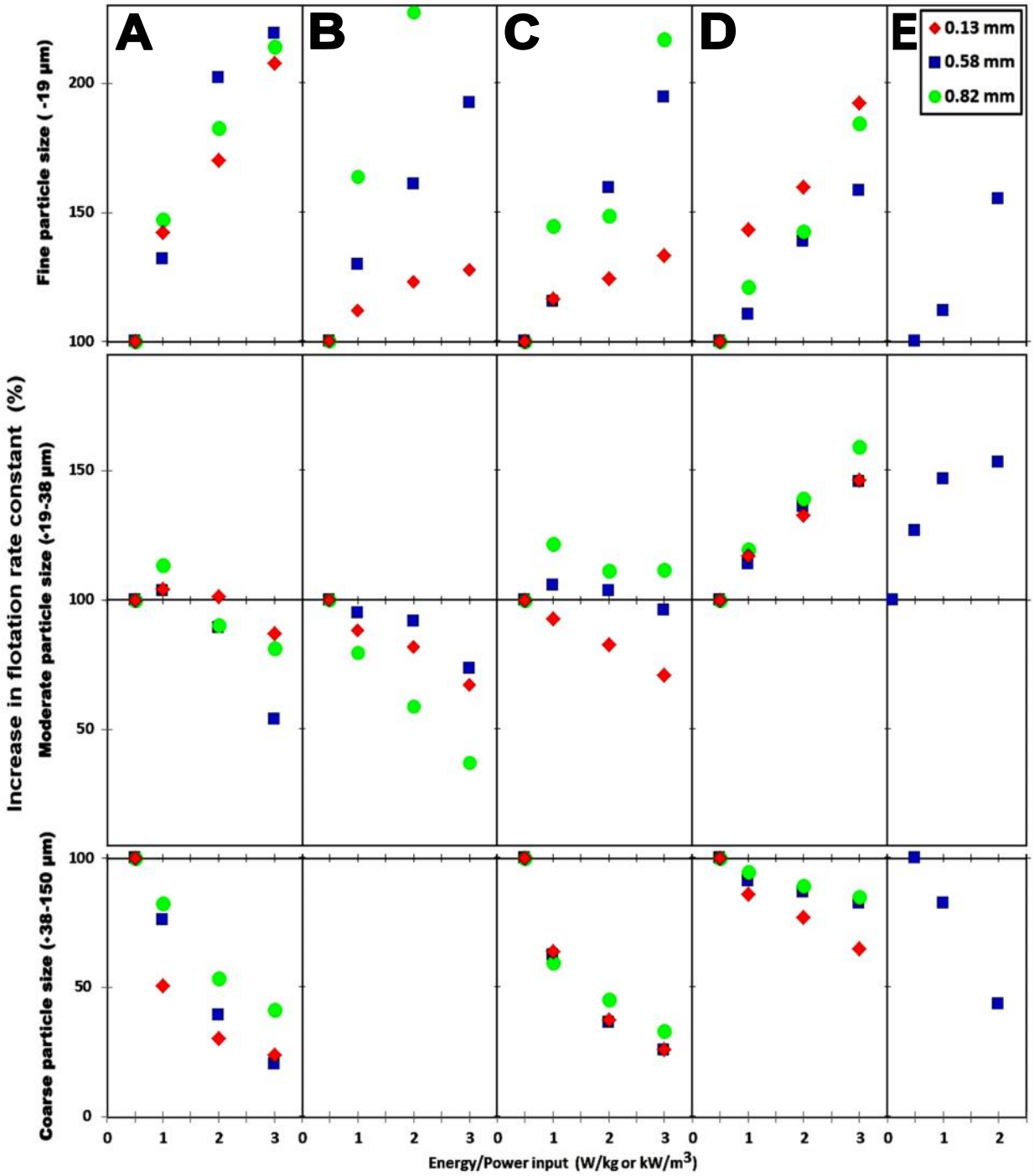

Figure 4.9: Percentage change in the flotation rate constants, relative to the rate at low energy input (0.5 W/kg), versus energy input for all particle sizes, bubble sizes and moderate collector dosage, sorted for all minerals based on their density, A: Galena, B: Hematite, C: Pyrite, D: Pentlandite, E: Apatite

4.1.4. Simulated Effect of Energy Input on Flotation Kinetics

This section presents and discusses simulated results for the effect of energy input on the flotation rate constants for the sulphide minerals. The purpose of this section is to both augment and interrogate the interpretation of results from Sections 4.1.1 to 4.1.3 through simulation of the flotation rate constants using the best available fundamental models from the flotation literature. The method used to calculate the simulated flotation rate constants is given in Section 4.1.4.1. Results for the simulated flotation

rate constants are given in Sections 4.1.4.2 & 4.1.4.3. Here, collision frequencies, collision efficiencies, attachment efficiencies, stability efficiencies and flotation rate constants are simulated and presented based on the flotation conditions used for the sulphide minerals.

4.1.4.1. Flotation Rate Constant Calculations

Flotation rate constants were calculated using Equation 2.55 developed by Pyke, Fornasiero and Ralston 2003. This model is still considered by many researchers to be the best available fundamental model for flotation in turbulent systems. Equation 2.55 determines the flotation rate constant using expressions for the collision frequency, collision efficiency, attachment efficiency and stability efficiency, as discussed in Section 2.3. The collision frequency is calculated using a modified form of the equation for collision in turbulent systems developed by Abrahamson 1975 with expressions for turbulent velocities developed by Liepe and Mockel 1976 (Equation 2.21). The collision efficiency is determined using the Generalised Sutherland Equation presented by Dai et al. 2000. The attachment efficiency is calculated using a model developed by Dobby and Finch 1987 (Equation 2.33) and the sliding time model used by Pyke et al. 2003. Here, the induction time is calculated from the particle contact angle using an empirical correlation (Equation 2.35) similar to that used by Pyke et al. 2003 and Dai et al. 1999. The stability efficiency is calculated using the modified Schulze model (Equation 2.38).

4.1.4.2. The Simulated Effect of Principal Parameters on Flotation Kinetics

This section presents and discusses the effect of the principle flotation parameters particle size, bubble size and contact angle (collector dosage) on the simulated flotation rate of sulphide minerals at low energy input (0.5 W/kg). Flotation results for the effect of particle size are presented for the -30 μm (finer) size class where bubble-particle detachment is minimal. Flotation results for the effect of bubble size and contact angle are presented for three particle size classes for comparative purposes, namely, -19 μm (fine), +19-38 μm (intermediate) and +38-150 μm (coarse). Galena, pyrite and pentlandite flotation results are indicated as “A”, “B” and “C”, respectively on all figures.

4.1.4.2.1. Effect of Particle Size

Figure 4.10 shows the relationship between the simulated flotation rate constant, collision efficiency, attachment efficiency, stability efficiency and particle size for the three bubble sizes and high collector dosage at low energy input. Here, trends in the flotation rate constants are affected primarily by the collision and attachment efficiencies as the collision frequency and stability efficiency remain relatively constant. The bubble-particle collision efficiency increases dramatically with increasing particle size and decreasing bubble size, which is well established in the flotation literature. It is

notable that the collision efficiencies for very hydrophobic particles (θ= 90°) with diameters below 5.0 µm are less than 5 %, highlighting the fact that the low flotation rate of fine particles is primarily a bubble-particle collision problem. It is also worth noting that there is no minimum in the collision efficiency for very fine particles, despite their small Stokes numbers.

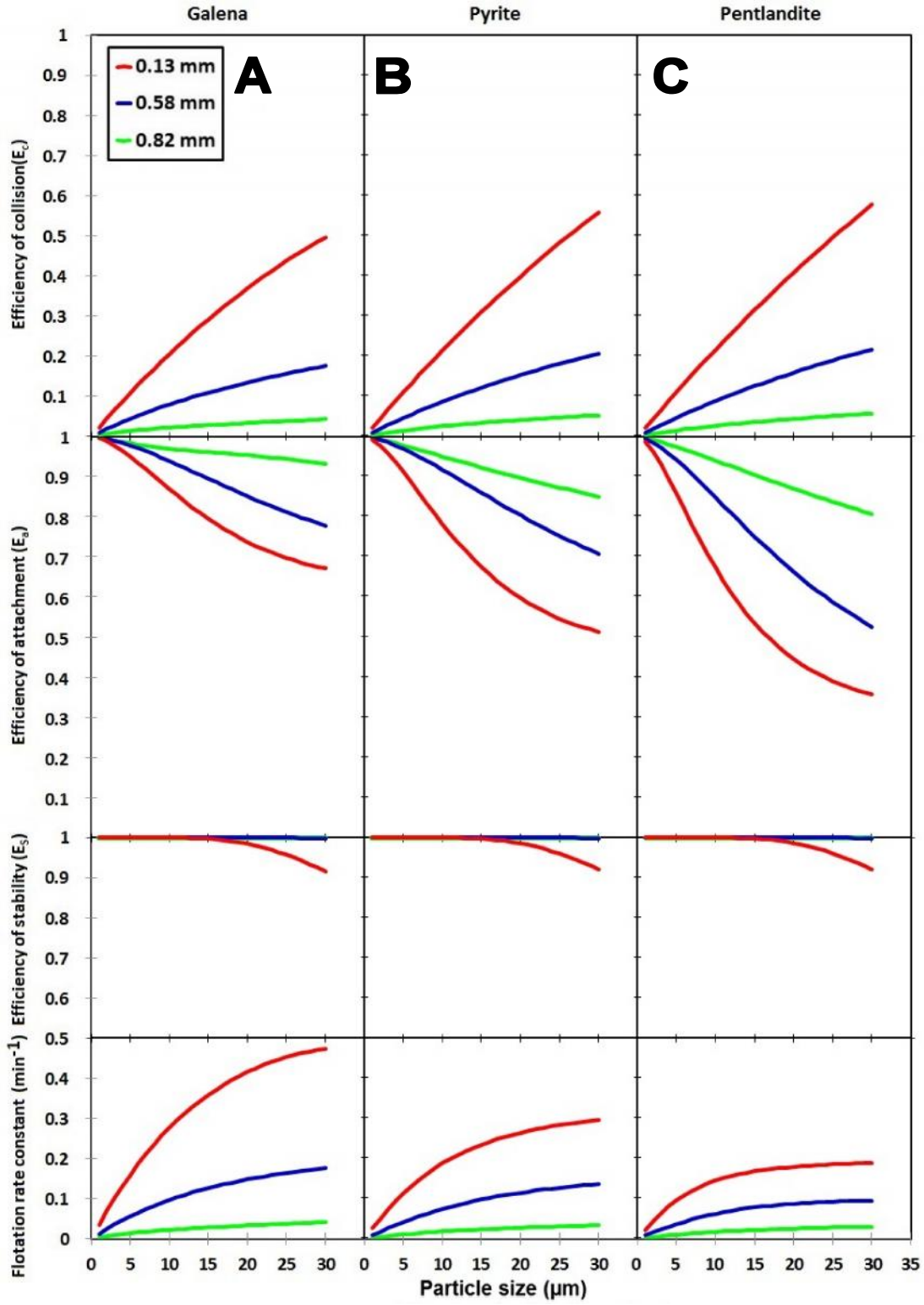

Figure 4.10: Flotation rate constant (min^{-1}) (k), collision efficiency (Ec), attachment efficiency (Ea), stability efficiency (Es) versus particle size (µm) for three bubble sizes and high collector dosage (¯=90) at low energy input (0.5 W/kg), A: Galena, B: Pyrite, C: Pentlandite

Nguyen et al. 2006 measured a minimum in collision efficiency at a particle diameter of 0.1 µm. The bubble-particle attachment efficiency decreases with increasing particle size and decreasing bubble size. This is in agreement with the experimental data of Hewitt et al. 1995, Dai et al. 1999 and Pyke et al. 2003. Attachment efficiencies are higher in overall magnitude for the more dense galena and decrease with decreasing mineral density. The flotation rate constant increases with increasing particle size and decreasing bubble size. This is attributed primarily to increases in bubble-particle collisions, as discussed in Section 4.1.1.1. Here, increases in collision efficiencies dominate over decreases in attachment efficiencies. The flotation rate constant decreases in overall magnitude with decreasing mineral density due to changes in the attachment efficiency discussed previously. The simulated flotation rate constants compare well to the experimental data presented in Figure 4.1 in terms of both trends and magnitude. The average relative error between simulated and experimental data is around 30% which is surprising good given that Equation 2.55 is based entirely on fundamental models and parameters i.e. no fitted quantities. However, it should be noted that the simulated flotation rate constants are for the -30 µm (finer) size class only in order to allow for direct comparison with Figure 4.1. This size class was chosen as bubble-particle detachment is minimal. This allows for direct comparison with literature studies where the effect of particle size is commonly expressed as $k \propto d_p^n$.

4.1.4.2.2. Effect of Bubble Size

Figure 4.11 shows the relationship between the simulated flotation rate constant, collision efficiency, attachment efficiency, stability efficiency and bubble size for the three particle size fractions and high collector dosage at low energy input. The bubble-particle collision efficiency increases with increasing particle size and decreasing bubble size, as noted previously. The bubble-particle attachment efficiency is strongly dependent on the particle size, bubble size and mineral density, with galena having the highest attachment efficiencies, as noted previously. The increase in the attachment efficiency with increasing bubble size is more pronounced for larger particles than for smaller particles, which is in agreement with the literature. The bubble-particle stability efficiency is also strongly dependent on the particle size and bubble size, but is less dependent on mineral density. Here, the stability efficiency for fine particles is near unity under all conditions but is very low for coarse particles and small bubbles. In general, the flotation rate constant increases significantly with decreasing bubble size, as commonly observed in the literature and discussed in Section 4.1.1.2. However, this trend is particle size dependent with intermediate particles having the highest overall rates due to the poor stability efficiencies for coarse particles. The simulated flotation rate constants compare well to the experimental data presented in Figure 4.2 in terms of general trends but differ in magnitude. Here, the average relative error between simulated and experimental data is around 60%. This is still considered reasonably good for a fundamental model given that rate constants in Figure 4.11 vary in magnitude by several hundred percent.

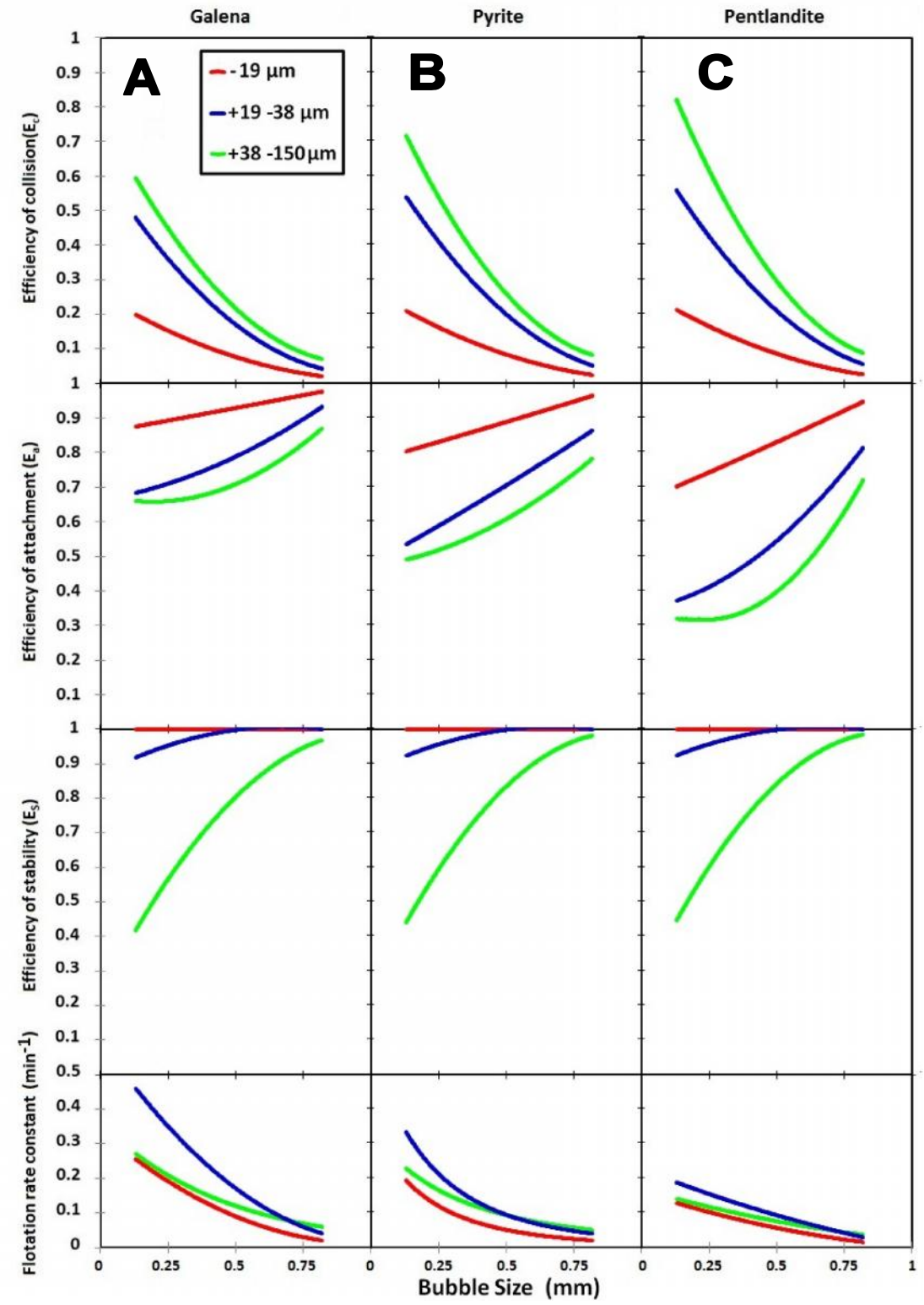

Figure 4.11: Flotation rate constant (min^{-1}) (k), collision efficiency (Ec), attachment efficiency (Ea), stability efficiency (Es) versus bubble size (mm) for three particle size fractions (µm) and high collector dosage ($\bar{}$=90) at low energy input (0.5 W/kg), A: Galena, B: Pyrite, C: Pentlandite

4.1.4.3. The Simulated Effect of Energy Input on Flotation Kinetics

This section presents and discusses results for the effect of energy input on the simulated flotation rate constants for the sulphide minerals. Flotation results are presented in three particle size classes for comparative purposes, namely, fine (-19 μm), intermediate (+19 -38 μm) and coarse (+38 -150 μm). Galena, pyrite and pentlandite flotation results are indicated as “A”, “B” and “C”, respectively on all figures.

It is important to note that the bubble-particle collision and attachment efficiencies are only dependent on the particle size, bubble size, contact angle and mineral density. Consequently, these quantities vary in magnitude in the results presented in this section, but are independent of changes in energy input. Here, the collision efficiency increases with increasing particle size, decreasing bubble size and decreasing mineral density while the attachment efficiency follows completely contrary trends. These efficiencies affect the overall magnitude of the flotation rate constant but not the variation of the rate constant with changes in energy input and will not be discussed in this section.

4.1.4.3.1. Fine Particles

Figure 4.12 shows the relationship between the flotation rate constant, collision efficiency, attachment efficiency, stability efficiency and the energy/power input for the fine particles (-19 μm) and for all bubble sizes and a high collector dosage. The bubble-particle stability efficiency is near unity under all conditions. Consequently, changes in the flotation rate constant with increasing energy input are entirely due to changes in the collision frequency, which is dependent on the energy input, bubble size and mineral density.

The flotation rate constant increases steadily with increasing energy input due to an increase in the bubble-particle collision frequency. The flotation rate constant decreases in overall magnitude with decreasing mineral density due to changes in the attachment efficiency discussed previously. The simulated flotation rate constants compare well to the experimental data presented in Figure 4.4 in terms of both trends and magnitude. The average relative error between simulated and experimental data is around 35%. This suggest that the turbulent collision model used is appropriate for fine particles (Equation 2.21). In addition, this supports the arguments presented in Section 4.1.2.1.1 where the increase in the flotation rate constant with increasing energy input was attributed to increases in bubble-particle collisions.

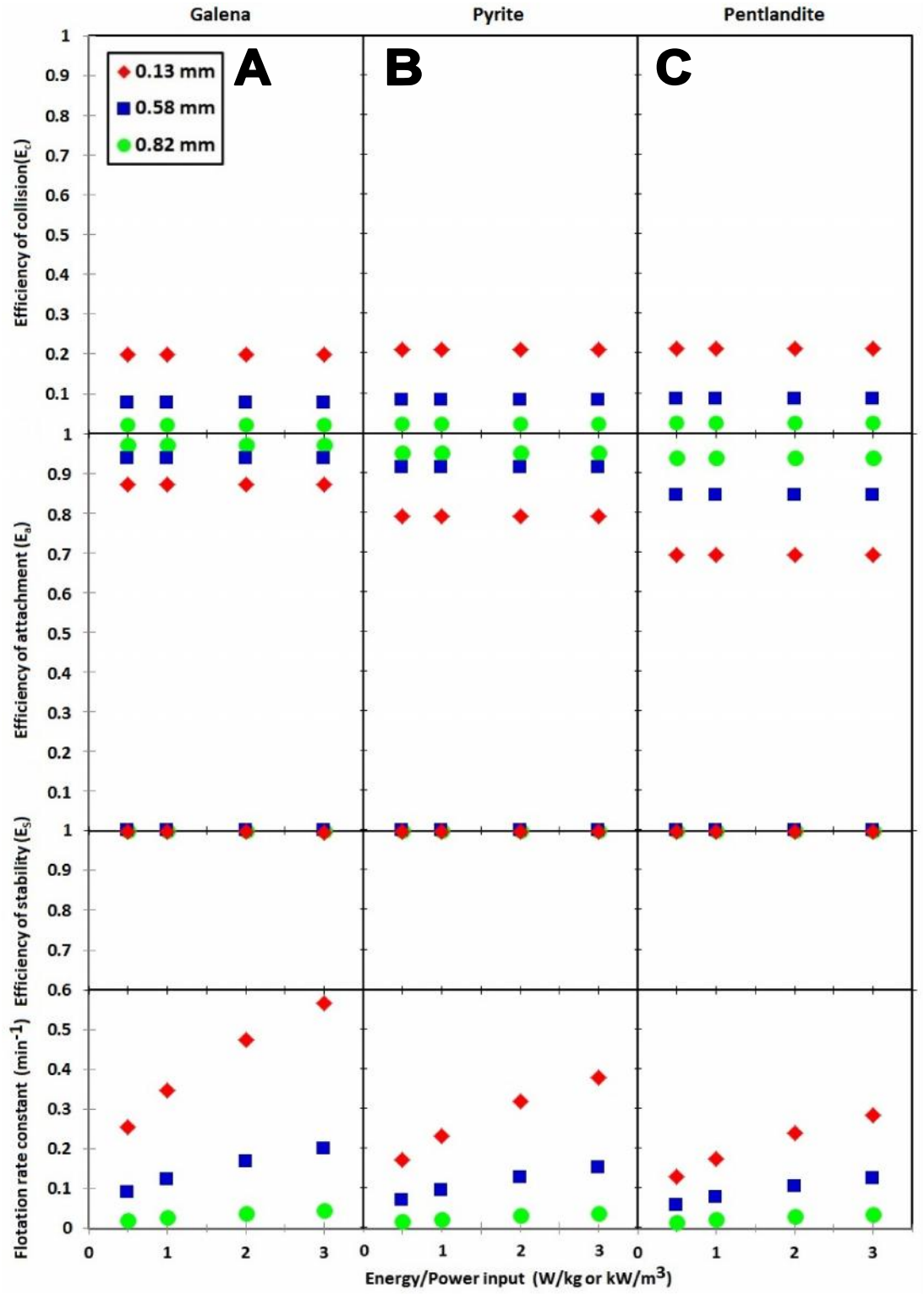

Figure 4.12: Flotation rate constant (min^{-1}) (k), collision efficiency (Ec), attachment efficiency (Ea), stability efficiency (Es) versus energy input (W/kg) for the flotation of fine particles (-19 µm), all bubble sizes and high collector dosage (¯=90), A: Galena, B: Pyrite, C: Pentlandite

4.1.4.3.2. Intermediate Particles

Figure 4.13 shows the relationship between the flotation rate constant, collision efficiency, attachment efficiency, stability efficiency and the energy/power input for the intermediate particles (+19 -38 µm) and for all bubble sizes and a high collector dosage. The bubble-particle stability efficiency is near

unity under most conditions. Consequently, as with the fine particles, changes in the flotation rate constant with increasing energy input are entirely due to changes in the collision frequency. Again, the flotation rate constant increases steadily with increasing energy input due to an increase in the bubble-particle collision frequency.

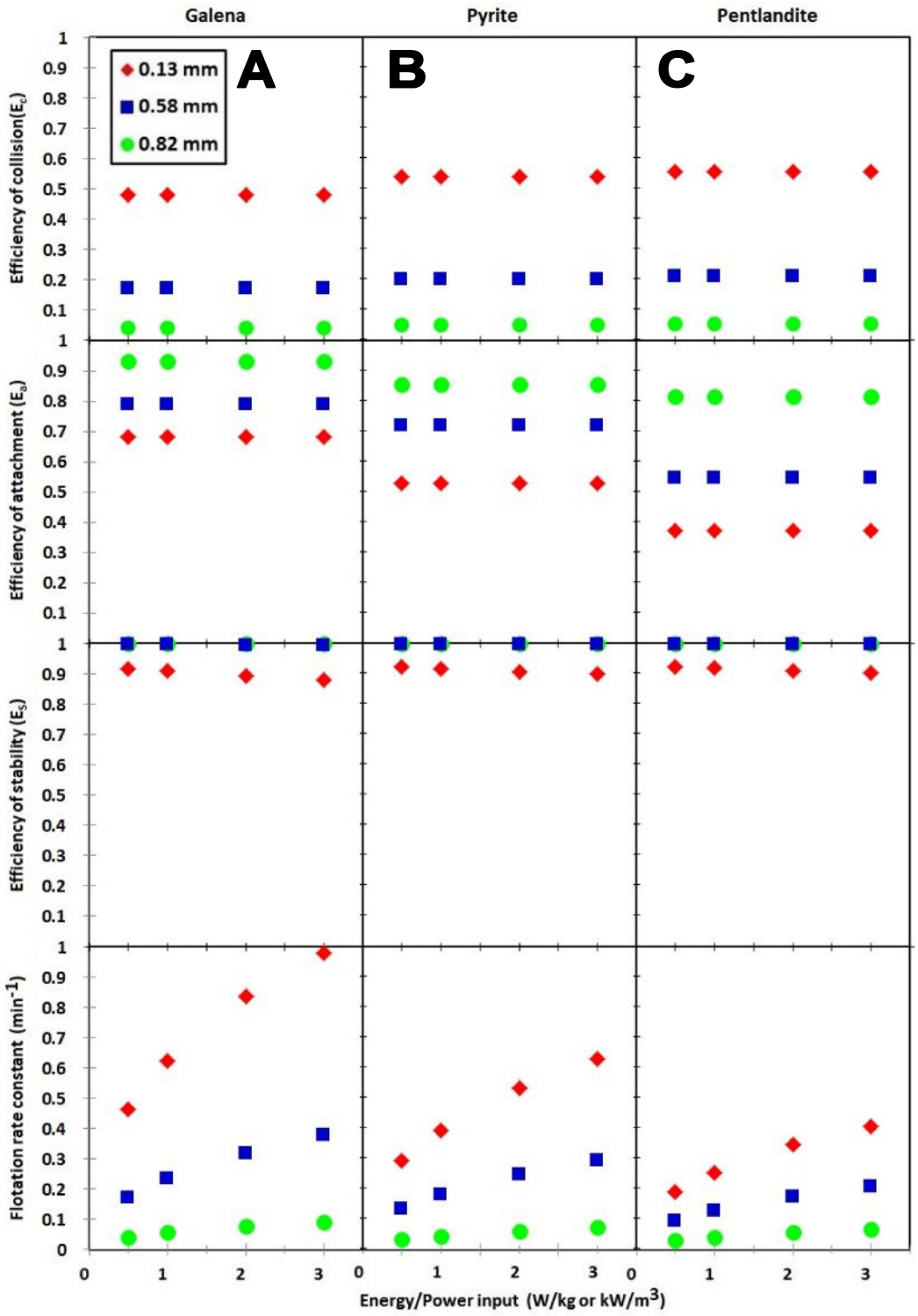

Figure 4.13: Flotation rate constant (min^{-1}) (k), collision efficiency (Ec), attachment efficiency (Ea), stability efficiency (Es) versus energy input (W/kg) for the flotation of intermediate particles (+19 -38 µm), all bubble sizes and high collector dosage (¯=90), A: Galena, B: Pyrite, C: Pentlandite

However, there are differences between the simulated flotation rate constants and the experimental data presented in Figure 4.5 primarily in terms of trends. The average relative error between simulated and experimental data is around 53%. This is still considered reasonably good for a fundamental model given that rate constants in Figure 4.12 vary in magnitude by several hundred percent. However, of more concern is that there are clear differences between the trends in the simulated and experimental data for galena and pyrite. The simulated rate constants increase steadily with increasing energy input under all conditions whereas there are clear optimums in the experimental rate constants for most of the galena and pyrite data. This deviation could be due to a number of reasons and will discussed further in Section 4.1.4.2.3 for coarse particles.

4.1.4.3.3. Coarse Particles

Figure 4.14 shows the relationship between the flotation rate constant, collision efficiency, attachment efficiency, stability efficiency and the energy/power input for the coarse particles (+38 -150 µm) and for all bubble sizes and a high collector dosage. The bubble-particle stability efficiency is dependent on the bubble size and energy input, Here, the stability efficiency decreases dramatically with decreasing bubble size and more steadily with increasing energy input. The stability efficiency is very low for coarse particles and small bubbles, even at low energy inputs i.e. relatively quiescent conditions. Again, the flotation rate constant increases with increasing energy input, although this increase is lower than that for the fine/intermediate particles and appears to be approaching an optimum. However, there are very large differences between the simulated flotation rate constants and the experimental data presented in Figure 4.6 in terms of both trends and magnitude. The average relative error between simulated and experimental data is over 100% and for certain data points exceeds 200%.

The trends in the simulated and experimental data for all three minerals are completely different. Here, the simulated flotation rate constants increase steadily with increasing energy input whereas the experimental rate constants decrease sharply under all conditions. This deviation could be due to a number of reasons but the two most likely are as follows. The difference in magnitude could be due to an under prediction of the collision frequency/efficiency. The collision efficiency is based on the Generalised Sutherland Equation which has been known to under predict this quantity for coarser particles. The collision efficiency could also be influenced by the bubble rise velocity which affects the maximum possible collision angle (θt) in the GSE. The bubble rise velocity has a large effect on the collision efficiency (Pyke et al., 2003). However, an increase in the collision frequency/efficiency would increase the overall magnitude of the simulated flotation rate constants but would not affect the trends with increasing energy input. The stability efficiency would have to change significantly in order to explain the sharp decreases in the experimental rate constants for the coarse particles and the existence of optimums for the intermediate particles. Here, the stability efficiency would have to have

a much stronger dependence on energy input than shown in Figure 4.14, with less of a dependence on bubble size at lower energy inputs. Hence the stability efficiency would have to be much higher at low energy inputs an much lower at high energy inputs. This would require modification of the Schulze model for the stability efficiency (Equation 2.38).

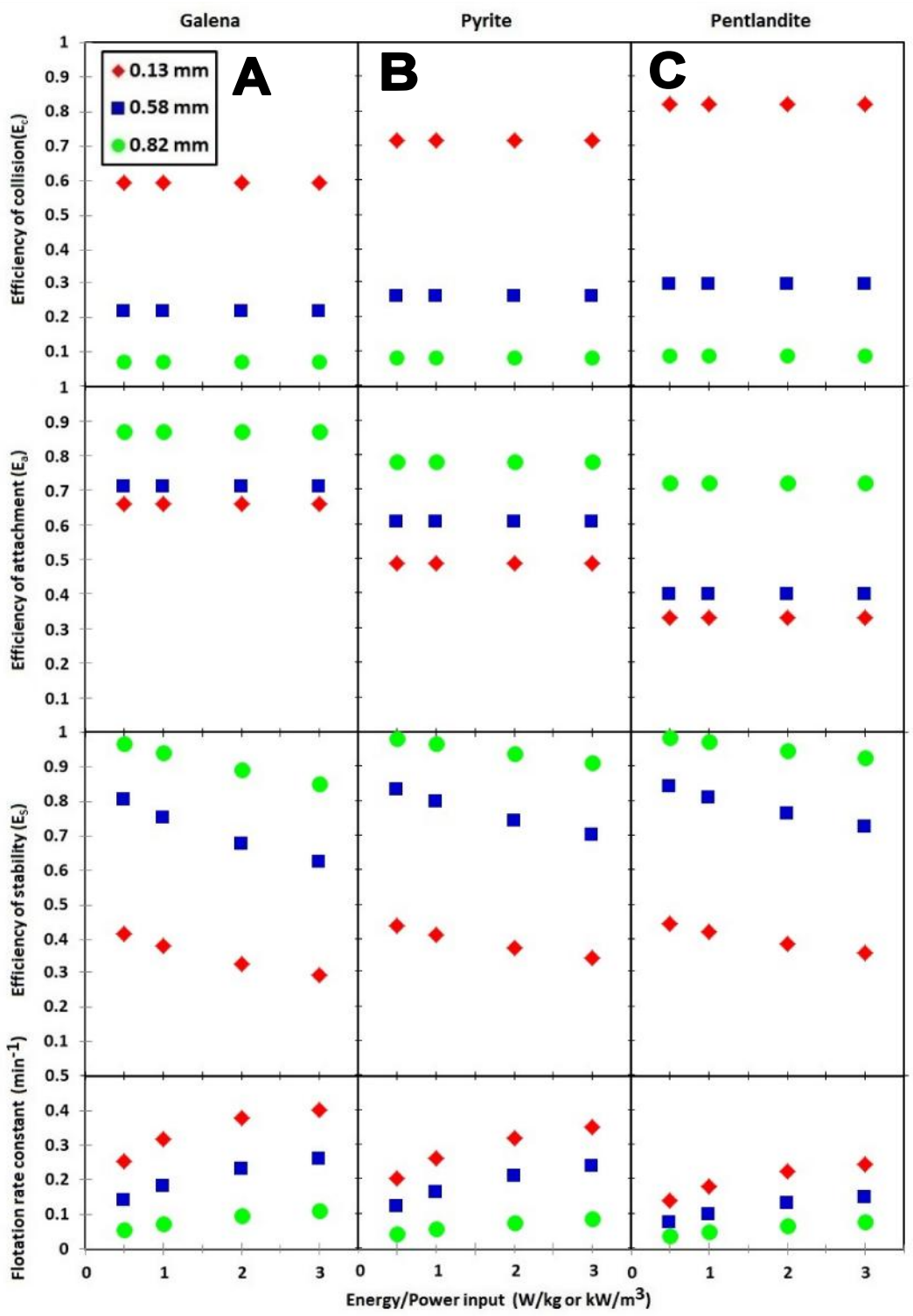

Figure 4.14: Flotation rate constant (min^{-1}) (k), collision efficiency (Ec), attachment efficiency (Ea), stability efficiency (Es) versus energy input (W/kg) for the flotation of coarse particles (+38-150 µm), all bubble sizes and high collector dosage (¯=90), A: Galena, B: Pyrite, C: Pentlandite

4.2. Pilot Scale Oscillating Grid Cell

This section presents and discusses results for the effect of energy/power input on the flotation of a platinum ore (PGM) in the pilot scale oscillating grid flotation cell. The results of flotation tests in the laboratory oscillating grid flotation cell are used for comparative/benchmarking purposes as PGMs are generally treated as a sulphide float. The results are presented for three particle size classes, referred to as fine (-25 μm), intermediate (+25 -53 μm) and coarse (+53 μm). Results are discussed in terms of trends in the flotation rate constant, rather than the overall magnitude, as the two OGC flotation cells had very different operating conditions.

The pilot scale OGC was operated over a broad range of test conditions. Recoveries and grades (platinum and palladium) varied from 10.23 to 43.94% and 4.24 to 65.11 ppm, respectively. Mass pull and water recoveries varied from 0.51 to 14.81% and 0.32 to 11.66%, respectively. These are large differences in metallurgical performance, given that the cell was operated at constant feed conditions, air flow rate and froth depth. Large changes in the performance of individual flotation cells are usually achieved by varying parameters such as feed properties (rate, grade, grind etc.), reagent dosage, air flow rate and froth depth. The relative differences range from hundreds to thousands of percent. The cell achieved reasonable flotation performance (rate, recovery, grade etc.) while operating on a fine, relatively low grade feed (≈ 1 ppm).

4.2.1. The Effect of Energy Input on Flotation Kinetics

Figure 4.15 shows the relationship between the normalized PGM (platinum and palladium) flotation rate constant and the energy input for three particle size classes and two bubble sizes. Primary cleaner tails and secondary rougher feed flotation results are indicated as “A” and “B”, respectively on this figure. All data are normalized relative to the maximum flotation rate constant for each series of experiments i.e. 0.14 min^{-1} and 0.16 min^{-1} for the primary cleaner tail and secondary rougher feed respectively. As with the laboratory OGC results, the flotation rate constant increases significantly with decreasing bubble size. This has been observed previously by other researchers in platinum flotation (Hernandez-Aguilar et al., 2006). However, the flotation rate constant does not increase with increasing particle size. This is not unexpected as -25 μm PGM ore is relatively fast floating. Furthermore, PGM particles may be poorly liberated in the coarser fractions. The lower flotation rate for coarser particles is probably due to a combination of liberation and increased detachment.

Results for the primary cleaner tail indicate that the flotation rate constant for fine and intermediate particles increases steadily with increasing energy input for the large bubbles (1.47 mm) but decreases for the small bubbles (0.71 mm). For example, for the large bubbles the flotation rate constant increase by around 300% with increasing energy input from 0.1 to 1.7 W/kg for the fine and intermediate particles. However, for coarse particles increasing energy input leads to an optimum in the flotation rate constant for the large bubbles, but significant decreases for the small bubbles. For the large

bubbles the flotation rate constant increase by around 400% with increasing energy input to an optimum at around 0.9 W/kg. Results for the secondary rougher feed show that increasing energy input leads to an optimum in the flotation rate constant for the large bubbles, but significant decreases for the small bubbles. This optimum is at around 2 W/kg for the fine and intermediate particles and 1.5 W/kg for the coarse particles. For the large bubbles the flotation rate constant increases by around 250% with increasing energy input from 0.1 to 1.9 W/kg for the fine particles while this increase is over 400% for the intermediate particles.

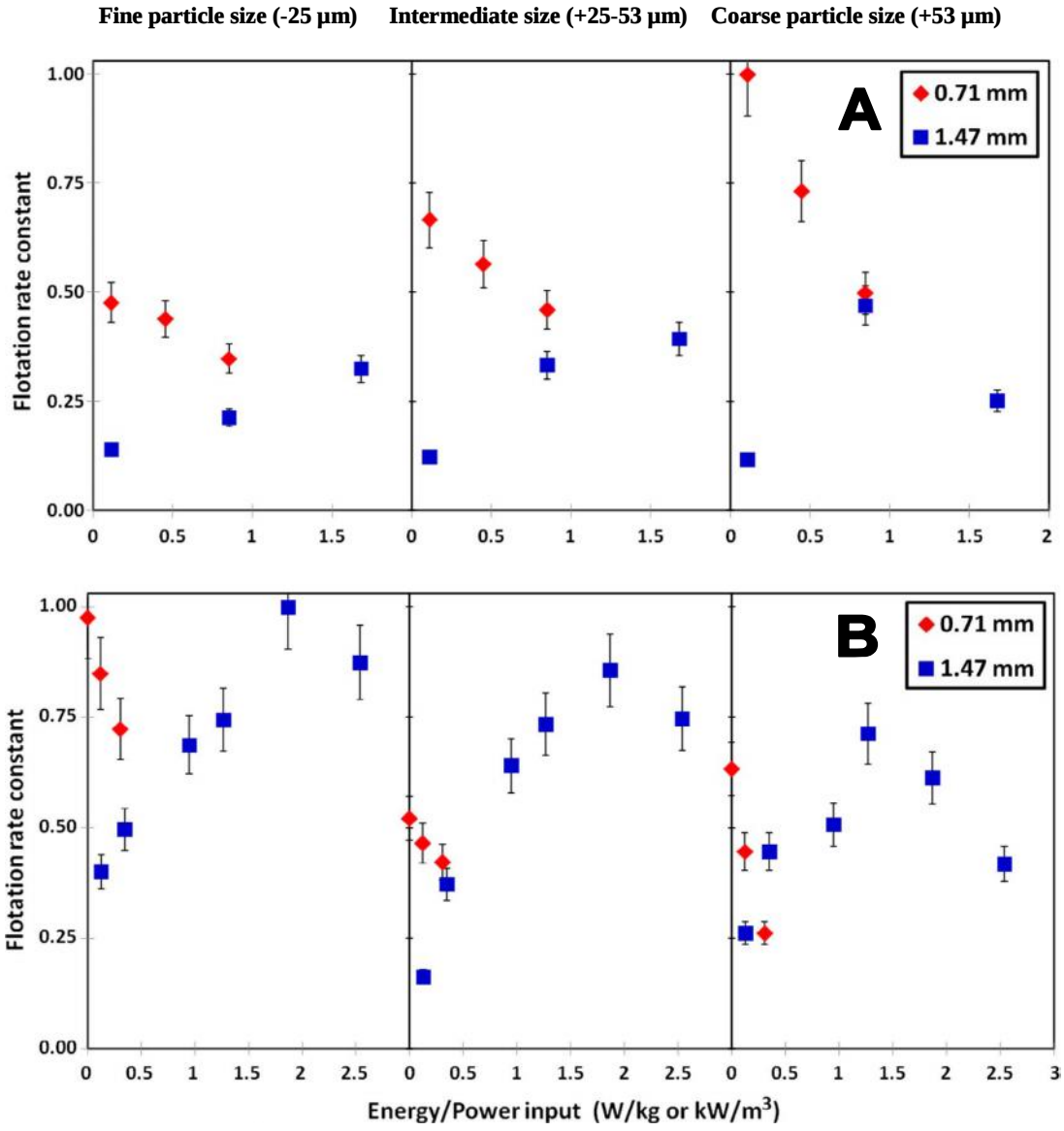

Figure 4.15: Normalized flotation rate constant versus energy input for the flotation of PGM minerals with three particle size fractions, two bubble sizes and plant collector dosage, A: Primary cleaner tail, B: Secondary rougher feed

Trends in the pilot-scale OGC results for the fine and intermediate particles and for the large bubbles are similar to those for the laboratory OGC. For the fine particles, increasing energy input generally leads to a steady increase in the flotation rate constant, although this approaches an optimum at higher energy inputs for galena and the secondary rougher feed. For intermediate particles, a similar increase

is observed with a clearer indication of an optimum in the vicinity of 1 to 2 W/kg. Results for the coarse particles cannot be compared directly due to differences in the size ranges. However, for the small bubbles increasing energy input leads to a decrease in the flotation rate constant for all conditions. The laboratory OGC results showed that flotation with small bubbles tends to be more sensitive to increasing energy input, but not as marked as in the pilot-scale OGC. In general, pilot-scale OGC results show that optimum conditions for PGM flotation are using small bubbles at lower energy inputs, or large bubbles at higher energy inputs. This suggests that higher energy inputs are generally beneficial for the flotation of platinum ores as these consist predominantly of finer particles and most industrial flotation applications operate with larger bubbles (1.0-2.0 mm), as observed in the flotation literature (Manlapig, 2000; Deglon, 2005; Wei et al., 2014).

4.3. Flotation Modelling

Flotation rate constants calculated using the fundamental flotation model (Equation 2.55) compared reasonably well to the experimental rate constants for the fine particles but not for the intermediate and coarse particles. Trends in the experimental flotation rate constants clearly showed that the rate constant was an outcome of the competitive processes of bubble-particle collision/attachment and detachment. In order to extract as much information from this large flotation data set as possible, it was decided to model this using a suitable kinetic model. The attachment-detachment kinetic model presented in Section 2.4.2 was used as this is a kinetic model which allows for the two separate processes of particle-bubble collision/attachment and detachment. Section 4.3.1 presents an overview of the attachment-detachment kinetic model. The empirical correlations for the attachment and detachment rate constants are compared to findings from the flotation literature in Section 4.3.2. Finally, the attachment-detachment model is used to simulate the flotation rate constant over a broad range of conditions in Section 4.3.3.

4.3.1. The Attachment-Detachment Kinetic Model

The development of the attachment-detachment kinetic model is described in Section 4.3.1.1 while testing/validation of the model is presented in Section 4.3.1.2.

4.3.1.1. Model Development

General empirical correlations for the attachment and detachment rate constants were developed based on clear trends observed in the experimental data, as shown in Equations 4.1 & 4.2. These correlations describe the relationship between the attachment and detachment rate constants and the particle size, particle density, bubble size, contact angle and energy input. The correlations were applied to the entire laboratory OGC sulphide and oxide flotation data set of several thousand size-by-size rate

constants to determine best-fit regression values for individual empirical coefficients (C_1 & C_2) for each mineral type and common empirical exponents (n_1 to n_5) for all minerals. Here, rate constants were calculated using the equations presented in Section 2.4.2. Results for the common empirical coefficients are summarized in Table 4.1. The coefficients (C_1 & C_2) varied quite significantly between the mineral types. For example, the coefficient C_1 for the attachment rate constant for the sulphide minerals was found to be 33.7, 7.0 and 2.40 ($x10^{-5}$) for galena, pyrite and pentlandite respectively. Similarly, the coefficient C_1 for the detachment rate constant was found to be 1.0, 1.5 and 1.8 ($x10^{-6}$) for these same minerals. These coefficients are entirely empirical and would have to be determined experimentally for other minerals/ores and flotation conditions. The coefficients for the attachment rate constant appear to correlate with the mineral's natural floatability e.g. galena is known to be fast floating. In addition, these coefficients will vary with gas flow rate as the attachment rate constant was defined to be consistent with the flotation rate constant. Hence, it is likely that these coefficients will increase proportionately with increasing superficial gas velocity. However, the coefficients for the detachment rate constant are relatively similar (in overall magnitude) and average values could probably be used for all minerals. In addition, it is possible that these coefficients may not vary significantly with gas flow rate as a gas phase was incorporated in the definition of this rate constant. The empirical exponents (n_1 to n_5) are common for all mineral types and will be discussed further in Section 4.2.

$$k_a = d_p^{\,n_1}\left(c_1 + c_2 \pounds^{\,n_2}\right)(1-\cos^{-})^{n_3} d_b^{\,n_4 \circ n_5} \tag{4.1}$$

$$k_d = d_p^{\,n_1}\left(c_1 + c_2 \pounds^{\,n_2}\right)(1-\cos^{-})^{n_3} d_b^{\,n_4 \circ n_5} \tag{4.2}$$

Table 4.1: Empirical exponents for all experimental data

	Attachment Rate Constant (k_a)		**Detachment Rate Constant (k_d)**	
All Minerals	n_1	0.72	n_1	2.17
	n_2	0.91	n_2	1.33
	n_3	0.47	n_3	-1.17
	n_4	-0.77	n_4	0.67
	n_5	1.81	n_5	0.67
# Valid for d_p (μm), d_b (mm), Θ (°), ρ (ton/m^3), ε (W/kg)				

Figure 4.16 is a parity chart comparing the experimental to the model predicted flotation rate constant for the entire flotation data set. Rate constants are plotted on a log-log axis as they varied by orders of magnitude. The 99% confidence interval (CI), prediction interval (PI) and relative prediction interval (RPI) are also included in this figure. There is a reasonably good correlation between the experimental and model predicted rate constants, with an overall R^2 value of 0.91. More importantly, the parity

chart indicates a direct correlation with no apparent bias in the data. This suggests that the empirical exponents are relatively robust as these were determined by fitting few parameters to a very large flotation data set over a wide range of particle sizes, particle densities, bubble sizes, contact angles and energy inputs.

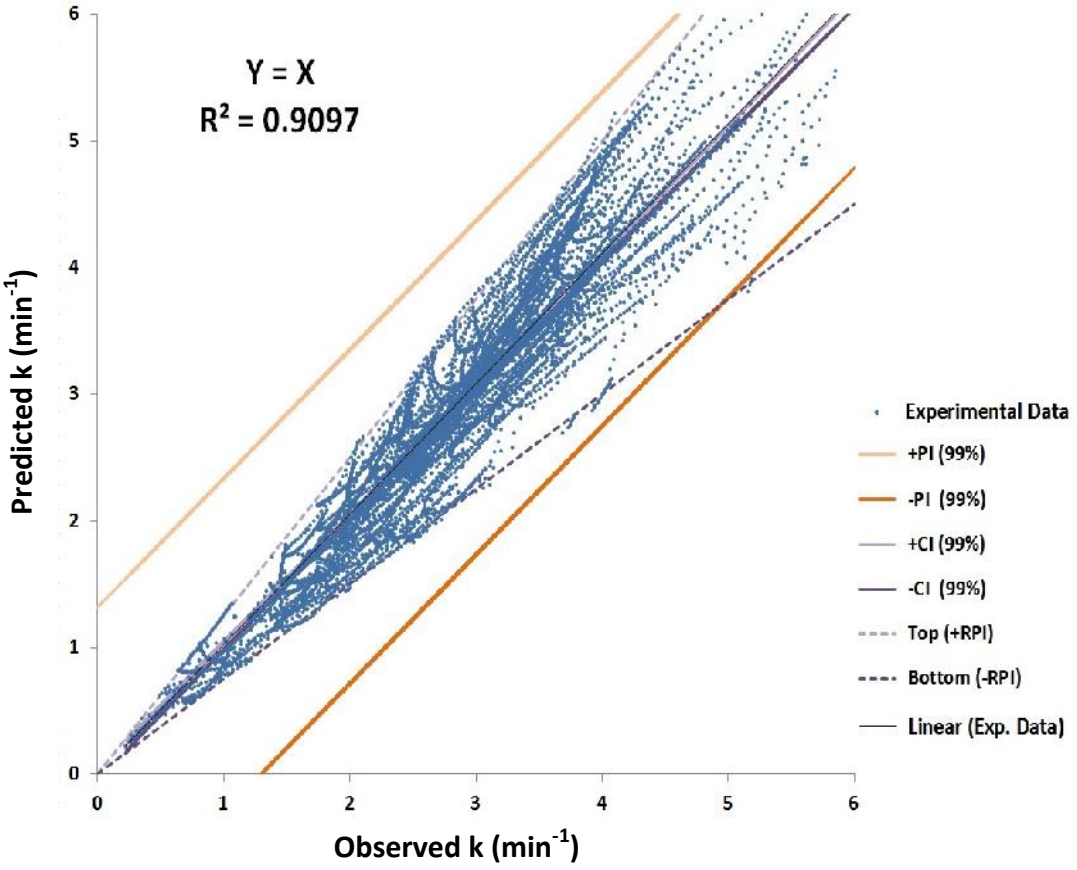

Figure 4.16: Model predicted versus experimental flotation rate constant (-ln(k)) for full experimental data set

4.3.1.2. Model Testing

Figure 4.16 suggests that the attachment-detachment model, used in conjuction with the empirical correlations for the attachment and detachment rate constants, gives a reasonable estimation of the entire flotation data set. However, this is only meaningful if the trends predicted by the model are consistent with those observed in the experimental data. Figure 4.17 shows the relationship between the flotation rate constant and the energy/power input for pyrite for three particle size classes (fine, moderate, coarse), three bubble sizes (0.13, 0.58, 0.82 mm) and three collector dosages (low, moderate, high). It is clear from this figure that in general the model predicts the trends in the experimental data reasonably well. There are clear differences between modelled and experimental data in certain instances but trends are generally similar, which is reassuring given that rate constants vary by well over an order of magnitude.

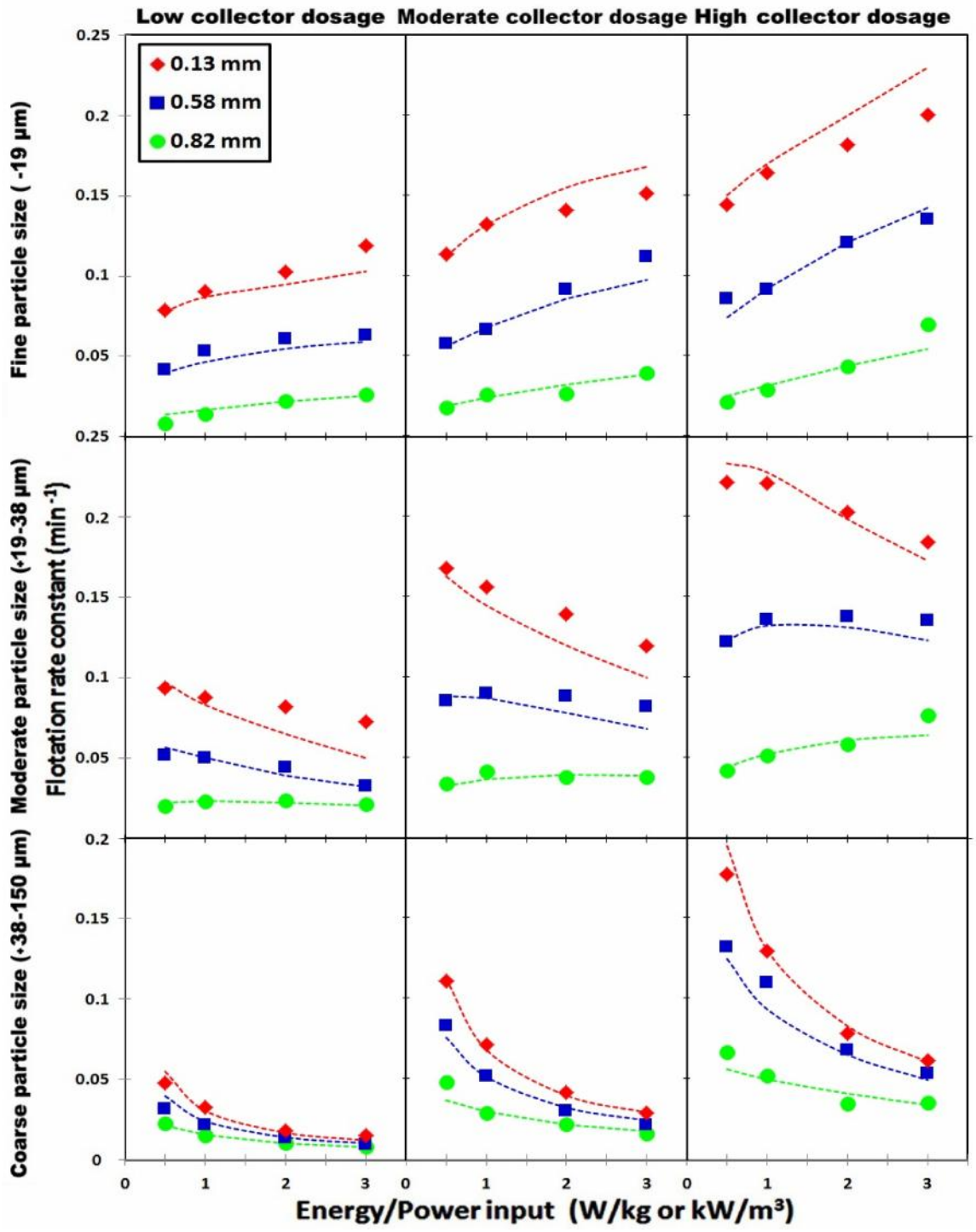

Figure 4.17: Experimental (symbols) and predicted (dash lines) flotation rate constant (min^{-1}) versus energy input (W/kg) for all the pyrite experimental data

Based on consistent trends in the predicted data, which were shown to be in reasonably good agreement with the experimental data, it was decided to test the attachment-detachment model against other flotation data sets in the literature. Three flotation data sets with a broad range of operating conditions were selected (Deglon, 1998; Pyke, 2004; Massey, 2012). Deglon 1998 and Pyke 2004 conducted flotation tests in stirred flotation cells while Massey 2012 used an oscillating grid flotation cell. The attachment-detachment model was applied to these three data sets using the same

methodology presented in Section 4.3.1.1. Here, the same empirical exponents (n_1 to n_5) presented in Table 4.1 were used and only the four coefficients (C_1 and C_2) were fitted to the data. Figure 4.18 is a parity chart comparing the experimental to the model predicted flotation rate constants for the three data sets. It is clear from this figure that the attachment-detachment model provides a reasonably good prediction for the experimental data. There is scatter in the data but no significant bias is observed. The predictions are surprising good given that the three researchers used very different operating conditions and that rate constants vary by several orders of magnitude.

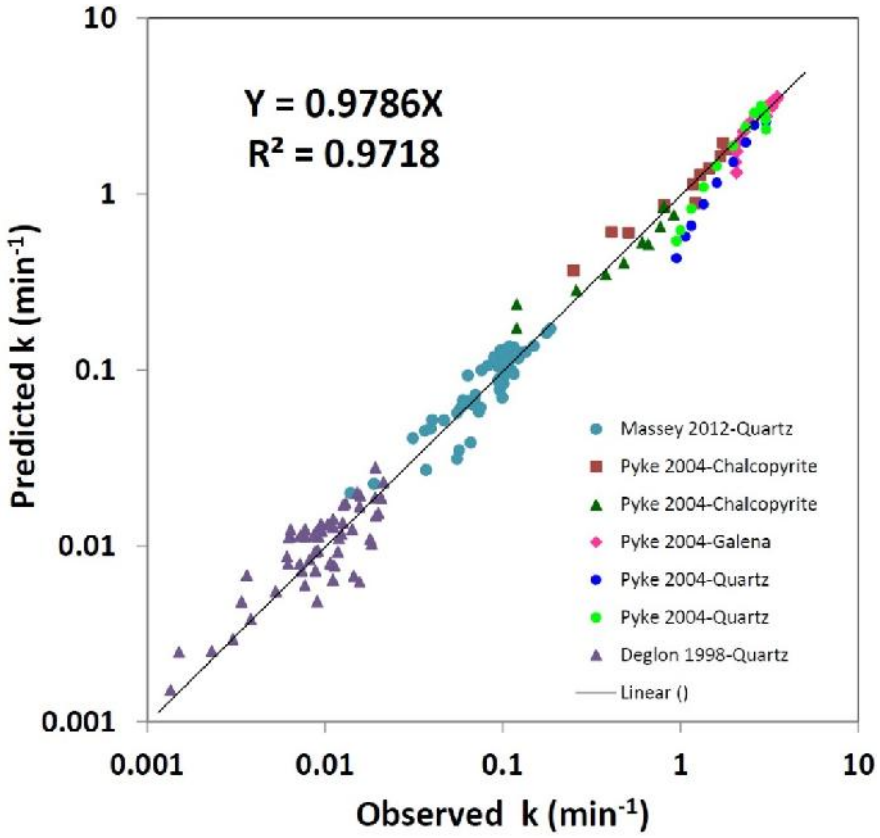

Figure 4.18: Model predicted versus experimental flotation rate constant (min^{-1})

4.3.2. Empirical Correlations for the Rate Constants

As discussed previously the coefficients for the attachment and detachment rate constants are empirical and would have to be determined experimentally for other minerals/ores. However, the exponents for the attachment and detachment rate constants (n_1 to n_5) were found to be similar for all mineral types. For these exponents to be meaningful, rather than merely regression parameters, they should be consistent with trends/values in the flotation literature. Table 4.2 compares the empirical exponents (n_1 to n_5) with a range of comparable values from the flotation literature. It should be noted that direct comparison is difficult as, to the authors' knowledge, there is no equivalent kinetic model of this nature in the flotation literature.

Table 4.2: Comparison of empirical exponents to the flotation literature

Attachment Rate Constant (k_a)				Detachment Rate Constant (k_d)			
For This Study		Flotation Literature		For This Study		Bond Number	
n_1	0.72	n_1	0.15 to 1	n_1	2.17	n_1	2
n_2	0.91	n_2	0.44 to 1	n_2	1.33	n_2	0.67
n_3	0.47	n_3		n_3	-1.17	n_3	-1
n_4	-0.77	n_4	-0.4 to -2.2	n_4	0.67	n_4	1
n_5	1.81	n_5	0.67-1	n_5	0.67	n_5	1

4.3.2.1. Attachment Rate Constant

The attachment rate constant was defined to be consistent with the flotation rate constant. Several of the exponents for the attachment rate constant are similar to those for the flotation rate constant commonly found in the flotation literature. The value of n_1=0.72 for the particle size is within the range observed in the literature for turbulent systems (0.15 to 1.0). The value of n_2=0.91 for the energy input is higher than the range used in theoretical turbulent collision models (0.44 to 0.75) but comparable to the range found in other experimental studies (0.7 to 1.0). The value of n_4=-0.77 for the bubble size is within the range found in the flotation literature for turbulent systems (-0.4 to -2.2). The values of n_5=1.81 for the particle density is higher than the typical value of 0.67 used in theoretical turbulent collision models but higher densities are also considered to increase the collison efficiency. It is difficult to comment on the value of n_3=0.47 for the contact angle as there are no suitable kinetic correlations for this quantity in the literature. However, the rate constant is expected to increase with increasing contact angle.

4.3.2.2. Detachment Rate Constant

Models for particle-bubble detachment generally predict the maximum stable aggregate/particle size rather than the rate of detachment. Here, the destabilising influence (probability of detachment, stress on aggregate, detachment force etc.) has be shown to be proportional to the particle size and the specific power input to the power of between 2/3 & 7/3 and 2/3 & 1 respectively (Deglon, 2002). Consequently, it is difficult to comment on the form of the detachment expression other than to indicate that it is dominated by the robust value of n_1=2.17 for the particle size, which is similar to the theory of Mika and Fuerstenau who found the detachment rate to be proportional to $d_p^{7/3}$. An exception to this is Bloom and Heindel who defined a detachment rate constant as the product of the number of collisions of a particle-bubble aggregate with a destabilising influence, times the stability efficiency, expressed as an exponential function of the modified Bond number (Goel and Jameson 2012). The exponent in the Bond model for the particle size (d_p^2) is comparable to the value of n_1=2.17 found in this study. The exponent in the Bond model for the bubble size (d_b^1) is higher than the value of n_4=0.67 determined in this study. This higher dependence on bubble size was noted previously in

Section 4.1.4.3.3. The exponent for the contact angle (n_3=-1.17) is comparable to that for Bond equation while the exponent for particle density (n_5=0.67) is lower than that for the Bond equation (ρ^1). The exponent in the Bond model for the energy input ($\varepsilon^{2/3}$) is much lower than the value of n_2=1.33 found in this study. This suggests that the stability efficiency has a much stronger dependence on energy input, as noted previously in Section 4.1.4.3.3.

4.3.3. The Flotation Rate Constant

The attachment-detachment kinetic model provides a reasonably good prediction for the experimental data in this study and other literature data sets. In addition, the exponents in the empirical correlations are consistent with several trends/values in the flotation literature The model can be used to predict experimentally observed phenomena such as the optimum in the rate of flotation as a function of energy input and the classical optimum particle size range found in flotation. It is possible that this model may be used to extrapolate beyond the range of parameters used in this study, given its applicability to such a broad range of particle sizes, particle densities, bubble sizes, contact angles and energy inputs. This section presents simulated results for pyrite flotation for energy/power inputs of up to 10 W/kg, which is 7 W/kg more than range of energy inputs used in this study.

Figure 4.19 shows simulated pyrite flotation rate constants for a wide range of particle sizes (-150 µm) and energy inputs (0 - 10 W/kg) using micro bubbles (0.1 mm) and a high collector dosage (Contact angle = 90°). It is clear from this figure that the flotation rate constant for very fine particles (-10 µm) increases significantly with increasing energy input. Furthermore, intermediate particles (+10 -50 µm) have a maximum flotation rate constant in the vicinity of 1 - 2 W/kg, which is the average range of energy inputs used in industry. On the other hand, the flotation rate constant for coarse particles (+50 µm) decreases significantly with increasing energy input, showing that coarse particles do not benefit from energy input. Here, coarser particles should be floated at an energy input closer to the just-suspended criterion whereas fine particles require significantly higher energy inputs These results support the general view that different size fractions should be treated in separate flotation circuits with different energy intensities, as practiced in some plants (e.g. Western Australia Ni plants and ElSoldado copper concentrate in Chile).

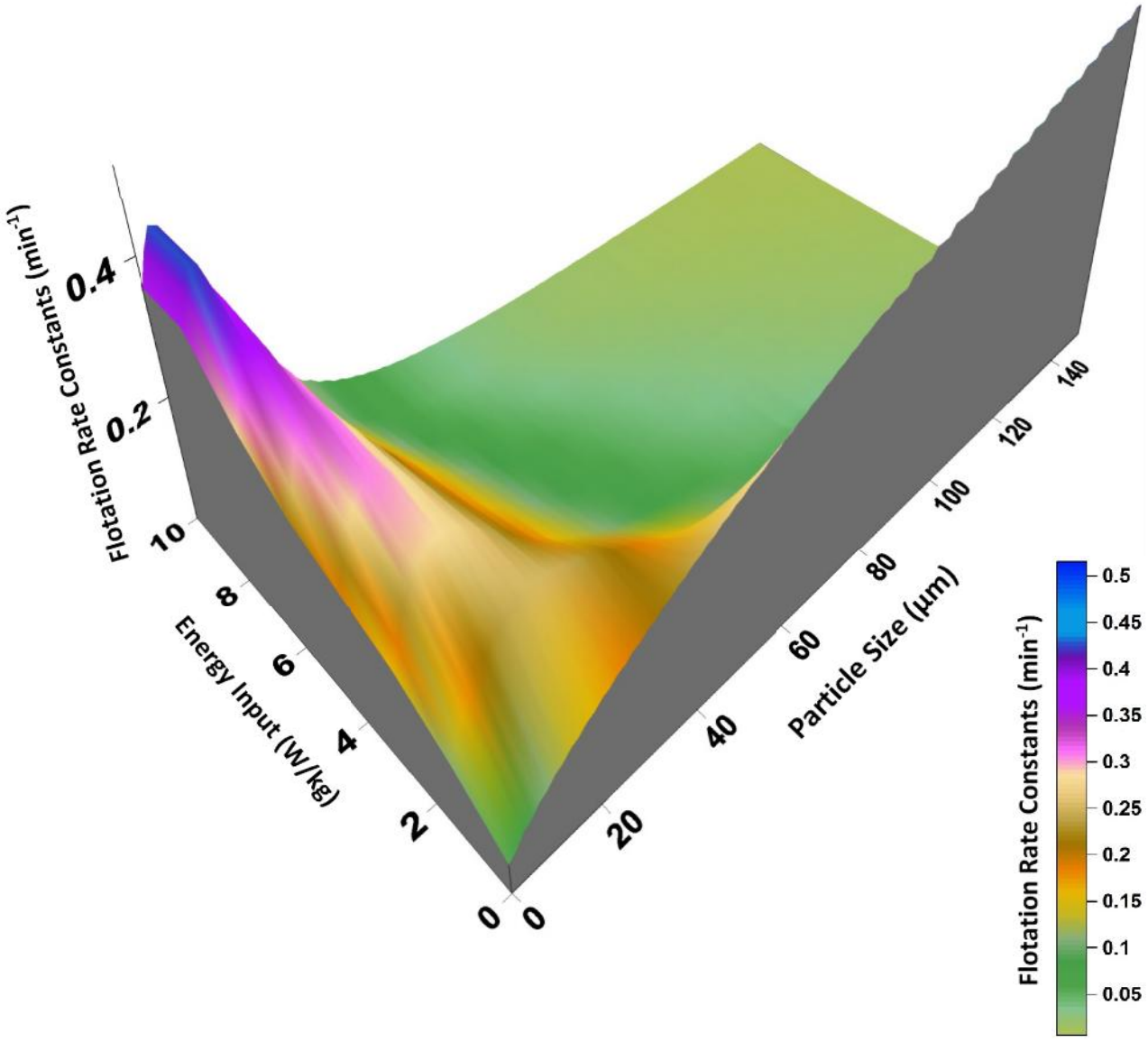

Figure 4.19: Variation of predicted flotation rate constants (min^{-1}) versus particle size (µm) and energy input (W/kg) for the pyrite sample with high collector dosage (Contact angle = 90°) and 0.1 mm bubble size

Figure 4.20 shows simulated pyrite flotation rate constants for a wide range of particle sizes (-150 µm) and energy inputs (0 - 10 W/kg) using normal bubbles (0.9 mm) and a high collector dosage (Contact angle = 90°). As illustrated in this figure, results are similar to Figure 4.19 but the flotation rate constants are much lower in magnitude. This is the reason why the flotation industry has been trying to use small bubbles (-0.5 mm) with new sparging technologies in novel flotation cells in order to increase flotation performance. Furthermore, the optimum particle size for flotation of pyrite particles with larger bubbles is higher compared to micro bubbles. For example, here fine particles up to 30 µm benefit from increasing energy input. Moreover, intermediate particles (+30 -70 µm) have a maximum flotation rate in the vicinity of 1 - 3 W/kg, which is higher than that for micro bubbles. This supports the findings in this study that optimum conditions for flotation are using small bubbles at lower energy inputs, or large bubbles at higher energy inputs.

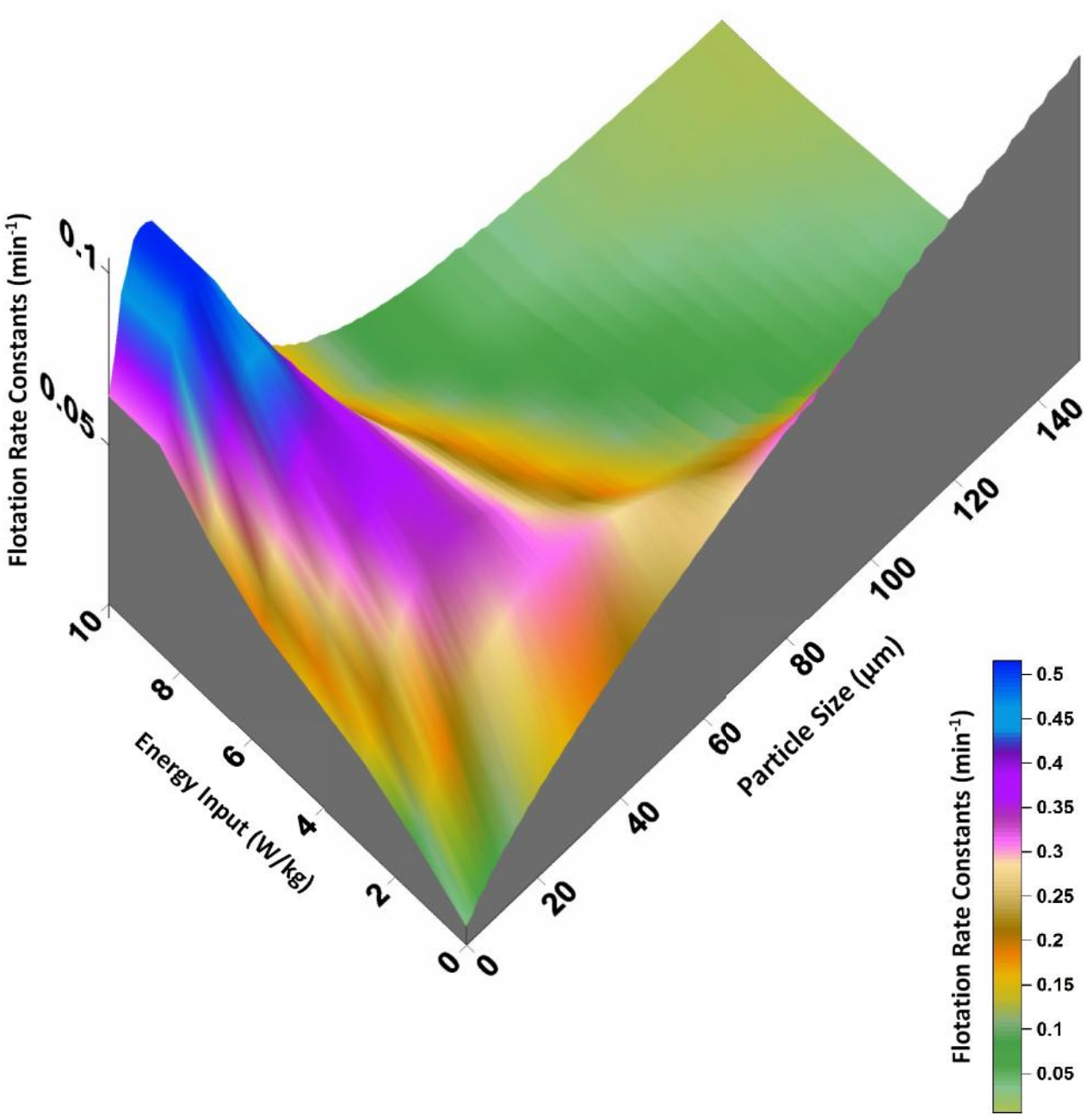

Figure 4.20: Variation of predicted flotation rate constants (min^{-1}) versus particle size (µm) and energy input (W/kg) for the pyrite sample with high collector dosage (Contact angle = 90°) and 0.9 mm bubble size

4.4. Summary of the Effect of Energy Input on Flotation Kinetics

This study investigated the effect of energy/power input on the flotation of three sulphide minerals (galena, pyrite and pentlandite) and two oxide minerals (apatite and hematite) in a laboratory OGC and a PGM ore in a pilot scale OGC. The effect of energy input was interpreted through trends in experimental flotation rate constants, simulated flotation rate constants from the best available literature fundamental model and attachment-detachment rate constants from a kinetic model.

Experimental flotation results show that the effect of energy input on the flotation rate is strongly dependent on the particle size and particle density and less dependent on bubble size and contact angle. Flotation rates generally increase with increasing particle size, decreasing bubble size and increasing contact angle, as is commonly found in the literature. Increasing energy input generally leads to an increase in the flotation rate for fine particles, an optimum flotation rate for intermediate particles and a decrease in the flotation rate for coarse particles. The optimum in the flotation rate for minerals with higher density is at a lower energy input than that for lower density minerals. The changes (increases/decreases) in the flotation rate with increasing energy input are very large for most of the conditions, indicating that this is an important parameter in flotation. Pilot scale results generally support the trends observed in the laboratory OGC. These findings are attributed to the effect of energy/power input on bubble-particle collection which is a balance between two competing effects, those of bubble-particle collision/attachment and those of bubble-particle detachment. Increasing energy input generally leads to significant increases in the flotation rate of fine particles, due to increased bubble-particle collision/attachment. Increasing energy input generally leads to an optimum flotation rate for intermediate particles, due to a combination of increased bubble-particle collision/attachment and detachment. For coarse particles, increasing energy input leads to significant increases in bubble-particle detachment. The relationship between the flotation rate and energy input is often described as $k \propto \varepsilon^N$, in the absence of significant bubble-particle detachment. The typical values of N are in the range of 0.44-0.75 for theoretical studies and 0.7-1 for experimental studies. The values of N found in the current study are in the range of 0.7-1, which suggests that bubble-particle collision/attachment has a stronger dependence on energy input than theory suggests.

Simulated flotation results for fine particles compare well to the experimental data in terms of both trends and magnitude. This suggest that the turbulent collision model used is appropriate for fine particles. For intermediate particles there are differences between the simulated flotation rate constants and the experimental data, primarily in terms of trends. For coarse particles there are very large differences between simulated flotation rate constants and the experimental data. This is attributed to under prediction of the collision frequency/efficiency and incorrect prediction of the stability efficiency. Here, the stability efficiency is considered to be under predicted at low energy inputs and over predicted at high energy inputs. This suggests that the stability efficiency has a much stronger dependence on energy input than theory suggests. Attachment-detachment results show that the attachment rate constant has a stronger dependence on energy input than theory suggest, supporting finding from the experimental results and simulated results for coarser particles. In addition, the detachment rate constant has a much stronger dependence on energy input than theory suggests, supporting findings from both the experimental and simulated results.

Chapter 5:
Conclusions and Recommendations

This thesis investigated the effect of energy input on flotation kinetics in an oscillating grid flotation cell. The first objective of this thesis was to determine the effect of energy/power input on the flotation kinetics of sulphide minerals (galena, pyrite & pentlandite) and oxide minerals (apatite & hematite) in a laboratory scale oscillating grid flotation cell. The second objective was to compare the results from the laboratory OGC to comparative studies in the flotation literature and to fundamental models for particle-bubble contacting. The third objective was to determine whether the experimental results from the laboratory OGC were consistent with those from the pilot scale OGC operating on a platinum ore. The effect of energy input on flotation kinetics was interpreted through trends in experimental flotation rate constants, simulated flotation rate constants and attachment-detachment flotation rate constants. Here, simulated flotation rate constants were calculated using a literature fundamental model for flotation in turbulent systems. This model is based on suitable expressions for the collision frequency, collision efficiency, attachment efficiency and stability efficiency, Attachment-detachment flotation rate constants were calculated using a kinetic model which allows for the two separate processes of bubble-particle collision/attachment and detachment. This model is based on kinetic expressions using empirical correlations for the attachment and detachment rate constants. Section 5.1.1 presents a summary of the effects of principal parameters (i.e. particle size, bubble size and contact angle) on flotation kinetics. In Section 5.1.2, the findings on the effect of energy input on flotation kinetics are summarized. Section 5.1.3 makes some recommendations for future work.

5.1. The Effect of Principal Parameters on Flotation Kinetics

This section presents a summary on the effect of particle size, bubble size and contact angle on the flotation rate constant. From this thesis one may conclude:

Particle Size: The flotation rate constant increased approximately linearly with increasing particle size after which there was a steady decline. Increasing flotation rate with increasing particle size is due to increases in the bubble-particle collision efficiency, which is well established in the flotation literature. However, both the attachment and stability efficiencies decreased with increasing particle size. The combination of these processes produces the characteristic shape of the flotation rate constant versus particle size curve, with a maximum at intermediate particle sizes.

Bubble Size: The flotation rate constant increased in inverse proportionality with decreasing bubble size. The increase in the flotation rate with decreasing bubble size is primarily due to an increase in the bubble-particle collision efficiency, as reported in the flotation literature. The influence of bubble size on the stability efficiency is less clear as some authors suggest that the stress on a bubble-particle aggregate should increase with increasing bubble size while others have postulated that the forces disrupting bubble particle aggregates should increase with decreasing bubble size. The flotation rate constant was less strongly dependent on the bubble size than suggested in the literature. In addition, this dependence was found to decreases with increasing energy input.

Contact Angle: The flotation rate constant increased proportionally with increasing contact angle, as found in the flotation literature. Increasing the contact angle has no effect on the bubble-particle collision efficiency since collisions are mainly controlled by hydrodynamic properties in the flotation cell. Therefore, increasing the flotation rate with increasing contact angle is due to increases in the attachment and stability efficiencies.

5.2. The Effect of Energy Input on Flotation Kinetics

This section presents a summary on the effect of energy input on the flotation rate constant. From this thesis one may conclude:

Energy Input: Energy input is one of the physical parameters most influential in all of the flotation sub-processes. The flotation rate is a function of the collision frequency, collision efficiency, attachment efficiency and stability efficiency. Increasing energy input results in an increase in the collision frequency due to increase in turbulence. Increasing energy input has no/minimum effect on the collision efficiency. Increasing energy input may result in an increase in the attachment efficiency

between bubbles and particles since a higher energy input helps to overcome the energy barrier and improves particle-bubble contacting. However, increasing energy input results in a decrease in the stability efficiency. Energy input has both beneficial and detrimental effects on flotation performance and, consequently, may result in an optimum in the flotation rate constant as a function of energy input.

Fine Particles: The flotation rate constant of fine particles increased approximately linearly with increasing energy input for all bubble sizes and collector dosages used in this study. This is due to an increased bubble-particle collision/attachment. The relationship between the flotation rate and energy input is often described as $k \propto \varepsilon^N$, in the absence of bubble-particle detachment i.e. for fine particles. The typical values of N are in the range of 0.44-0.75 for theoretical studies and 0.7-1 for experimental studies. The values of N found in the current study are in the range of 0.7-1, which suggests that bubble-particle collision/attachment has a stronger dependence on energy input than theory suggests. The optimum flotation conditions for fine particles was using small bubbles and high energy inputs.

Intermediate Particles: Increasing energy input generally led to an optimum flotation rate for intermediate particles, due to a combination of increased bubble-particle collision/attachment and detachment. The combination of these two processes produces the characteristic shape of the flotation rate constant versus energy input curve, with a maximum obtained at a different level of energy input for each mineral depending on their particle hydrophobicity and density. The optimum in the flotation rate for minerals with higher density was at a lower energy input than that for lower density minerals.

Coarse Particles: The flotation rate constant of coarse particles decreased approximately linearly with increasing energy input for all bubble sizes and collector dosages used in this study. This is due to increased bubble-particle detachment since the greater detaching forces result in decreased aggregate stability. It was found that detachment rate increased with increasing energy input, particle size and particle density. However, the detachment rate increased with decreasing bubble size and contact angle. Therefore, detachment was more prevalent for the coarser/denser particles, smaller bubbles and less hydrophobic particles. The optimum flotation conditions for coarse particles was using small bubbles and low energy inputs.

Simulated Flotation Rate Constants: Simulated flotation results for fine particles compared well to the experimental data in terms of both trends and magnitude. This suggest that the turbulent collision model used is appropriate for fine particles. For intermediate particles there were differences between the simulated flotation rate constants and the experimental data, primarily in terms of trends. For

coarse particles there were very large differences between simulated flotation rate constants and the experimental data. This is attributed to under prediction of the collision frequency/efficiency and incorrect prediction of the stability efficiency. Here, the stability efficiency was considered to be under predicted at low energy inputs and over predicted at high energy inputs. This suggests that the stability efficiency has a much stronger dependence on energy input than theory suggests.

Attachment-Detachment Rate Constants: The attachment-detachment model, used in conjunction with the empirical correlations for the attachment and detachment rate constants, was found to give a reasonable estimation of the entire flotation data set and several other data sets from the flotation literature. Attachment-detachment results showed that the attachment rate constant has a stronger dependence on energy input than theory suggest, supporting finding from the experimental results and simulated results for coarser particles. In addition, the detachment rate constant had a much stronger dependence on energy input than theory suggests, supporting findings from both the experimental and simulated results.

Hypotheses: Based on the objectives of this study and literature reviewed, the following hypotheses were made at the outset 1) Increasing energy/power input will increase the rate of flotation of fine particles but will result in an optimum for intermediate and coarse particles. The position of this optimum will depend on the particle density, bubble size and contact angle. 2) Fundamental models based on the RMS turbulent velocity will be appropriate for describing flotation kinetics as turbulence in the oscillating grid cell is relatively homogeneous and isotropic and 3) Trends in flotation results for a laboratory and pilot-scale oscillating grid flotation cell will be comparable as the distribution of turbulence in OGCs at equivalent specific power inputs is scale independent. Hypothesis 1 was found to be valid for both fine and intermediate particles, but for coarse particles increasing energy input resulted in sharp decreases in the flotation rate. In addition, the increase in the flotation rate with increasing energy input was found to be more dependent on the particle size and particle density than the bubble size and contact angle. Hypothesis 2 was found to be valid for fine particles but not for intermediate or coarse particles. Here, it was found that the processes of bubble-particle collision/attachment and detachment have a stronger dependence on energy input than theory suggests. Hypothesis 3 was supported by general trends in results for the laboratory and pilot-scale oscillating grid flotation cells, but was not convincingly demonstrated.

5.3. Recommendations for Future Work

It is recommended that the effect of energy input on the flotation kinetics for other ore types with different levels of liberation be investigated in an oscillating grid cell as this study excluded the effect

of liberation. Furthermore, investigation of the effect of energy input on flotation kinetics in different experimental condition from this study such as higher gas rate and higher solid percentage is highly recommended. It is also recommended that the effect of the froth zone be investigated. Given the findings of this thesis, it is strongly recommended that further work be done to evaluate the effect of energy input in a continuous system, on a larger scale. In industrial cells the energy input is non-homogeneous, and the results from the current study might not be directly applicable. It is proposed that CFD (computational fluid dynamics) simulations of the energy input distribution in larger scale may be used, in conjunction with flotation rate data from experiments in the oscillating grid cell, to estimate the flotation performance of a flotation cell.

References

Abrahamson, J., 1975. Collision rates of small particles in a vigorously turbulent fluid Chemical Engineering Science 30, 1371-1379.

Ahmed, N., Jameson, G., 1985. The effect of bubble-size on the rate of flotation of fine particles. International Journal of Mineral Processing 14 (3), 195-215.

Ahmed, N., Jameson, G.J., 1989. Flotation kinetics. Mineral Processing Extract. Metall., Rev 5, 77-99.

Amelunxen, R., 1995. The contact cell, a future generation of flotation machines. Promotional Literature, Amelunxen-Wales Technologies Inc.

Amini, E., 2012. Influence of Flotation Cell Hydrodynamics on the Flotation Kinetics and Scale up of Flotation Recovery. Ph.D. Thesis, University of Queensland.

Anderson, C., Harris, M.C., Deglon, D.A., 2009. Flotation in a novel oscillatory baffled column. Minerals Engineering 22, 1079-1087.

Anderson, C. J., 2008. Flotation in a novel oscillatory baffled column. PhD Thesis, University of Cape Town, Department of Chemical Engineering, Cape Town.

Anfruns, J.F., Kitchener, J.A., 1977. The rate of capture of small particles in flotation. Trans. Inst. Mineral Metall. 86, C9-C15.

Arbiter, N., Harris, C.C., 1962. Flotation kinetics. In, D.W. Fuerstenau (Editor), Froth Flotation. A.I.M.E., New York, 215-246.

Attalla, M., Chao, C., Nicol, S.K., 2000. The Role of Cavitation in Coal Flotation', Proc. Eighth Australian Coal Preparation Conference, Port Stephens, Paper H3.

Awatey, B., Thanasekaran, H., Kohmuench, J., Skinner, W., Zanin, M., 2013. Optimization of operating parameters for coarse sphalerite flotation in the HydroFloat® fluidised-bed separator, Minerals Engineering 50-51, 99-105.

Awatey, B., Thanasekaran, H., Kohmuench, J., Skinner, W., Zanin, M., 2014. Critical contact angle for coarse sphalerite flotation in a fluidised-bed, Minerals Engineering 60, 51-59.

Bache, D.H., Rasool, E., 1996. Measurement of the rate of energy dissipation around an oscillating grid by an energy balance approach. Chemical Engineering and Biochemical Engineering Journal 63, 105-115.

Bache, D.H., Rasool, E., 2001. Characteristics of turbulence in a multi grid mixer. Chemical Engineering 83, 67-78.

Baines, W.D., Peterson, E.G., 1951. An investigation of flow through screens. Trans. ASME, 73, 467-480.

Barbery, G., 1984. Engineering aspects of flotation in the minerals industry, flotation machines, circuits and their simulations. The scientific basis of flotation, NATO advanced institute services, series E. Appl. Science 25, 289-348.

Barnwal, J.P., Majumder, A.K., Govindarajan, B., Rao, T. 2006. Modeling of coal flotation in a batch and continuous cell operation, Part 1-kinetic approach. Coal Preparation 26, 123-136.

Bascur, O. A., Herbst, J. A., 1983. Dynamic modeling of a flotation cell with a view toward automatic control. Toronto, Can. CIM, Montreal, Que, Can, 111-1122.

Batchelor, G. K., 1951. Pressure fluctuations in isotropic turbulence. Proceedings of the Cambridge Philosophical Society 47, 359-374.

Bennett, A.J.R., Chapman, W.R., Dell, C.C., 1958. Studies in froth flotation of coal. Proc. 3rd Int. Coal Prep. Cong., Liege, 452-462.

Bergh, L., Yianatos, J., 2003. Flotation column automation, state of the art. Control Engineering Practice 11 (1), 67–72.

Bischofberger, C., Schubert, H., 1980. Untersuchungen zur hydrodynamischen optimierung des flotationsprozesses bei der kalisalz-flotation. Neue Bergbautechnik, 10, 58-62.

Blake, P., Ralston, J., 1985. Particle size, surface coverage and flotation response. Colloid Surface 16, 41-53.

Bloom, F., Heindel, T. J., 2003. Modelling flotation separation in a semi-batch Processing Chemical Engineering Science 58, 353-365.

Bloom, F., Heindel, T.J., 2002. On the structure of collision and detachment frequencies in flotation models. Chemical Engineering Science 57, 2467-2473.

Bogdanov, O.S., Emelyanov, M.F., Maximov, I.I., Otrozhdennova, L.A., 1980. Influence of some factors on fine particle flotation. In, P. Somasundran (Editor), Fine Particle Processing. S.M.E., New York, 706-719.

Brady, M. R., Telionis, D. P., Vlachos, P. P., Yoon, R.-H., 2006. Evaluation of multiphase flotation models in grid turbulence via particle image velocimetry. International Journal of Mineral Processing 80 (2-4), 133 - 143.

Breytenbach J.N., 1995. An Investigation of Particle Collection Efficiency in Different Particle-Bubble Contacting Environments in Flotation. MSc Thesis, Chemical Engineering, University of Cape Town.

Brown, D.J., 1965. A photographic study of froth flotation. Fuel Soc. J., 16, 22-34.

Brumley, B. H., Jirka, G. H., 1987. Near-surface turbulence in a grid-stirred tank. Journal of Fluid Mechanics 183, Cambridge, U.K., 235-263.

Brunk, B., Weber-Shirk, M., Jensen, A., Jirka, G., Lion, L.W., 1996. Modelling natural hydrodynamic systems with a differential-turbulence column. Journal of Hydraulic Engineering, ASCE 122, 373-380.

Brunk, B. K., Koch, D. L., Lion, L.W., 1998. Observations of coagulation in isotropic turbulence. Journal of Fluid Mechanics 371, 81-107.

Cameron, A.W., Kelsall, D.F., Restarick, C.J., Stewart, P.S.B., 1971. A detailed assessment of concentrator performance at Broken Hill South Ltd. Proc. Australas. Inst. Mineral Metall. 240, 53-67.

Changgen, L., Bahr, A., 1992. Flotation of copper ore in a Pneumatic flotation cell. Minerals Metallurg. Proc., 9, 7-12.

Changunda, K., Harris, M., Deglon, D. A., 2008. Investigating the effect of energy input on flotation kinetics in an oscillating grid flotation cell. Minerals Engineering 21 (12-14), 924-929.

Chipfunhu, D., Massimiliano Z., Stephen G., 2011. The dependency of the critical contact angle for flotation on particle size - Modelling the limits of fine particle flotation. Minerals Engineering 24, 50-57.

Chipfunhu, D., Zanin M., Grano S., 2012. Flotation behaviour of fine particles with respect to contact angle. Chemical Engineering Res Des 90(1), 26-32.

Collins, G.L., Jameson, G.J., 1976. Experiments on the flotation of fine particles - The influence of particle size and charge. Chemical Engineering Science 31, 985-991.

Comte-Bellot, G., Corrsin, S., 1966. The use of a contraction to improve the isotropy of grid-generated turbulence. Journal of Fluid Mechanics 25, Cambridge, U.K., 657-682.

Cowburn, J., Harbort, G., Manlapig, E. Pokrajcic, Z., 2006. Improving the recovery of coarse coal particles in Jameson cell, Minerals Engineering 19, 609-618.

Crawford, R., Ralston, J., 1988. The influence of particle size and contact angle in mineral flotation. International Journal of Mineral Processing 23, 1-24.

Crawford, R. J., 1986, Particle Size, Hydrophobicity and Flotation Response, Master of Applied Science Thesis, Swinburne Institute of Technology, Melbourne.

Daniel B. Blum, Surendra Kunwar, James Johnson, Greg A. Voth, 2009. Effects of non-universal large scales on conditional structure functions in turbulence, Journal of physics fluid dynamic.

Dai, Z., Dukhin, S., Fornasiero, D., Ralston, J., 1998. The inertial hydrodynamic interaction of particles and rising bubbles with mobile surfaces. Journal of Colloid and Interface Science 197 (2), 275 - 292.

Dai, Z., Fornasiero, D., Ralston, J., 1999. Particle-bubble attachment in mineral flotation. Journal of Colloid and Interface Science 217 (1), 70 - 76.

Deglon D.A., 1998. A hydrodynamic investigation of fine particle flotation in a batch flotation cell. PhD Thesis, Department of Chemical Engineering, University of Cape Town.

Deglon, D.A., Sawyerr, F., O'Connor, C.T., 1999. A model to relate the flotation rate constant and the bubble surface area flux in mechanical flotation cells. Minerals Engineering 12, 599-608.

Deglon, D., Egya-mensah, D., Franzidis, J., 2000. Review of hydrodynamics and gas dispersion in flotation cells on South African platinum concentrators. Minerals Engineering 13 (3), 235-244.

Deglon D.A., 2002. A novel attachment-detachment kinetic model. Flotation and Flocculation - From Fundamentals to Applications, Hawaii.

Deglon, D.A., 2003, A novel attachment-detachment kinetic model, in Proc of the Strategic Conference, Australia, Flotation and Flocculation, From Fundamentals to Applications, 109-116.

Deglon, D.A., 2005. The effect of agitation on the flotation of platinum ores. Minerals Engineering 18 (8), 839-844.

De Bruyn, P.L., Modi, H.J., 1956. Particle size and the flotation rate of quartz. Mineral Engineering 8, 415-419.

De Silva, I.P.D., H.J.S. Fernando., 1994. Oscillating grids as a source of nearly isotropic turbulence. Physics Fluids 6, 2455-2464.

Degner, V.R., Sabey, J.B., 1988. WEMCO/Leeds flotation column development. In, Sastry, K. V. S. (Ed.), Column '88. Pheonix, Arizona, SME.

Deng, H., Mehta, R. K., Warren, G. W. 1996. Numerical modeling of flows in flotation columns. International Journal of Mineral Processing 48, 61-72.

Derjaguin, B.V., Dukhin, S.S., 1961. Theory of flotation of small and medium sized particles. Trans. Inst. Mineral Metall. 70, 221-245.

Diaz-Penafiel, P., Dobby, G.S., 1994. Kinetic studies in flotation columns - Bubble size effects. Mineral Engineering 7, 465-478.

Dickey, T. D., Mellor, G. L., 1980. Decaying turbulence in stratified and normal fluids. Journal of Fluid Mechanics 99, Cambridge, U.K., 13-31.

Do, H., 2010. Development of a Turbulent Flotation Model from First Principles, PhD Dissertation, Virginia Polytechnic Institute and State University, Blacksburg, VA.

Dobby, G.S., Finch, J.A., 1986. A model of particle sliding time for flotation size bubbles. Journal of Colloid and Interface Science 109, 493-498.

Dobby, G.S., Finch, J.A., 1987. Particle size dependence in flotation derived from a fundamental model of the capture Processing. International Journal of Mineral Processing 21, 241-260.

Dobby, G.S., Finch, J.A., 1990. Column Flotation. Pergamon Press, Toronto.

Dobby, G.S., Savassi, O.N., 2005. An Advanced Modelling Technique for Scale-Up of Batch Flotation Results to Plant Metallurgical Performance. Centenary of Flotation Symposium, 2005 Brisbane, Australia.

Duan J., Fornasiero D., Ralston J., 2003. Calculation of the flotation rate constant of chalcopyrite particles in an ore. International Journal of Mineral Processing 72, 227- 237.

Eriez HydroFloat Separator, 2014, www.eriez.com.

Ettema, R., Karim, F., Kennedy, J.F., 1984. Laboratory experiments on frazil ice growth in super cooled water. Cold Regions Science and Technology 10(1), 43-58.

Eidelman, A., Elperin, T., Kleeorin, N., Markovich, A., Rogachevskii, I., 2002. Oscillating grids turbulence generator for turbulent transport studies. Nonlinear Processes in Geophysics 9, 201-205.

Evans, G., Doroodchi, E., Lane, G., Koh, P., Schwarz, M., 2008. Mixing and gas dispersion in mineral flotation cells. Chemical Engineering Research and Design 86 (12), 1350–1362, international Symposium on Mixing in Industrial Processes.

Feng, D., Aldrich, C., 1999. Effect of particle size on the flotation performance of complex sulphide ores. Minerals Engineering 12, 721-731.

Fichera, M.A., Chudacek, M.W., 1992. Batch cell flotation models - A review. Mineral Engineering 5, 41-55.

Finch, J.A., 1995. Column flotation, a selected review - part IV, Novel flotation devices. Minerals Engineering 8 (6), 587-602.

Finch, J.A., Dobby, G.S., 1990. Column Flotation. Perg. Press, Flotation. McGraw-Hill, New York.

Finch, J.A., Hardie, C.A., 1999. An example of innovation from the waste management industry, deinking flotation cells. Minerals Engineering 12, 476-475.

Gaudin, A.M., 1957. Flotation (2nd Edition), McGraw-Hill, New York.

Gaudin, A.M., Schuhmann, R., Schlecten, W., 1942. The effect of size on the behaviour of galena particles. Journal Phys. Chemical, 46, 902-910.

Glencore Technology, 2015

Gontijo, C.D.F., Fornasiero, D., Ralston, J., 2007. The limits of fine and coarse particle flotation. Canadian Journal of Chemical Engineering 85, 739-747.

Gorain, B.K., Franzidis, J.P., Manlapig, E.V., 1996. Studies on impeller type, impeller speed and air flow rate in an industrial scale flotation cell. Part 3: Effect on superficial gas velocity. Minerals Engineering 9, 639–654.

Gorain, B.K., Franzidis, J.P., Manlapig, E.V., 1997. Studies on impeller type, impeller speed and air flow rate in an industrial scale flotation cell. Part 4, Effect of bubble surface area flux on flotation performance. Minerals Engineering 10, 367-379.

Gorain, B., 2000. P9L Final Report. Queensland, JKMRC.

Gorain, B. K., 2006. The Effect of Bubble Size on The Kinetics Of Flotation And Its Relevance To Scale-Up. Ph.D., University of Queensland.

Gorain, B.K., Napier-Munn, T.J., Franzidis, J.P., Manlapig, E.V., 1998. Studies on impeller type, impeller speed and air flow rate in an industrial scale flotation cell. Part 5, validation of k-S_b relationship and effect of froth depth. Minerals Engineering 11 (7), 615-626.

Gruber, G. A., Kelahan, M. E., 1988. Flotaire cell applications in phosphate flotation. In, Sastry, K. V. S. (Ed.), Column Flotation '88. Pheonix, Arizona.

Grau, R., Heiskanen K., 2005. Bubble size distribution in laboratory scale flotation cells. Minerals Engineering 18, 1164-1172.

Guadayol, O., Peters, F., Stiansen, J.E., Marrase, C., Lohrmann, A., 2009. Evaluation of oscillating grids and orbital shakers as means to generate isotropic and homogeneous small-scale turbulence in laboratory enclosures commonly used in plankton studies. Limnology And Oceanography - Methods 7, 287-303.

Hafez, M.M., Prochazka, J., 1974. The dynamic effects in vibrating-plate and pulsed extractors - I. Theory and experimental technique. Chemical Engineering Science 29, 1745- 1753.

Harris, C.C., Raja, A., 1970. Flotation machine impeller speed and air rate as scale-up criteria. Trans. Inst. Mineral Metall. 79, C295 - C297.

Harris, M.C., Franzidis, J.P., O'Connor, C.T., Stonestreet, P., 1992. An evaluation of the role of particle size in the flotation of coal using different flotation technologies. Minerals Engineering 5, 1225-1238.

Heindel, T.J., Bloom, F., 1999. Exact and Approximate Expressions for Bubble-Particle Collision. Journal of Colloid and Interface Science 213(1), 101-111.

Heiskanen, K., 2000. On the relationship between flotation rate and bubble surface area flux. Minerals Engineering 13, 141-149.

Herlina, Jirka, G. H., 2008. Experiments on gas transfer at the air-water interface induced by oscillating grid turbulence. Journal of Fluid Mechanics 594, 183-208.

Hernandez-Aguilar, J.R., Cunningham, R., Finch, J.A., 2006. A test of the Tate Equation to predict bubble size at an orifice in the presence of frother. International J. of Mineral Processing 79, 89-97.

Hewitt, D., Fornasiero, D., Ralston, J., 1993. Aqueous film drainage at the quartz/water/air interface. Journal Chemical Soc. Faraday Trans., 89, 817-822.

Hopfinger, E.J., J.A. Toly. 1976. Spatially decaying turbulence and its relation to mixing across density interfaces. Journal of Fluid Mechanics 78, Cambridge, U.K., 155-188.

Huppert, H.E., Turner, J.S., Hallworth, M.A., 1995. Sedimentation and entrainment in dense layers of suspended particles stirred by an oscillating grid. Journal of Fluid Mechanics 289, 263-293.

Ityokumbul, M.T., de Aquino J.A., O'Connor C.T., Harris, M.C., 2000. Fine pyrite flotation in an agitated column cell". International Journal of Mineral Processing 58, 167-178.

Janzen, J.G., 2003. Details of turbulence properties in water agitated through a pair of oscillating grids. MSc Thesis, School of Engineering at São Carlos, University of São Paulo, Brazil (Portuguese).

Janzen, J.G., de Souza, L.B.S., Schultz, H.E., 2003. Kinetic energy in grid turbulence, comparison between data and theory. Journal of Brazilian Society and Mechanical Science and Engineering 4, 347-351.

Janzen, J.G., 2006. Gas transfer near the air-water interface in an oscillating grid tanks and properties of isotropic turbulent flows. PhD Thesis, São Carlos, University of São Paulo, Brazil (in Portuguese).

Jameson, G., Nam, S., Young, M., 1977. Physical factors affecting recovery rates in flotation. Mineral Science Engineering 9, 103-118.

Jameson, G.J., 2010. New directions in flotation machine design. Minerals Engineering 23, 835- 841.

Jameson, G. J., 2007. New concepts in coarse and ultrafine flotation. Flotation '07. Cape Town, MEI.

Jenne, M., M. Reuss, 1999. A critical assessment on the use of k-e turbulence models for simulation of the turbulent liquid flow induced by a Rushton-turbine in baffled stirred tank reactors. Chemical Engineering Science 54 (17), 3921-3941.

Jirka, G. H., 1991. Gas transfer processes at the air/water interface. Environmental hydraulics, J.H.W. Lee, Y.K. Cheung, eds., Balkema, Rotterdam, The Netherlands, 357-370.

Jordan, C.E., Spears, D.R., 1990. Evaluation of a turbulent flow model for fine-bubble and fine-particle flotation. Mineral Metall. Processing 7, 65-73.

Jordan, C.E., Susko, F.J., 1992. Rapid flotation using a modified bubble-injected hydrocyclone and a shallow-depth froth separator for improved flotation kinetics. Mineral Engineering 5, 1239-1257.

Jowett, A., 1980. Formation and disruption of particle-bubble aggregates in flotation. In, P. Somasundran (Editor), Fine Particle Processing. S.M.E., New York, 720-754.

Julien Saint Amand, F., 1999. Hydrodynamics of de-inking flotation. International Journal of Mineral Processing 56 (1-4), 277-316.

Kelsall, D.F., 1961. Application of probability in the assessment of flotation systems. Trans. Inst. Mineral Metall. 70, C191-C204.

King, R.P., 1973. Model for design and contol of flotation plants. In, Tenth International Symposium - Application of Computer Methods in the Mineral Industry Johannesburg, South Africa, 341-350.

King, R.P., 1976. The use of simulation in the design and modification of flotation plants, in Flotation, A.M. Gaudin Memorial Volume, (Ed, M.C. Fuerstenau), AIME 2, Chapter 32, 937-961.

King, R.P., 1978. A pilot-plant investigation of a kinetic model for flotation, Journal of the South African Institute of Mining and Metallurgy, July, 325-338.

Kirchberg, H, Topfer, E., 1965. The mineralization of air bubbles in flotation. Proc. VII International Mineral Processing Cong., New York, 157-168.

Koh, P.T.L., Schwarz, M.P., 2003. CFD modelling of bubble-particle collision rates and efficiencies in mineral flotation cells. Minerals Engineering 16, 1055-1059.

Koh P.T.L., Schwarz M.P., 2006. CFD Modelling of Bubble-Particle Attachments in a Flotation Cells. Minerals Engineering 19, 619-626.

Kolmogorov, A. N., 1941. Dissipation of energy in a locally isotropic turbulence. Doklady Akad. Nauk SSR 32, 141.

Kostazos, A. E., Apikides, P. S., Kastrinakis, E. G., Nychas, S. G., 1994. Oscillating grid turbulence and bulk mixing at high Schmidt numbers. Canadian Journal of Chemical Engineering 72, 431-439.

Krasowska, M., MALYSA K., 2007. Kinetics of Bubble Collision and Attachment to Hydrophobic Solids, I. Effect of Surface Roughness, International Journal of Mineral Process, 81, 205-216.

Laplante, A. R., Toguri, J.M., Smith, H.W. 1989. The effect of air flow rate on the kinetics of flotation. Part 1, The transfer of material from the slurry to the froth. Int. Jour. Min. Proc., 203 - 219.

Laplante, A. R., Toguri, J.M., Smith, H.W. 1989. The effect of air flow rate on the kinetics of flotation. Part 2, The transfer of material from the froth over the cell lip. Int. Jour. Min. Proc., 221-234.

Leal Filho, L.S.R., Rodrigues, W. J., Ralston, J., 2002. Importance of Hydrodynamics in Coarse Particle Flotation. In, J.M.J. Ralston, J. Rubio (Editor), Flotation and Flocculation, 203-212.

Lee, C. H., Erickson, L. E., 1987. Bubble breakup and coalescence in turbulent gas- liquid dispersions. Chemical Engineering Communications 59(1-6), 65-84.

Lee, C., Yianneskis, M., 1988. Turbulence properties of the impeller stream of a Rushton turbine. American Institute of Chemical Engineering Journal 44, 13-24.

Lelinski, D., Govender, D., Dabrowski, B., Traczyk, F., Mulligan, M., 2011. Effective use of energy in the flotation Processing 6th Southern African Base Metals Conference.

Li, R., Hoberg, H., Schneider, F.U., 1993. Investigation on the influence of particle size in flotation. Proc. XVIII International Mineral Processing Cong., Sydney, 689-697.

Liepe, F., Mockel, O.H., 1976. Untersuchungen zum stoffvereinigen in flussiger phase. Chemical Techn., 28, 205-209.

Liem, L. E., Smith, D. W., Stanley, S. J., March 1999. Turbulent velocity in flocculation by means of grids. Journal of Environmental Engineering 125 (3), 224-233.

Luttrell, G.H., 1986. Hydrodynamic studies and mathematical modelling of fine coal flotation. Ph.D. Thesis, Virginia Polytechnic Institute and State University, USA.

Lyn, D. A., 1995. Observations of initial sediment motion in a turbulent flow generated in a square tank by a vertically oscillating grid. Proc., 1st Int. Conf. on Water Resource, Vol. 1, ASCE, 608-612.

Mackenzie, J.M.W., Matheson, G.H., 1963. Kinetic and dynamic relationships in coal flotation. Trans. Soc. Mineral Engineering 226, 68-75.

Malhotra, D., Hoover, R.M., Bender, F.N., 1980. Effect of agitation and aeration on flotation of Molybdenite. Mineral Engineering, 1392-1397.

Mao, L., Yoon, R.-H., 1997. Predicting flotation rates using a rate equation derived from first principles. International Journal of Mineral Processing 51 (1-4), 171 - 181, application of Surface Science to Advancing Flotation Technology.

Massey, W.T., Harris, M.C, Deglon, D. A., 2012. The effect of energy input on the flotation of quartz in an oscillating grid flotation cell. Minerals Engineering.

Matiolo, E., Gonzaga, L., Guedes, L., 2015. An alternative flotation process for apatite concentration of the itataia carbonaceous uranium-phosphate ore.Worley-Parsons Services, ECI Symposium Series.

Matsunga, N., Sugihara, Y., Komatsu, T., Masuda, A., 1999. Quantitative properties of oscillating-grid turbulence in a homogeneous fluid. Fluid Dynamic Research 25, 147-165.

Medina, P., Sánchez, M.A., Redondo, J.M., 2001. Grid stirred turbulence, applications to the initiation of sediment motion and lift-off studies. Phys. Chemical Earth, Vol. 26, No. 4, 299-304.

Metso, 2015, Flotation columns - Metso. www.metso.com.

McDougall, T., 1979. Measurements of turbulence in a zero-mean-shear mixed layer. Journal of Fluid Mechanics 94, 409-431.

McKenna, S. P., McGillis, W. R., 2004. Observations of flow repeatability and secondary circulation in an oscillating grid-stirred tank. Physics of Fluids 16 (9), 3499 - 3502.

Miettinen, T., Ralston, J., Fornasiero, D., 2010. The limits of fine particle flotation. Minerals Engineering 23, 420 - 437.

Miettinen, T., 2007. Fine Particles Flotation. PhD Thesis. University of South Australia, M. Lakes.

Miettinen, M., Stén, P., Bäckman, S., Leppinen, J., Aaltonen, J., 2000. Determination of chemicals bound to mineral surfaces in flotation processes. Minerals Engineering 13, 245-254.

Mika, T.S., Fuerstenau, D.W., 1968. A microscopic model of the flotation Processing Proc. VIII Int. Mineral Processing Cong., Leningrad, 246-269.

Mohamed, M.S., LaRue, J.C. 1990. The Decay Power Law in Grid Generated Turbulence. Journal of Fluid Mechanics 219), 195-214.

Mohanty, M. K., Honaker, R. Q., 1999. A comparative evaluation of the leading advanced flotation technologies. Minerals Engineering 12, 1-13.

Mokgethi, B., 2010. The effect of energy input on precipitation in an oscillating grid reactor. MSc Thesis, Department of Chemical Engineering, University of Cape Town.

Muganda, S., Zanin, M., Grano, S., 2008. Flotation behaviour of sulphide mineral size fractions with controlled contact angle. Chemeca Conference Proceedings, Towards a sustainable Australasia. Newcastle City Hall, New South Wales, Australia, Engineers Australia.

Munoz-Diaz, C., 2007. Performance and enhancement methods for coal flotation. M.S. Thesis. University of Kentucky, Lexington, KY.

Nelson, M.G., TRACZYK, F. P., LELINSKI, D., 2002. Design of mechanical flotation machine. Mineral processing plant design, practice, and control proceedings, V. 1, 1179-1204. SME.

Newell, R., Grano, S., 2006. Hydrodynamics and scale up in Rushton turbine flotation cells, Part 2. flotation scale-up for laboratory and pilot cells. International Journal of Mineral Processing 81, 65-78.

Newell, R., Bradshaw, D., Harris, P.J., 2005. The effect of heavy oxidation upon flotation and potential remedies for Merensky type sulphides. Centenary of Flotation Symposium, Brisb., Australia.

Newell, R., Grano, S., 2007. Hydrodynamics and scale-up in Rushton turbine flotation cells, Part 1. Cell hydrodynamics. International Journal of Mineral Processing 81, 224-236.

Nguyen, A., Schulze, H., 2004. Colloidial Science of Flotation. Vol.118 of Surfactant Science Series.

Nguyen, A. V., George, P., Jameson, G. J., 2006. Demonstration of a minimum recovery of nanoparticles by flotation, Theory and experiment. Chemical Engineering Science 61, 2494- 2509.

Nguyen, A.V., Schulze, H.J., Ralston, J., 1997. Elementary steps in particle-bubble attachment. International Journal of Mineral Processing 51, 183-195.

Nielsen, P., 1993. Turbulence effects on the settling of suspended particles. Journal of Sed. Petrology 63, 835-838.

Nonaka, M., Inoue, T., Imaizumi, T., 1982. A micro-hydrodynamic flotation model and its application to the flotation Processing. Proc. XIV Int. Mineral Processing Cong., Toronto, III-9.1-III-9.18.

Orlins, J., Gulliver, J., 2003. Turbulence quantification and sediment resuspension in an oscillating grid chamber. Experiments in Fluids 34, 662 - 677.

Oteyaka, B., Soto, H., 1995. Modelling of negative bias column for coarse particles flotation, Minerals Engineering 8, 91-100.

Ott, S., Mann, J., 2000. An experimental investigation of the relative diffusion of particle pairs in three-dimensional turbulent flow. Journal of Fluid Mechanics, Vol. 422, 207-223.

Outotec, 2016, OTE_Outotec_Flotation_Modernization_Guidebook_eng_web. www.outotec.com.

Peters, F., T. Gross., 1994. Increased grazing rates of micro plankton in response to small-scale turbulence. Mar. Ecol. Prog. Ser. 115,299-307.

Pushkarova, R.A., Horn, R.G., 2008. Bubble-solid interactions in water and electrolyte solutions [J]. Langmuir 24(16), 8726 - 8734.

Pyke, B., Fornasiero, D., Ralston, J., 2003. Bubble particle heterocoagulation under turbulent conditions. Journal of Colloid and Interface Science 265, 141- 151.

Pyke, B., 2004. Bubble-particle capture in turbulent flotation systems. Ph.D. Thesis, University of South Australia, Ian Wark Research Institute.

Ralston, J., 1983. Thin films and froth flotation. Advance Colloid Interface Science 19, 1-26.

Ralston, J., 1992. The influence of particle size and contact angle in flotation. In, J.S. Laskowski and J. Ralston (Editors), Colloidal Chemistry in Mineral Processing. Elsevier, Oxford, 203-224.

Ralston, J., Fornasiero, D., Hayes, R., 1999. Bubble-particle attachment and detachment in flotation. International Journal of Mineral Processing 56 (1-4), 133 – 164.

Reay, D., Ratcliff, G.A., 1973. Removal of fine particles from water by dispersed air flotation - Effects of bubble size and particle size on collection efficiency. Can. J. Chemical Engineering 51, 178-185.

Reay, D., Ratcliff, G.A., 1975. Experimental testing of the hydrodynamic collision model of fine particle flotation. Can. Journal Chemical Engineering 53, 481-486.

Rodrigues, R. T., Rubio, J., 2007. DAF-dissolved air flotation, Potential applications in the mining and mineral processing industry. International Journal of Mineral Processing 82 (1), 1 - 13.

Rodrigues, W.J., Leal Filho, L.S., Masini, E.A., 2001. Hydrodynamic dimensionless parameters and their influence on flotation performance of coarse particles. Minerals Engineering 14(9),1047-1054.

Rouse, H., 1939. Experiments on the mechanics of sediment suspension Processing, 5th International Congress of Applied Mechanic, Cambridge, Mass., 550- 554.

Rouse, H., Dodu, J., 1955. Diffusion Turbulente à Travers Une Discontinuité de Densité, La Houille Blanche, No. 4, 522-529.

Rubio, J., Souza, M. L., Smith, R. W., 2002. Overview of flotation as a wastewater treatment technique. Minerals Engineering 15, 139-155.

Safari, M., Deglon, D.A., Harris, M.C., Filho, L.L., Testa, F., 2016. The effect of energy input on flotation kinetics", International Journal of Mineral Processing, doi : 10.1016/j.minpro.2016.05.008.

Saffman, P.G, Turner, T.S., 1956. On the collision of drops in turbulent clouds. Journal Fluid Mechanics 1, 16-30.

Sanchez, M.A., Redondo, J.M., 1998. Observations from grid stirred turbulence. Appl. Science Res. 59, 243-254.

Sayed-Ahmed, A.S., 2013. Bubble-particle interactions in nanobubble enhanced froth flotation. Poster presentation in the 2013 SME Annual Meeting, Denver, Colorado.

Schafer, M., Hofken, M., Durst, F., 1997. Detailed LDV measurements for visualization of the flow within a stirred reactor equipped with a Rushton turbine. Transactions of Institute of Chemical Engineering 75, 729-739.

Scheiner, B.J., Jordan, C.E., 1989. Hydrodynamic effects in flotation of ores. In S. Chander and R.R. Klimpel (Eds). Advances in Coal and Mineral Processing Using Flotation, S.M.E., Littleton, 219-224.

Schimmoller, B.K., Luttrell, G.H., Yoon, R-H., 1993. A combined hydrodynamic surface force model for bubble-particle collection. XVIII International Mineral Processing Congress, Sydney, 751-756.

Schneider, J.C., Van Weert, G., 1988. Design and operation of the Hydrochem flotation column. In, Sastry, K. V. S. (Ed.), Column Flotation '88. Pheonix, Arizona.

Schubert, H., Bischofberger, C, 1998. On the microprocesses air dispersion and particle bubble attachment in flotation machines as well as consequences for the scale-up of macro processes, International Journal of Mineral Processing 52, 245-259.

Schubert, H., 1985. On some aspects of the hydrodynamics of flotation processes, in Flotation of Sulphide Minerals (ed, K S E Forssberg), 337-355 (Elsevier, Amsterdam).

Schubert, H., 1999. On turbulence-controlled microprocesses in flotation machines. International Journal of Mineral Processing 56, 257-276.

Schubert, H., 2008. On the optimization of hydrodynamics in fine particle flotation. Minerals Engineering 21 (12-14), 930 -936, selected Papers from Flotation ’07.

Schubert, H.J., Bischofberger, C., 1978. On the hydrodynamics of flotation machines. International Journal Mineral Processing 5, 132-142.

Schubert, H.J., 2008. On the optimization of hydrodynamics in fine particle flotation. Minerals Engineering 21, 930-936.

Schubert, H., Bischofberger, G., Koch, P., 1982. ber den einfluss der hydrodynamik auf flotationsprozesse. Aufbereitungs-Technik, 23, 306-315.

Schulze, H.J., 1977. New theoretical and experimental investigations on stability of bubble/particle aggregates in flotation - A theory on the upper particle size of floatability. International Journal Mineral Processing 4, 241-259.

Schulze, H.J., 1982. Dimensionless number and approximate calculation of the upper particle size of floatability in flotation machines. International Journal Mineral Processing 9, 321-328.

Schulze, H.J., 1989. Hydrodynamics of bubble-mineral particle collisions. Mineral Processing Extract. Metall., Rev. 5, 43-76.

Schulze, H. J., 1993. Flotation as a heterocoagulation process, possibilities of calculating the probability of flotation. In, Dobias, B. (Ed.) Coagulation and Flocculation, Theory and Applications. New York, Marcel Dekker.

Schulze, H.J., Radoev, B., Geidel, T., Stechmesser, H., Topfer, E., 1989. Investigations of the collision process between particles and gas bubbles in flotation. International Journal Mineral Processing 27, 263-278.

Sherrell, I., Yoon, R.H., 2005. Development of a turbulent flotation model. In, Centenary of Flotation Symposium, Brisbane.

Sherrell, I. M., 2004. Development of a flotation rate equation from first principles under turbulent flow conditions. Ph.D. thesis, Virginia Polytechnic Institute and State University, Blacksburg, Virginia.

Goel, S., Jameson, G.J., 2012. Detachment of particles from bubbles in an agitated vessel. Minerals Engineering 36-38, 324-330.

Shy, S.S, Jang, R.H., Tang, C.Y., 1996. Simulation of turbulent burning velocities using aqueous autocatalytic reactions in an ear homogeneous turbulence. Combustion and Flame, Vol. 105, 54-67.

Spears, D.R., Jordan, C.E., 1989. The effect of turbulence on the flotation rate of galena when using fine bubbles. In S. Chander and R.R. Klimpel (Eds). Advances in Coal and Mineral Processing Using Flotation, S.M.E., Littleton, 77-84.

Srdic, A., Fernando, H., Montenegro, L., 1996. Generation of nearly isotropic turbulence using two oscillating grids. Experiments in Fluids 20 (5), 395-397.

Stamenkovic´, Ivica S., Ivana B. Bankovic´ -Ilic´, Predrag B. Jovanic´, Vlada B. Veljkovic´, Dejan U. Skala, 2010, Hydrodynamics of a co current up flow liquid-liquid reciprocating plate reactor for homogeneously base-catalyzed methanolysis of vegetable oils, Fuel 89, 3971-3984

Subrahmanyam, T.V., M.B.M. Monte, A. Middea, E. Valdiviezo, F.F. Lins, 1999. Mineral Engineering 12, 1347.

Sun, S.C., Zimmerman, R.E., 1950. The mechanism of coarse coal and mineral froth flotation. Trans. Soc. Mineral Engineering 187, 616-622.

Sutherland, K.L., 1948. Kinetics of the flotation Processing. Journal Phys. Colloid, 52, 394-425.

Tabosa, E., Rubio, J., 2010. Flotation of copper sulphides assisted by high intensity conditioning (HIC) and concentrate recirculation. Mineral Engineering 23, 1198-1206.

Tabosa, E., 2012. The effect of cell hydrodynamics on flotation kinetics. Ph.D. Thesis, University of Queensland.

Tabosa, E., Runge, K., Holtham, P., 2016. The effect of cell hydrodynamics on flotation performance. International Journal of Mineral Processing, http://dx.doi.org/10.1016/j.minpro.2016.05.019.

Tabosa, E., Runge, K., Holtham, P., Duffy, K., 2016. Improving flotation energy efficiency by optimizing cell hydrodynamics. Mineral Engineering, http://dx.doi.org/10.1016/j.mineng.2016.05.002.

Tao, D. 2004. Role of bubble size in flotation of coarse and fine particles-A review. Separation Science and Technology 39(4), 741–760.

Taylor, G. I., 1935. Statistical theory of turbulence. Proc. Roy. Soc. Lon. A 151, 421-454.

Tennekes, H., J.L. Lumley, 1972. A first course in turbulence. Cambridge, MA, MIT Press, 300.

Tennekes H., 1975. Eulerian and Lagrangian time microscales in isotropic turbulence. Fluid Mechanic 67, 561-567.

Thompson, S.M., Turner, J.S., 1975. Mixing across an interface due to turbulence generated by an oscillating grid. Journal of Fluid Mechanics 67, Cambridge, U.K., 349-368.

Tomlinson, H.S., Fleming, M.G., 1963. Flotation rate studies. Proc. VI Int. Mineral Processing Cong., Cannes, 563-579.

Tojo, K., Miyanami, K., Minami, I., Yano, T., 1979. Power dissipation in a vibrat- ing disc column. Chemical Engineering Journal and the Biochemical Engineering Journal 17 (3), 211–218.

Trahar, W., 1981. A rational interpretation of the role of particle size in flotation. International Journal of Mineral Processing 8 (4), 289-327.

Ulan, W. W., Green, D., Kosick, G. A., 1991. In-plant testing of the Outokumpu high grade flotation cell. In, Agar, G. E., Huls, B. J., Hyma, D. B., Column Flotation '91. Sudbury, Ontario, Canada.

Varbanov, R., 1984. Flotation of spherical particles. Trans. Inst. Mineral Metall. 93, C6-C8.

Vienna, S., 2004. The effect of particle size, collector coverage and liberation on the floatability of galena particles in an ore. PhD thesis, University of Queensland.

Wei, Z., 2010. On the interpretation of floatability using the bubble load. Ph.D. Thesis, University of Queensland.

Weiss, T., Schubert, H., 1988. The effect of fine particles on the hydrodynamics of flotation processes. XVI. Int. Minerall Process Forssberg K.S.E., Elsevier, 807-818.

Westhuizen, A.P., Deglon, D.A., 2008. Solids suspension in a pilot-scale mechanical flotation cell, A critical impeller speed correlation. Minerals Engineering 21, 621-629.

Wheeler, D.A., 1988. Historical view of column flotation development. Column 88 - Proc. Int. Conf., S.M.E., Phoenix, 3-4.

Villermaux, E., Sixou, B., Gagne, Y., 1995. Intense vertical structures in grid generated turbulence. Physics of Fluids 7 (8).

Washburn, E.W., 1921. The dynamics of capillary flow. Physical Review XVII (3), 273–283.

Weiss, N.L. (editor), 1985. SME Mineral Processing Handbook, AIME.

Wierink, G.A., K. Heiskanen, T. Niitti, J. Turunen, 2008. The dual outlet device - Key to size-selective flotation. Minerals Engineering 21, 894-898.

Woodburn, E.T., King, R.P., Colborn, R.P., 1971. The effect of particle size distribution on the performance of a phosphate flotation Processing Metall. Trans., 2, 3163-3174.

Wu, H., Patterson, G.K., 1989. Laser-doppler measurements of turbulent-flow parameters in a stirred mixer. Chemical Engineering Science 44, 2207-2221.

Xinghau, C., 1998. Technical note, Study and test on a new flotation device, LM flotation cell. Minerals Engineering 11, 457-462.

Ye, Y., Gopalakrishnan, S., Pacquet, E., Miller, J.D., 1988. Development of the air-sparged hydrocyclone. In, Sastry, K. V. S. (Ed.), Column Flotation '88. Pheonix, Arizona, SME.

Yianatos, J., Henrquez, F., Tapia, L., 2008. Evaluation of the largest flotation cells at Minera Los Pelambres. Minerals Engineering 21 (12-14), 841 – 845, selected Papers from Flotation 07.

Yoon, R.H., 1991. Hydrodynamic and surface forces in bubble-particle interaction. Aufbereitungs Technik 32, 474.

Yoon, R.H., 2000. The role of hydrodynamic and surface forces in bubble–particle interaction. International Journal Mineral Processing 58, 129-143.

Yoon, R.-H., Mao, L., 1996. Application of extended DLVO theory, IV, Derivation of flotation rate equation from first principles. Journal of Colloid and Interface Science 181 (2), 613 - 626.

Yoon, R.J., Luttrell, G.H., 1986. The effect of bubble size on fine coal flotation. Coal Prep. , 179-192.

Yoon, R.H., Luttrell, G.H., 1989. The effect of bubble size on fine particle flotation. Mineral Processing Extract. Metall. Rev. 5, 101-122.

Yan, J., Cheng N.S, Tang H.W., Tan S.K., 2010. Oscillating-grid turbulence and its applications, a review. Journal of Hydraulic Research 45 (1), 26-32.

Zanin, M., Ametov, I., Grano S., Zhou, L., Skinner, W., 2009. A study of mechanisms affecting molybdenite recovery in a bulk copper/molybdenum flotation circuit, In. J. of Min. Pro. 93, 256-266.

Zheng, X., Johnson, N.W., Franzidis, J.P. 2006. Modelling of entrainment in industrial flotation cells, Water recovery and degree of entrainment. Minerals Engineering 19, 1191-1203.

Zuninga, H.G., 1935. Flotation recovery is an exponential function of its rate, Bol. Soc. Nac. Min., Santiago 47, 83-86.

Appendices

A.1: Galena Flotation Data

Table A.1: Flotation rates for Galena particles floated with 0.13 mm bubbles

	Particle Size (µm)	**Energy Input (W/kg)**			
Low Collector Dosage	d_p \ E	0.5	1	2	3
	- 19 µm	0.07	0.09	0.11	0.48
	+ 19 - 38 µm	0.03	0.02	0.02	0.02
	+ 38 - 150 µm	0.01	0.00	0.00	0.01
Moderate Collector Dosage	d_p \ E	0.50	1.00	2.00	3.00
	- 19 µm	0.27	0.39	0.47	0.57
	+ 19 - 38 µm	0.48	0.50	0.49	0.42
	+ 38 - 150 µm	0.38	0.19	0.11	0.09
High Collector Dosage	d_p \ E	0.50	1.00	2.00	3.00
	- 19 µm	0.25	0.35	0.60	0.74
	+ 19 - 38 µm	0.55	0.70	0.84	0.66
	+ 38 - 150 µm	0.81	0.73	0.43	0.22

Table A.2: Flotation rates for Galena particles floated with 0.58 mm bubbles

	Particle Size (µm)	**Energy Input (W/kg)**			
Low Collector Dosage	d_p \ E	0.5	1	2	3
	- 19 µm	0.02	0.04	0.06	0.21
	+ 19 - 38 µm	0.01	0.01	0.01	0.02
	+ 38 - 150 µm	0.00	0.00	0.00	0.01
Moderate Collector Dosage	d_p \ E	0.50	1.00	2.00	3.00
	- 19 µm	0.11	0.15	0.23	0.25
	+ 19 - 38 µm	0.23	0.24	0.20	0.12
	+ 38 - 150 µm	0.16	0.12	0.06	0.03
High Collector Dosage	d_p \ E	0.50	1.00	2.00	3.00
	- 19 µm	0.12	0.12	0.26	0.30
	+ 19 - 38 µm	0.28	0.32	0.38	0.29
	+ 38 - 150 µm	0.58	0.43	0.22	0.15

Table A.3: Flotation rates for Galena particles floated with 0.82 mm bubbles

	Particle Size (µm)	**Energy Input (W/kg)**			
Low Collector Dosage	d_p \ E	0.5	1	2	3
	- 19 µm	0.01	0.02	0.03	0.09
	+ 19 - 38 µm	0.01	0.01	0.01	0.01
	+ 38 - 150 µm	0.00	0.00	0.00	0.01
Moderate Collector Dosage	d_p \ E	0.50	1.00	2.00	3.00
	- 19 µm	0.05	0.07	0.09	0.10
	+ 19 - 38 µm	0.08	0.09	0.07	0.06
	+ 38 - 150 µm	0.05	0.04	0.03	0.02
High Collector Dosage	d_p \ E	0.50	1.00	2.00	3.00
	- 19 µm	0.07	0.08	0.10	0.12
	+ 19 - 38 µm	0.15	0.19	0.20	0.15
	+ 38 - 150 µm	0.24	0.23	0.15	0.09

A.2: Pyrite Flotation Data

Table A.4: Flotation rates for Pyrite particles floated with 0.13 mm bubbles

	Particle Size (µm)	**Energy Input (W/kg)**			
Low Collector Dosage	d_p \ E	0.5	1	2	3
	- 19 µm	0.08	0.09	0.10	0.16
	+ 19 - 38 µm	0.09	0.09	0.08	0.07
	+ 38 - 150 µm	0.05	0.03	0.02	0.02
Moderate Collector Dosage	d_p \ E	0.50	1.00	2.00	3.00
	- 19 µm	0.11	0.13	0.14	0.15
	+ 19 - 38 µm	0.17	0.16	0.14	0.12
	+ 38 - 150 µm	0.11	0.07	0.04	0.03
High Collector Dosage	d_p \ E	0.50	1.00	2.00	3.00
	- 19 µm	0.14	0.16	0.18	0.20
	+ 19 - 38 µm	0.22	0.22	0.20	0.18
	+ 38 - 150 µm	0.18	0.13	0.08	0.06

Table A.5: Flotation rates for Pyrite particles floated with 0.58 mm bubbles

	Particle Size (µm)	**Energy Input (W/kg)**			
Low Collector Dosage	d_p \ E	0.5	1	2	3
	- 19 µm	0.04	0.05	0.06	0.10
	+ 19 - 38 µm	0.05	0.05	0.04	0.03
	+ 38 - 150 µm	0.03	0.02	0.01	0.01
Moderate Collector Dosage	d_p \ E	0.50	1.00	2.00	3.00
	- 19 µm	0.06	0.07	0.09	0.11
	+ 19 - 38 µm	0.09	0.09	0.09	0.08
	+ 38 - 150 µm	0.08	0.05	0.03	0.02
High Collector Dosage	d_p \ E	0.50	1.00	2.00	3.00
	- 19 µm	0.09	0.09	0.12	0.14
	+ 19 - 38 µm	0.12	0.14	0.14	0.14
	+ 38 - 150 µm	0.13	0.11	0.07	0.05

Table A.6: Flotation rates for Pyrite particles floated with 0.82 mm bubbles

	Particle Size (µm)	**Energy Input (W/kg)**			
Low Collector Dosage	d_p \ E	0.5	1	2	3
	- 19 µm	0.01	0.01	0.02	0.05
	+ 19 - 38 µm	0.02	0.02	0.02	0.02
	+ 38 - 150 µm	0.02	0.02	0.01	0.01
Moderate Collector Dosage	d_p \ E	0.50	1.00	2.00	3.00
	- 19 µm	0.02	0.03	0.03	0.04
	+ 19 - 38 µm	0.03	0.04	0.04	0.04
	+ 38 - 150 µm	0.05	0.03	0.02	0.02
High Collector Dosage	d_p \ E	0.50	1.00	2.00	3.00
	- 19 µm	0.02	0.03	0.04	0.07
	+ 19 - 38 µm	0.04	0.05	0.06	0.08
	+ 38 - 150 µm	0.07	0.05	0.03	0.04

A.3: Pentlandite Flotation Data

Table A.7: Flotation rates for Pentlandite particles floated with 0.13 mm bubbles

	Particle Size (µm)	**Energy Input (W/kg)**			
Low Collector Dosage	d_p \ E	0.5	1	2	3
	- 19 µm	0.03	0.05	0.05	0.11
	+ 19 - 38 µm	0.05	0.06	0.07	0.08
	+ 38 - 150 µm	0.04	0.03	0.03	0.03
Moderate Collector Dosage	d_p \ E	0.5	1	2	3
	- 19 µm	0.06	0.08	0.09	0.11
	+ 19 - 38 µm	0.07	0.09	0.10	0.11
	+ 38 - 150 µm	0.05	0.05	0.04	0.03
High Collector Dosage	d_p \ E	0.5	1	2	3
	- 19 µm	0.10	0.11	0.14	0.16
	+ 19 - 38 µm	0.13	0.15	0.15	0.16
	+ 38 - 150 µm	0.10	0.08	0.08	0.06

Table A.8: Flotation rates for Pentlandite particles floated with 0.58 mm bubbles

	Particle Size (µm)	**Energy Input (W/kg)**			
Low Collector Dosage	d_p \ E	0.5	1	2	3
	- 19 µm	0.02	0.03	0.04	0.08
	+ 19 - 38 µm	0.04	0.05	0.06	0.06
	+ 38 - 150 µm	0.03	0.03	0.03	0.02
Moderate Collector Dosage	d_p \ E	0.5	1	2	3
	- 19 µm	0.04	0.05	0.06	0.07
	+ 19 - 38 µm	0.05	0.06	0.07	0.08
	+ 38 - 150 µm	0.04	0.04	0.03	0.03
High Collector Dosage	d_p \ E	0.5	1	2	3
	- 19 µm	0.06	0.09	0.10	0.11
	+ 19 - 38 µm	0.10	0.10	0.12	0.12
	+ 38 - 150 µm	0.09	0.07	0.06	0.06

Table A.9: Flotation rates for Pentlandite particles floated with 0.82 mm bubbles

	Particle Size (µm)	**Energy Input (W/kg)**			
Low Collector Dosage	d_p \ E	0.5	1	2	3
	- 19 µm	0.01	0.02	0.03	0.06
	+ 19 - 38 µm	0.02	0.03	0.03	0.04
	+ 38 - 150 µm	0.02	0.02	0.02	0.02
Moderate Collector Dosage	d_p \ E	0.5	1	2	3
	- 19 µm	0.03	0.03	0.04	0.05
	+ 19 - 38 µm	0.03	0.04	0.05	0.05
	+ 38 - 150 µm	0.03	0.03	0.03	0.02
High Collector Dosage	d_p \ E	0.5	1	2	3
	- 19 µm	0.05	0.06	0.08	0.08
	+ 19 - 38 µm	0.06	0.07	0.07	0.08
	+ 38 - 150 µm	0.05	0.04	0.04	0.03

A.4: Apatite Flotation Data

Table A.10: Flotation rates for Apatite particles floated with 0.58 mm bubbles

	Particle Size (µm)	**Energy Input (W/kg)**			
Low Collector Dosage	d_p \ E	0.1	0.5	1	2
	- 38 µm	0.05	0.06	0.07	0.09
	+ 38 - 150 µm	0.13	0.10	0.08	0.04
	+ 150 - 650 µm	0.15	0.06	0.04	0.02
Moderate Collector Dosage	d_p \ E	0.1	0.5	1	2
	- 38 µm	0.03	0.05	0.06	0.07
	+ 38 - 150 µm	0.07	0.06	0.05	0.03
	+ 150 - 650 µm	0.09	0.03	0.02	0.01

A.5: Hematite Flotation Data

Table A.11: Flotation rates for Hematite particles floated at moderate collector dosage

Bubble Size	**Particle Size (µm)**	**Energy Input (W/kg)**					
0.13 mm	d_p \ E	0.5	1	2	3	4	5
	- 19 µm	0.06	0.07	0.07	0.08	0.08	0.09
	+ 19 - 45 µm	0.04	0.03	0.03	0.02	0.02	0.01
0.24 mm	d_p \ E	0.5	1	2	3	4	5
	- 19 µm	0.05	0.05	0.06	0.07	0.07	0.08
	+ 19 - 45 µm	0.03	0.03	0.02	0.02	0.02	0.02
0.82 mm	d_p \ E	0.5	1	2	3	4	5
	- 19 µm	0.01	0.02	0.03	0.03	0.04	0.04
	+ 19 - 45 µm	0.02	0.02	0.01	0.01	0.00	0.00